An *in vitro* investigation of the spatial control involved in collagen mineralization

by

Janice Jing Song

A thesis submitted in conformity with the requirements
for the degree of Master of Applied Science

Department of Materials Science and Engineering and
The Institute of Biomaterials and Biomedical Engineering
University of Toronto

© Copyright by Janice Song 2010

An *in vitro* investigation of the spatial control involved in collagen mineralization

Janice Jing Song

Master of Applied Science

Department of Materials Science and Engineering and
The Institute of Biomaterials and Biomedical Engineering
University of Toronto

2010

Abstract

An *in vitro* model system utilizing de-mineralized periodontium tissues was developed for investigating the molecular controls involved in the spatial deposition of minerals on collagenous tissues. Preferential mineral deposition was observed when the de-mineralized tissue sections were incubated in solutions containing a supersaturation of calcium and phosphate ions with respect to hydroxyapatite (HA). Energy dispersive X-Ray (EDX) analysis demonstrated that these minerals are likely to be octacalcium phosphate (OCP) or dicalcium phosphate dihydrate (DCPD); further characterization with a secondary technique is required to draw a more definitive conclusion. The role of collagen fibrils in mineralization was tested by removing all the non-collagenous components from the tissue sections with proteolytic enzymes and exposing them to similar mineralization conditions as the control samples. A substantially less amount of minerals were formed in these samples; this correlates well with the hypothesis in the literature that collagen fibrils alone cannot initiate mineral formation.

Acknowledgments

I want to thank my supervisor, Dr. Eli D. Sone, for his guidance and advice on this research project. I also want to thank my collaborator, Dr. Bernhard Ganss for continued support and advice throughout this project; and Dr. Craig Simmons, my committee member, for his technical advice and expertise.

I would like to acknowledge Feryal Sarraf, Vanessa Mendes, Doug Homyard, and Cecilia Bolarinho for their technical assistance without which this project would not have been possible. I want to thank my fellow group members, Nikrooz Farzad, Trevor Gilbert, and Bryan Quan for all their help and assistance in the laboratory, it is much appreciated. I would also like to acknowledge Na-Rae Park and Henry Leopold for their contribution to a set of experiments completed as their fourth year thesis project, included as part of this thesis.

I'm grateful for the funding provided by the Bone and Minerals Scholarship, U of T Open fellowship, and Ontario Graduate Scholarship (OGS).

I want to thank my parents for their support throughout the duration of my studies. I would also like to thank all my friends for all their encouragement along the way, especially Seema Nagaraj, Elizabeth Pham, and Zahra Mirzaei. And lastly, yet foremost, I would like to express my heartfelt gratitude for my God who upheld me through the hardest times in life and made this Master's project possible.

Table of Contents

List of Tables

List of Figures

List of Appendices

List of Abbreviations

ACP – Amorphous calcium phosphate

BGP – Bone gla-protein

BSE – Backscattered electron

BSP – Bone sialoprotein

CaP – Calcium phosphate

c-SBF – Conventional SBF

DCPD – Dicalcium phosphate dihydrate

DMPI – Dentin matrix protein I

DSP – Dentin sialoprotein

DSPP – Dentin sialophosphoprotein

DPP – Dentin phosphoprotein (also known as phosphophoryn)

ECM – Extracellular matrix

EDTA – Ethylenediamine-tetraacetic acid

EDX – Energy dispersive X-ray analysis

ESEM – Environmental scanning electron microscope/microscopy

GAGs – Glycosaminoglycans

HA – Hydroxyapatite

HEPES – 4-(2-hydroxyethyl)-1-piperazineethanesulfonic acid

HMDS – Hexamethyldisilazane

i-SBF – Ionized SBF

LDPE – Low density polyethylene

m-SBF – Modified SBF

MEPE – Matrix extracellular phosphoglycoprotein

MGP – Matrix Gla-protein

MVs- Matrix vesicles

NCPs – Non-collagenous proteins

OC – Osteocalcin, also known as

OCP – Octacalcium phosphate

ON – Osteonectin

OPN – Osteopontin

PBS – Phosphate buffered saline

PDL – Periodontal ligament

PFA – paraformaldehyde

PG – Proteoglycans

PVC – Polyvinyl chloride

r-SBF – Revised SBF

RGD – Arginine-glycine-aspartate

SBF – Simulated body fluid

SEM – Scanning electron microscope/microscopy

SIBLING proteins – Small Integrin Binding LIgand N-Link Glycoproteins

TCP – Tricalcium phosphate

Tris – Tris(hydroxymethyl)aminomethane

TEM – Transmission electron microscope

VP – Variable pressure

Chapter 1
Introduction and literature review

1 Introduction and literature review

1.1 Why does collagen mineralize?

Collagen mineralization is a meticulously regulated process *in vivo*. A loss of spatial control in mineral deposition could result in a number of diseases either caused by excessive mineral formation in soft connective tissues (e.g. pathologically calcified heart valves) or insufficient mineral formation in hard connective tissues (e.g. osteoporosis). Therefore, a more thorough understanding of the controls and mechanisms involved in collagen mineralization can potentially lead to the prevention and treatment of a number of diseases [1].

The collagen fibrils of hard connective tissues become infiltrated with plate-like mineral crystals during the mineralization process. They are in the nano-meter size range and are oriented along the length of collagen fibrils [2]. These crystals have a similar crystal structure as synthetic hydroxyapatite (HA) and are often referred to as carbonated hydroxyapatite, or biological apatite [3-6].

According to thermodynamics, the concentration of calcium and phosphate ions in the body fluid is supersaturated with respect to calcium phosphate minerals and precipitates should form spontaneously in all tissues. However, the fact that HA crystals only forms in hard connective tissues under normal physiological conditions suggests that there's a chemical difference between the collagenous and non-collagenous components of hard and soft connective tissues. They either contain different types of collagen molecules or non-collagenous macromolecules

that are capable of preventing and/or inducing mineral formation. Strong experimental evidence suggests that both the collagen fibrils and various macromolecules play a role in regulating mineral deposition [1]. Collagen fibrils are hypothesized to act as a template for HA deposition, while different non-collageneous macromolecules are thought to promote or inhibit mineral nucleation and growth [1]. However, due to the complexity of the *in vivo* environment, the exact role of each of these components has not been thoroughly characterized [7].

The goal of this study is to first develop an *in vitro* mineralization model system that mimics the ECM components of the *in vivo* environment. Intact collagen tissues from the periodontium of mice will be utilized as the model tissue structure for this study. These tissues are especially suitable for investigating the spatial control of mineral deposition because they contain two soft-hard tissue interfaces, the periodontal ligament (PDL)-cementum interface and the PDL-bone interface. The former interface contains a sharp transition between the hard and soft connective tissues which requires a high degree of spatial control over mineral deposition; the latter contains an irregular interface due to constant remodeling that takes place in bone [8]. The periodontium tissues will be de-mineralized and re-mineralized in a solution that contains a similar ion concentration as the blood plasma. The pattern of mineral deposition will be characterized with histological stains and the Ca/P molar ratio of the mineral will be studied with Energy Dispersive X-ray (EDX) analysis.

Once this *in vitro* model system is well characterized, it will then be used to investigate the role of collagen fibrils in regulating mineral deposition. All the non-collagenous macromolecules will be removed from the collagen matrix with proteolytic enzymes; these samples will be re-mineralized in the same way as the non-enzyme treated ones. The ability of the collagen fibrils at inducing mineral deposition will be studied by comparing the re-mineralization pattern of the enzyme-treated samples and the non-enzyme treated ones.

The knowledge gained from this project will lead to a better understanding of the role of collagen fibrils in regulating collagen mineralization. The proposed *in vitro* model system will be utilized in the future to investigate the role of different groups of non-collagenous macromolecules by selectively removing them from the collagen matrix and studying the resulting re-mineralization pattern. These future investigations will lead to a clearer understanding of the molecular controls involved in collagen mineralization; this knowledge could be applied to preventive or treatment strategies of periodontal diseases such as ankylosis and periodontitis. Ankylosis is the fusion of the tooth root with the tooth socket caused by mineralization of the PDL. Periodontitis is a more advanced stage of gingivitis in which inflammation (or infection) of the gums spreads to the PDL and alveolar bone of the tooth; it eventually results in the detachment of the tooth from the tooth socket [9]. A better understanding of the mechanisms that control mineralization at the PDL-cementum interface could potentially lead to tissue engineering strategies for the treatment of these diseases.

1.2 Collagen fibrils and mineralization

1.2.1 The structure of collagen

Collagen is the main protein component of connective tissues. It is synthesized by various cell types including fibroblasts, smooth-muscle cells, and osteoblasts [10]. There are at least 16 types of collagens that have been identified to date, with type I, II and III being the most abundant [11].

The collagen matrix is composed of collagen fibers that are made up of bundles of collagen fibrils. Collagen fibrils have a characteristic banding pattern of 67 nm when viewed with the transmission electron microscope (TEM) [11]. Collagen fibrils are composed of microfibrils, a filamentous structure with a diameter of 4 nm. Each microfibril contains four or five strands of tropocollagen molecules that are staggered along the length of the fibrils [10, 12]. Tropocollagen molecules consist of three alpha chains of amino acids wound around each other in a triple helical configuration; each molecule is 280 nm long and 1.4 nm in diameter [10].

The alpha chains of the tropocollagen molecules contain two different sequence regions, the central triple helical region (~ 1014 residues) and the non-triple helical region at both ends of the molecule (~ 9-50 residues) [10].

The helical region is composed of repeating amino acid sequences with the motif Gly-X-Y; where X represents proline amino acid residues and Y represents any amino acid residue, but primarily hydroxyproline [11]. These proline rich units (e.g. Gly-Pro-Hyp and Gly-Pro-Y) form covalent cross-links that help stabilize the collagen molecules. The major contributions come from two types of borohydride-reducible cross-links, dihydroxylysinonorleucine (DHLNL) and

hydroxylysinonorleucine (HLNL)), and a tri-functional non-reducible crosslink, pyridinoline [13].

The non-helical regions contain polar charged and hydrophobic amino acids with functional groups useful for intermolecular bonding (e.g. lysine or hydroxylysine which can be oxidized to lysylaldehydes) [10]. The strongest interaction between different collagen molecules occurs when they are shifted by a distance of 67 nm from each other. The polar amino acid residues in the "overlap region" can be visualized in the TEM with phosphotungstic acid staining, which allows the characteristic 67 nm banding pattern of collagen to be observed (Figure 1) [10].

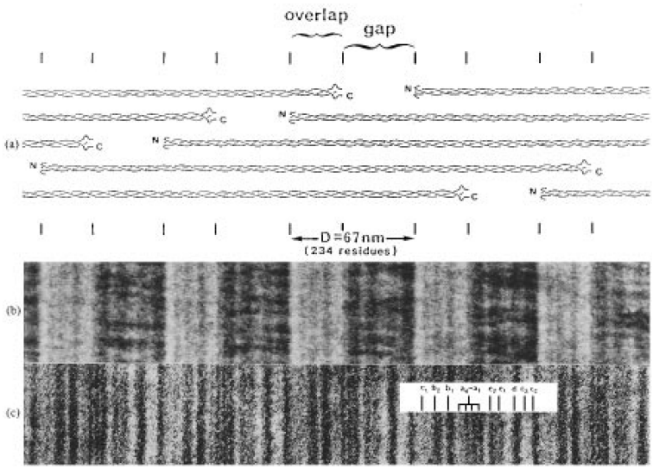

Figure 1 Schematic representation of the axial packing arrangement of triple-helical collagen molecules in a fibril, derived from analysis of the negative (b) and positive (c) staining patterns [14]. Figure reproduced with permission from K.E. Kadler, D.F. Holmes, J.A. Trotter and J.A. Chapman, 1996, (*Biochemical Journal*), (316), (**1-11). © the Biochemical Society.**

1.2.2 The process of mineral formation

The process of mineral formation in bone and dentin involves a complex series of events under close cellular (osteoblasts and odontoblasts) and molecular control (extracellular proteins) [1, 13]. While it is well agreed upon that the function of the hard tissue forming cells is to produce the organic components and create an extracellular (ECM) environment conductive to mineral formation, the mechanisms of initial mineral deposition remains a controversial topic. The observation of the first mineral deposits at both the "hole-zones" of collagen fibrils and in membrane bound vesicle structures secreted by calcifying cells has given rise to two separate nucleation mechanisms known as "heterogeneous nucleation" and "matrix vesicles (MVs)" [13, 15, 16].

The heterogeneous nucleation model was based on TEM observations of the close relationship between the inorganic substance and the periodic banding of collagen fibrils [15, 17]. Mineral nuclei deposits were seen at the "hole-zones" of collagen fibrils in newly formed embryonic chick bone [18, 19, 20]. This led to the hypothesis that the initial calcium phosphate crystals formed as a result of calcium binding at the "hole-zones" of collagen fibrils; these crystal nuclei would then grow in length and thickness into platelets aligned along the length of collagen fibrils [1, 21, 22].

The size and shape of mineral crystals are thought to be regulated by the binding of non-collageneous proteins (NCPs) to selected crystal facets [1, 23]. This is due to the close match between the polypeptide chain spacing of NCPs and the lattice spacing of inorganic crystals; an example is the selective binding of phosphophoryn to octacalcium phosphate (OCP) [24].

Matrix vesicles (MVs) are membrane bound structures that bud off from the membrane of calcifying cells (e.g. osteoblasts and odontoblasts) [25]; they contain a number of molecules such

as alkaline phosphatase, phospholipids and other proteins that favour the formation of calcium phosphate crystals [1, 25]. Once nucleated, the crystal nuclei grow in size until it perforates the vesicle membranes, it then deposits at the “hole zones” of collagen fibrils and continue to increase in size [1, 25].

MVs are often associated with the initial sites of HA formation, but the relationship of the crystal to the bulk mineral is still poorly understood [13]. MVs have been observed in different hard tissues such as bone, alveolar bone, and reparative dentin, and in many different species including rats, canines, rabbits, bovines, humans, chickens, deer and turkeys. They are a fundamental component of endochondral ossification and primary bone formation [13].

Regardless of the initial nucleation mechanism, the mature apatite crystals are deposited in a highly oriented manner, with their crystallographic c-axes parallel to the long axis of the fibril (see Figure 2) [2, 26]. This high degree of crystal orientation with respect to the collagen fibrils may be caused by the porous structure of collagen fibrils or the interactions between collagen fibrils and its bound macromolecules [13]. Once the mineral crystals have filled the intrafibrillar and interfibrillar spaces, they continue to mature chemically and structurally into more perfect crystals over time [13].

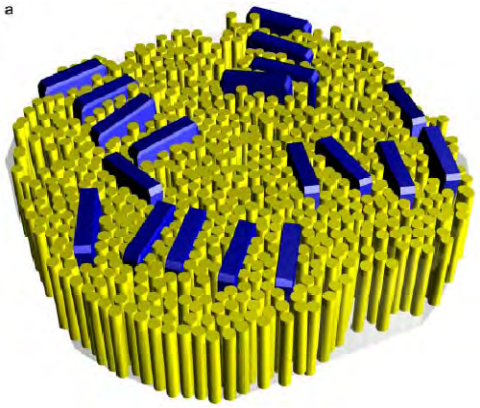

Figure 2 Schematic illustration of the lateral packing of mineral crystals in the collagen matrix. Thin apatite platelets are aligned nearly parallel within the stacks. The thickness of

crystals is typically 2 nm and the width is 20 nm. The crystal height in the c-axis dimension (preferentially aligned about the fibril axis, not visible in this figure) is ~ 30 nm [2].

1.2.3 Biological hydroxyapatite (HA)

The mineral found in bone and dentin is poorly crystalline carbonatoapatite, with a chemical formula and structure closest to synthetic hydrxyapatite (HA), $Ca_{10}(OH)_2(PO_4)_6$ [4-6]. It is sometimes referred to as calcium deficient hydroxyapatite due to the large amount of carbonate substitution observed [3]. Ionic substitutions can occur with a number of ions to varying degrees: Ca^{2+} can be replaced by Na^+, K^+, Li^+, Sr^{2+}, Ba^{2+}, Pb^{2+}, Mn^{2+}, Sn^{2+}, Zn^{2+}, Mg^{2+} and Al^{3+}; PO_4^{3-} can be replaced by HPO_4^{2-}, CO_3^{2-}, SO_4^{2-}, MnO_4^-, VO_4^{2-}, and BO_3^{3-}; and OH^- can be replaced by F^-, Cl^-, and CO_3^{2-} [27, 28]. Mineral phases that have been identified in mineralized tissues in addition to HA include octacalcium phosphate (OCP), amorphous calcium phosphate (ACP), dicalcium phosphate dihydrate (DCPD), and whitelockite (which is also known as β-Tricalcium phosphate) (see Table 1).

Calcium phosphate	**Mineral name**	**Chemical formula**	**Ca/P molar ratio**
Dicalcium phosphate dihydrate (DCPD)	Brushite	$CaHPO_4 \cdot 2H_2O$	1
β-Tricalcium phosphate (TCP)	Whitlockite	$Ca_3(PO_4)_2$	1.5
Octacalcium phosphate (OCP)		$Ca_8H_2(PO_4)_6 \cdot 5H_2O$	1.33
Hydroxyapatite (HAP)	Apatite	$Ca_{10}(OH)_2(PO_4)_6$	1.67
Carbonated apatite (CAP)		$Ca_{10}(OH)_2(PO_4, CO_3)_6$	

Table 1 Common calcium phosphate minerals and biominerals; figure adapted from [29].

The minerals found in mature mineralized tissues (bone and dentin) have a platelet shape, and can be found in a range of sizes in different tissues and animal species [1, 2, 13]. Human dentin and alveolar bone was found to contain HA monocrystals with a width of approximately 36 and 56 nm, and a thickness of approximately 10 and 8 nm, respectively [30]. The crystals of rat cartilage and bone were found to be 12 and 17 nm long and 50 nm wide [31]. Mesenchymal hard tissues contain HA crystals that are 10-20 nm long and 5 nm wide [1]. Embryonic chick tibia HA crystals are approximately 45 nm long and 3 nm wide [21]. The largest crystals are found in enamel, 140 nm long and 80 nm wide [1].

While the size and shape of HA crystals have been well characterized and agreed upon in recent years, the mechanism through which they form remains a controversial topic [32]. A less stable transient precursor phase (e.g. OCP, or ACP) has been proposed to form first and transform into HA by hydrolysis over time, since HA is the most thermodynamically stable phase of all the calcium phosphate minerals that form in biological systems [33, 34, 17]. This hypothesis is supported by both *in vivo* and *in vitro* observations, as well as evidence from invertebrate species [33, 35, 36].

In vivo studies: Several *in vivo* studies have identified the presence of amorphous calcium phosphate (ACP), dicalcium phosphate dihydrate (DCPD), and octacalcium phosphate (OCP) in newly formed bone tissues [28, 33, 36-40]. The calcium to phosphorus (Ca/P) molar ratio was observed to be higher in mature bone; it was 1.35 (corrected for carbonate) for the bone mineral of 9-day old chick embryos, but increased to 1.39 in chicks that are 15 days to 6 months old [41]. Another study performed on the growing rat tibial diaphyses obtained Ca/P molar ratios of approximately 1.3 and 1.6 in growing and mature bone, respectively [42]. It has been hypothesized based on these experimental data that the phase of the calcium phosphate mineral is associated with the maturity of mineralized tissues [13].

In vitro studies: *In vitro* precipitation studies of calcium phosphate minerals have provided indirect evidence for the existence of a transient precursor phase. The shape of the HA crystals formed *in vitro* has a needle-like shape when precipitated directly from solution; however, when precipitated by partial or complete hydrolysis of an OCP precursor, the crystals have a flat and platy shape similar to the HA crystals formed *in vivo* [43]. Under *in vitro* conditions (pH range of 7.4-9.2), OCP forms preferentially over HA because it has a lower crystal surface energy [34, 43-47]. Another factor that influences the phase of calcium phosphate minerals formed is the ion concentration of calcium and phosphate ions. HA forms directly in solutions with low super saturation levels (indicated by arrow 1); as the concentration of phosphate ions increase, less stable phases of calcium phosphate compounds (e.g. ACP and OCP) form initially and transform into HA over time (indicated by arrows 2-4) (Figure 3) [28].

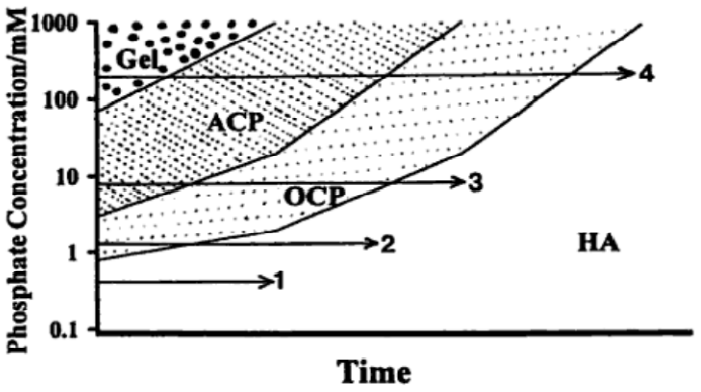

Figure 3 The formation, stability, and hydrolysis of calcium phosphate minerals, as a function of phosphate concentration (log(P)) in solutions at neutral pH [28].

Proponents that dispute the existence of precursor phases present the evidence that the percentage of ACP is fairly constant (approximately 12%) in both mature and immature bone [17]. The seemingly contradictory findings presented in the literature are possibly due to the fact that the different phases of calcium phosphate minerals are not clearly distinguishable with traditional characterization techniques such as X-Ray diffraction (XRD) and Energy-Dispersive X-Ray (EDX) analysis. The XRD pattern and crystal structure of HA and OCP are very similar, it is therefore difficult to distinguish the two phases with this technique alone [28]. EDX

analysis is a technique commonly used for obtaining the Ca/P molar ratios of calcium phosphate minerals, however, due to the large amount of ionic substitutions present in HA, and the significant amount of phosphorus ions present in tissues, it is therefore difficult to deduce the exact mineral phase (see Table A1 in Appendix I for a list of the Ca/P molar ratios of various calcium phosphate minerals). Therefore, it is imperative to use more than one characterization technique when determining the phase of calcium phosphate minerals. In recent year, techniques with lower resolution limits have been developed as an alternative or secondary method to aid the identification of calcium phosphate minerals, some of these techniques include Infrared spectroscopy (IR), Raman spectroscopy, and nuclear magnetic resonance (NMR) [28, 48-54].

1.2.4 The role of collagen fibrils in mineralization

Collagen of different types of tissues differs in its ability to induce mineral deposition. De-mineralized sheep bone and bovine dentin collagen were effective at inducing mineral formation *in vitro* when incubated in a solution containing calcium and phosphate ion [55-57]. On the other hand, collagen fibrils from soft connective tissues, reconstituted rat tail tendon and sheep PDL did not induce mineral formation *in vitro* [56, 58]. These observations led to two possible hypotheses: it is either the different distribution of non-collagenous macromolecules or the difference in collagen fibrils of hard and soft connective tissues that prevent and/or induce mineral formation [56, 58]. The hypothesized role of collagen fibrils is reviewed in the remainder of this section; the distribution of non-collagenous macromolecules and their role in mineralization will be reviewed in Section 1.3.

Some of the differences between hard and soft connective tissue collagen fibrils include: 1) fibril arrangement, 2) fibril width, 3) collagen type, 4) molecular structure, and 5) solubility in dilute acid solutions.

Collagen fibril arrangement: The arrangement of collagen fibrils may play a role in mineral deposition because it can alter the way that collagen molecules interact with each other and with surrounding macromolecules; this can ultimately affect the morphology and arrangement of minerals formed in the collagen matrix. The PDL contains loosely packed collagen fibrils that are arranged in an isotropic network intertwined with extracellular matrix proteins and cells [8]. The collagen fibrils found in bone are arranged irregularly in a three dimensional structures known as osteons [10]. The fibrils of dentin are densely packed and form tubular structures that are 1-3 μm thick in diameter [13].

Collagen fibril width: The collagen fibrils of mineralized tissues generally have greater width compared to soft connective tissues. The width of the collagen fibrils of the human PDL increases significantly at the PDL-cementum interface as they insert into the cementum (Figure 4) [8]. The collagen fibrils of the mineralizing osteoids of rat embryos fuse laterally and their diameter increase close to 8 times. The fusion of collagen fibrils and an increase in fibril diameter was hypothesized to be a means of providing room for subsequent mineral growth [59]. An *in vitro* study that investigated the role of dentin matrix protein 1 (DMP1) on mineral deposition supports this hypothesis. When irreversibly bound to DMP1, the re-constituted rat tail tendon collagen fibrils doubled in width and were able to accommodate mineral deposition. DMP1 was localized at the “hole-zones” of collagen fibrils, the initial site of mineral formation [60].

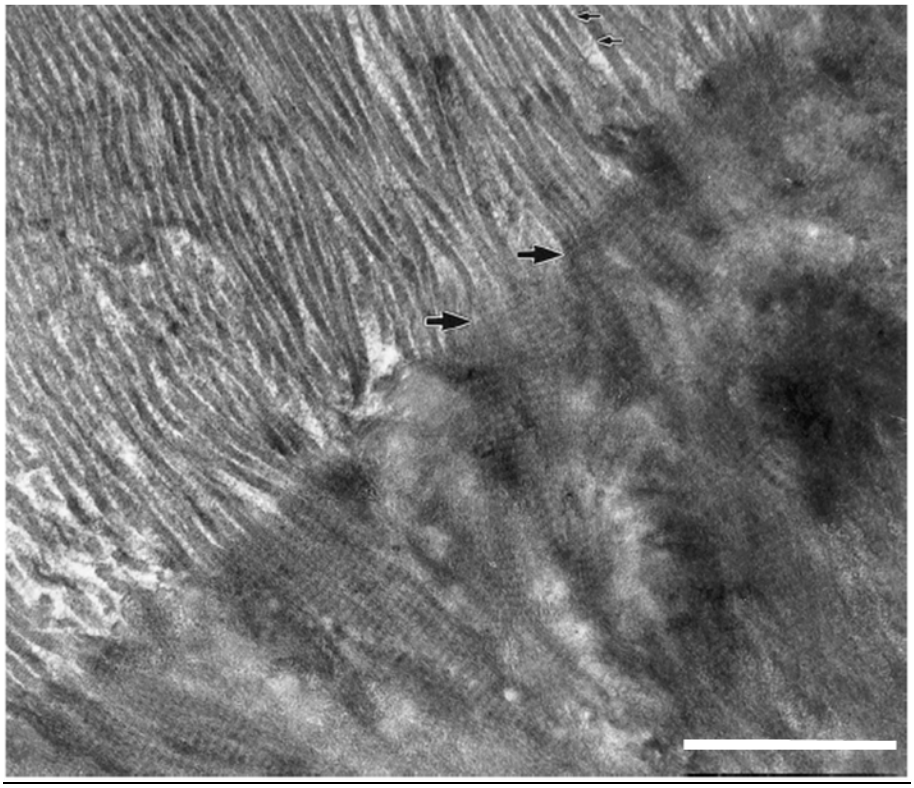

Figure 4 Transmission electron (TEM) micrograph taken at the PDL-cementum junction of a healthy human molar. A sharp mineralization front is clearly visible where the un-mineralized collagen fibrils (top left) insert into the cementum (bottom right), note the difference in fibril diameter. Scale bar = 1 μm [8].

Collagen type: The fibril diameter differs depending on collagen type: type III collagen fibrils are much thinner in diameter compared to type I collagen. Tissues containing a mixture of type I and type III collagen form thinner fibrils compared to type I collagen alone [14]. The PDL contains mostly type I collagen and approximately 20% type III collagen [61]. Dentin is composed primarily of type I collagen with almost no type III collagen [13]. Bone contains mainly type I collagen and a small proportion of type III collagen [13].

Molecular structure: The molecular structure of hard and soft tissue collagen is slightly different. Bone and dentin have an average intermolecular space of 0.6 nm, whereas the intermolecular space of tendon is 0.3 nm. This means that the intrafibrillar spaces (“gaps” and “pores”) of bone

are greater than soft tissue collagens, this could be the reason why hard tissues are able to accommodate more mineral [62, 63]. However, the molecular organization and intermolecular spaces of the collagen fibrils of bone and naturally calcified tendon is the same [64].

Solubility in dilute acid solutions: Tendon and skin collagen swell in dilute acids, while bone collagen does not. Bone collagen is less soluble in dilute acid and neutral salt solutions compared to other types of collagens [65]. However, this difference does not been shown to have a direct effect on collagen mineralization.

Despite the differences between the collagen fibrils of hard and soft connective tissues, collagen fibrils are hypothesized to act as a template for mineral deposition which support the binding of organic components that are involved in calcification, but do not directly induce mineral formation [13]. This is based on the observations that collagen fibrils are weak binders of Ca^{2+} ions and their molecular structure does not match the crystallographic parameters of HA, [13]. In addition, several *in vitro* studies showed that minerals formed as loosely bound clusters on the surface of collagen fibrils when a calcium binding protein (e.g. osteocalcin) or polymer (e.g. polyaspartate) was added in solution, but well aligned minerals in the shape of platelets formed inside the collagen fibrils when the protein or polymer was covalently bound the collagen fibrils [13, 66]; in one special case in which minerals formed through a polymer induced liquid precursor (PILP) process, well aligned minerals formed on collagen fibrils when polyaspartate was added to the mineralization solution (Figure 5) [32, 67]. One study found that removing the phosphate groups of the NCPs in de-mineralized chick bone resulted in a loss of the tissue's ability to nucleate mineral [68]. However, no study has tested the ability of collagen fibrils to induce mineral deposition on de-mineralized hard tissue collagen matrix with its non-collagenous contents removed.

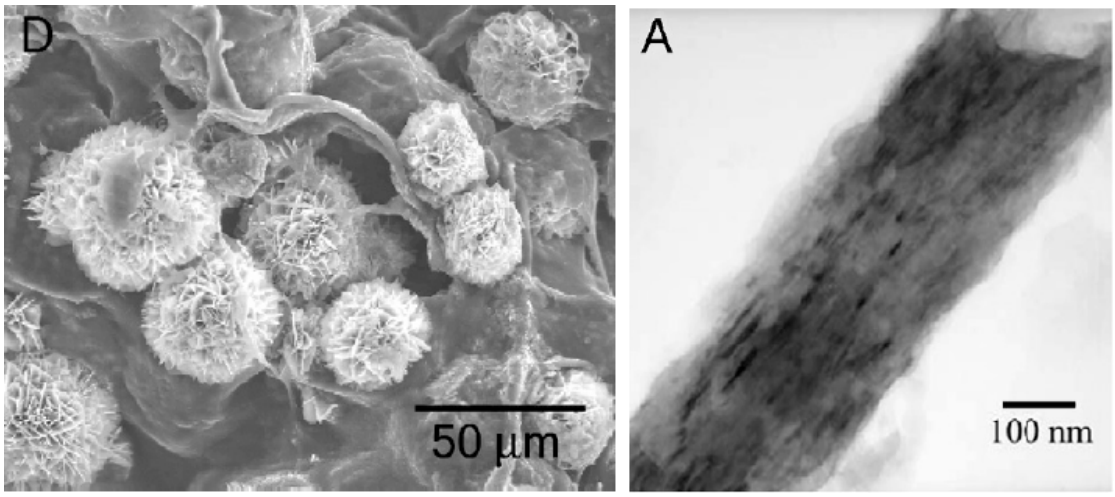

Figure 5 Left: Mineral crystals formed on collagen sponge re-mineralized in the absence of polyaspartate; the minerals are loosely attached to the collagen fibrils. Right: Re-mineralization of collagen sponge with polyaspartate, well aligned crystallites are formed inside the collagen fibrils [32].

1.3 Non-collagenous macromolecules and mineralization

The non-collagenous macromolecules have been hypothesized to facilitate the process of mineralization in hard connective tissues and prevent mineral deposition in soft connective tissues [1, 7, 13, 58, 69, 70]. They constitute approximately 10 % of the organic matrix of bone, dentin and the PDL [13, 71]. They are composed of three main groups of macromolecules: 1) proteoglycans (PGs), 2) glycoproteins and phosphoproteins, and 3) γ-carboxyglutamic acid-containing proteins [7, 72]. See Table A2 in Appendix I for a table of the protein structure and potential function of the various PGs and matrix proteins. The distribution and proposed function of some of the common non-collagenous proteins are summarized in Table 2. This table will be discussed in more detail in the following section, along with a review of the types of model systems utilized to study them.

Macromolecule	**Major constituent(s)**
Proteoglycans (PGs)	Decorin, biglycan, lumican, fibromodulin, versican [72]
Glycoproteins and phosphoproteins	bone sialoprotein (BSP), osteopontin (OPN), dentin matrix protein I (DMPI), dentin sialophosphoprotein (DSPP), matrix extracellular phosphoglycoprotein (MEPE), and osteonectin (ON) [69, 73]
γ-carboxyglutamic acid-containing proteins	Bone Gla protein (BGP) (80 %), Matrix Gla protein (MGP) (20 %) [72]

Table 2 The major constituents of the three major groups of non-collagenous macromolecules.

1.3.1 Proteoglycans (PGs) – Distribution and function

Proteoglycans (PGs) are macromolecules composed of a number of glycosaminoglycan (GAG) side chains covalently bound to a protein backbone [74, 75]. GAGs are made up of repeating dissacharide units, consisting of one uronic acid and one N-acetyl-hexosamine residue [13]. And

because the composition of the disaccharide units determines the type of PGs present, [70] the GAG content of tissues are often measured and reported. Table 3 shows a summary of the common types of GAGs present in connective tissues.

Glycosaminoglycan (GAG)	Distribution
Hyaluronic acid	Umbilical cord, synovial fluid, vitreous humor, cartilage
Chondroitin 4-sulfate	Brain, hyaline and elastic cartilages, bone
Chondroitin 6-sulfate	Articular cartilage, hyaline and elastic cartilages, bone
Dermatan sulfate	Skin, arterial adventitia, tendons, fasciae (collagen fibers)
Heparin sulfate	Smooth muscle, aortic intima + media (reticular fibers)
Heparin	Mast cell granules
Keratan sulfate	Cornea, cartilage from old specimens

Table 3 Distribution of GAGs in connective tissues (see Appendix I for the composition of each GAG); table modified from [76].

1.3.1.1 Distribution of PGs

The distribution of PGs is significantly different in hard and soft connective tissues. For example, decorin is abundant in the PDL while lumican and fibromodulin are the main PGs of the cementum [77, 78]. The PGs of the PDL are localized on collagen fibers while the PGs in dentin are localized in the dentinal tubules [13]. PGs constitute 10 % of all the non-collagenous macromolecules in bone [70]. Mineralized dentin and bone contain mainly biglycan and decorin; [13] the side chains of both biglycan and decorin are predominantly chondroitin-4-sulfate (C4S) and chondroitin-6-sulfate (C6S) [70], with a small amount of hybridized dermatan sulfate [79].

This difference in distribution of PGs in different tissues is hypothesized to be related to their role in mineralization. In the mineralizing osteoids of rat embryos, a significant decrease in

decorin concentration was directly linked to the mineralization of collagen fibrils; this suggests that decorin may serve a preventive role in collagen mineralization [59]. A study analyzing the GAG content of the sheep periodontal tissues showed that alveolar bone and cementum contained mainly C4-S and C6-S while the PDL contained primarily dermatan sulfate and close to equal amounts of CS and heparin sulfate and hyaluronic acid (Table 4) [58]. The same study showed that the removal of GAGs from the PDL resulted in mineralization of the tissue *in vitro*, suggesting that the role of CS GAGs may be to prevent mineralization in soft connective tissues [58]. C4S was found to be closely associated with mineralization because it was extractable only after demineralization [13].

Tissue	**Dermatan sulfate**	**Chondroitin-4- and -6-sulfate**	**Heparan sulfate and hyaluronic acid**
Periodontal ligament	45	25	30
Alveolar bone	12	84	4
Cementum	32	68	ND

Table 4 Relative proportions of different GAGs separated from sheep periodontal tissues; table modified from [58].

1.3.1.2 Function of PGs

The PGs found in mineralized tissues are very small in size compared to the PGs of the cartilage and serve a very different role physiologically [13]. PGs of the cartilage are highly hydrated macromolecules containing a large number of side chains; their role is to occupy space and dissipate force [80]. The PGs found in mineralized tissues are found in close association with collagen fibers [70], and have been proposed to control collagen fibril size and shape [14]. Specifically, the GAG "C4-S" is thought to be closely associated with mineralization because it was only extractable from dentin after de-mineralization [13]. The role of PGs on mineral formation is not clear and calls for further investigation. Some *in vitro* experiments that have

PGs immobilized on a solid support demonstrated HA formation at physiological pH [81], while other studies have demonstrated that PGs and PG aggregates inhibit mineral formation *in vitro* [82-85].

1.3.2 Glycoproteins and phosphoproteins – Distribution and function

The major phosphoproteins and glycoproteins of dentin and bone have been recently renamed as the SIBLING (Small Integrin-Binding LIgand N-linked Glycoprotein) family of proteins [69]. They were classified based on common molecular and proteomic characteristics. They are all acidic proteins with a random structure [69], with their genes clustered on the human chromosome 4q21 and mouse chromosome 5q21 [69]. They all contain an arginine-glycine-aspartate (RGD) cell attachment domain [86], and are distinct in their long-range sequence alignments [87].

The SIBLING proteins are not specific to mineralized tissues (except for DSP, which is only found in dentin) [72]. Most SIBLING proteins that were discovered in hard connective tissues are also present in soft tissues (e.g. BSP, DMP1, OPN, MEPE, and DSPP) [69, 72]. However, the function of these proteins may differ in hard and soft connective tissues depending on the type and extent of posttranslational modifications they have undergone [72]. For example, OPN loses its ability to inhibit mineral formation when in its dephosphorylated form [88, 89].

The distribution of non-collagenous proteins (NCPs) in hard and soft connective tissues is indicative of their roles in mineralization. NCPs that have been hypothesized to promote mineral nucleation and/or growth (e.g. BSP, DMP1, and DSPP) are found in greater amounts in mineralized tissues whereas those associated with mineral inhibition (e.g. OPN and MEPE) are found widely in both mineralized and nonmineralized tissues [69].

In mineralized tissues, the distribution of various NCPs during development and in mature tissues is a further indication of the role of each NCPs in mineralization. BSP is localized at the sites of mineralization in osteoids [69], cement-lines and the interfibrillar spaces of mineralized collagen fibrils (in bone and cementum) [90]. The level of BSP was shown to decrease rapidly with age, an indication that it is heavily involved in the mineralization process [69]. DMP1 is another protein heavily involved in the mineralization process. It is expressed in bone during development and remodeling, and is only expressed during development in dentin (since dentin does not remodel) [69].

OPN is localized in the extracellular matrix of endochondral and intramembraneous woven bone [91, 92], the osteoid, and mineralized bone matrix [93]. It is distributed non-uniformly in developing tooth, and is present in the dentin of rats [94]. In the growth plate of developing chick femurs, it is localized ahead of the mineralization front, and is thought to control the size of mineral crystals and the speed of mineralization during the initial mineralization event [95]. ON is a major constituent of developing bone (~15 %) [70], with its maximum amount found in mature lamellar bone [96]. It is found in fully mineralized matrix and is thought to have the role of controlling the size and speed of crystal formation [95]. It is absent in rat dentine, but present in porcine dentine [13].

1.3.3 Gla proteins – Distribution and function

The two major groups of γ-carboxyglutamic acid-containing proteins are bone Gla protein (BGP) and matrix Gla protein (MGP) [70].

Bone Gla protein (BGP) is also known as osteocalcin (OC) or Gla-protein; it constitutes 80% of the gla-protein content [70] and 20 % of the total amount of NCPs found in bone [66, 95]. It is

present in low amounts at early stages of bone formation and increases with age, reaching the maximal levels at maturity [70, 97, 98]. OC is localized in mineralized tissues and is found in young osteoblasts and odontoblasts [91, 99, 100]. *In vivo*, OC deposition in bone and dentin is observed in advance of mineralization [100, 101], and is less concentrated in mineralized matrix near the growth plate [98].

Matrix Gla protein (MGP) makes up approximately 20 % of the total Gla protein content [70]. It is expressed at earlier developmental stages than OC and remains fairly constant with increasing age [98]. It is present in both bone and dentin, but 40-50 times more in bone than other tissues [70, 102]. Its distribution is uniform in the mineralized matrix of the long bone growth plate [98]. It's thought to play a preventive role in mineralization. The growth plate cartilage of MGP knockout mice was found to calcify abnormally; calcification extended to the zone of proliferating chondrocytes which are mineral free in wild-type animals [103]. These mice also developed excessive calcification of the arterial media, and aortic lesions that became lethal within the first eight weeks of the animal's life [104].

1.3.4 *In vivo* investigations

Null mice models have been designed to study the effect of specific NCPs on collagen mineralization. Although these mice models provide excellent insight into what happens *in vivo*, caution must be taken when interpreting results because the missing NCP may be compensated partially or completely by other NCPs or other non-collagenous macromolecules, since many NCPs have overlapping roles in mineralization [69]. In addition, all the NCP involved in the mineralization process also play a role in other aspects of development and tissue repair, so the observed changes in null mice may not be a result of the altered mineralization process, it could well be caused indirectly by altering other aspects of development [69]. Nonetheless, the results

obtained with *in vivo* knockout mice studies provide useful insights into the function of individual NCPs.

BSP, DMP1, OPN, ON and OC knockout mice all showed normal skeletal development (possibly due to the compensating effect of other proteins and/or macromolecules); but hard tissue abnormalities become apparent in adult animals [7, 69, 105-108].

BSP knockout mice had thinner calvarias and cortical bones, smaller bone marrow spaces, and longer maxillary incisors compared to the wild-type [69, 105]. They also had greater trabecular bone volume and very low bone formation rate [69]. Knockout mice lacking DMP1 showed extensive cartilage calcification, enlarged growth plate, increased bone mineral density, and development of short limbs [69, 108]. MEPE deficient mice had increased bone mass due to increased osteoblastic activity and unaltered osteoclastic activity [69]. OPN knockout mice were observed to have higher bone density, mineral content, and larger mineral crystals [107, 109]. Bone remodeling was impaired in ON null mice, which resulted in bone osteopenia, decreased cancellous bone volume, increased mineral to matrix ratio, and increased mineral crystal size [106]. Both growing and mature DSPP knockout mice showed a higher volume fraction of trabecular bone and a lower degree of trabecular separation [86]. OC knockout mice showed an increase in bone formation [106].

These data suggest that each of the above mentioned NCPs plays a critical role in hard tissue formation. BSP is associated with mineral deposition and growth; DMP1, OPN, ON, MEPE and OC control the extent of mineralization and crystal size; and DSPP is hypothesized to regulate bone turnover.

1.3.5 *In vitro* investigations

1.3.5.1 *In vitro* model systems

A number of *in vitro* model systems have been designed to investigate the roles of individual macromolecules in collagen mineralization. They can be divided into five basic categories depending on the collagen substrate.

1. Double diffusion systems: The earliest experimental setup is the double diffusion system that utilizes gelatin or agarose gels as the substrate [73, 85, 88, 110]. The substrate is held in a construct in which solutions containing calcium and phosphate ions are continuously pumped into the gel from opposite ends. Calcium phosphate minerals precipitate near the centre of the gel where the ions come in contact with each other. The function of specific NCPs on mineralization is tested by binding them to the gel substrate and comparing the amount of minerals formed in their presence with the control gel containing no NCPs [88, 111]. NCPs that cause an increase in mineral formation are referred to as “mineral nucleators” and those that cause a decrease or prevent mineral formation are called “mineral inhibitors”. These systems are simple but are less than ideal representations of the *in vivo* environment since both the arrangement and structure of the collagen fibrils and NCPs are different from the native state. In some cases, the substrate is completely different from collagen (e.g. agarose gel).

2. Re-constituted collagen fibrils: Solubilized rat tail tendon is re-constituted and mineralized in a solution containing calcium and phosphate ions [112]. The effect of NCPs on mineralization can be tested by irreversibly binding them to the collagen fibrils; the amount of mineral formed on the fibrils with and without bound NCPs is used as an indicator of the nucleating effect of NCPs on mineralization [60, 67]. Although these

studies utilize collagen fibrils with native banding structures, the fibrils lack the three-dimensional orientation found in native collagen tissues.

3. Synthetic collagen sponges: Similar experimental setup as the re-constituted collagen fibrils [32]. This system provides a three dimensional framework of nearly native collagen fibrils, but its molecular composition is significantly different from that found *in vivo* because it does not contain non-collagenous macromolecules.

4. Turkey tendon: Turkey tendon is cut into smaller dimensions and mineralized *in vitro* with a double diffusion system or by soaking the samples in calcium and phosphate containing solutions [113-115]. Turkey tendon contains a collagen matrix with intact non-collagenous macromolecules, but the composition of these molecules is different from those found in mineralized tissues.

5. De-mineralized bone: Thin slices or small pieces of de-mineralized bone and dentin are re-mineralized *in vitro* in a solution containing calcium and phosphate ions supersaturated with respect to HA [55-57,116]. De-mineralized collagen matrix has been shown to mineralize *in vitro* while the soft connective tissue collagens did not. One study has shown that de-mineralized bone matrix loses its effect of inducing mineral formation when dephosphorylated [68]. This type of model system has the potential to be utilized for investigating the role of non-collagenous macromolecules in collagen mineralization.

1.3.5.2 Hypothesized function of NCPs

The first two categories are the most commonly employed *in vitro* model systems due to the ease of isolating individual NCPs. BSP was shown to be a potent mineral nucleator with a gelatin gel

based double diffusion system; very little or no HA is formed in its absence [73, 88]. MEPE inhibits phosphate uptake and mineralization *in vivo* and *in vitro* and is thought of as a mineral inhibitor [69].

However, when interpreting and comparing results from different experiments, several factors may affect the effect of NCPs on mineralization: 1) the extent of post-translational modifications, 2) whether or not the NCP(s) is bound to the substrate (e.g. collagen fibrils), and 3) the concentration of the NCPs.

The extent of post-translational modifications (e.g. phosphorylation) often changes the potency of a protein at inducing or inhibiting mineral formation. Highly phosphorylated OPN is a potent mineral inhibitor and prevents HA precipitation in double diffusion systems [73, 88, 89, 110, 117, 118]. However, it becomes less effective or not effective at all when in its dephosphorylated state [88, 89, 119]. rDMP1 is a mineral nucleator, but it becomes ineffective at inducing HA formation when dephosphorylated [108].

When working with re-constituted collagen fibrils, NCP(s) are only effective at inducing mineral formation when irreversibly bound to the fibrils. In the absence of a collagen substrate, rDMP1 induces HA nucleation when bound to a smooth glass surface [69, 120, 121]. DPP was a nucleator in the double diffusion system [73]; but when mineralized in the presence of re-constituted collagen fibrils, mineral nucleation only occurred when it was irreversibly bound to the collagen fibrils [122]. OC inhibits mineral nucleation weakly in double diffusion systems [73], but promotes the growth of platelet-like HA crystals when bound to reconstituted collagen fibrils [66].

The concentration of some NCPs can also alter their effect on mineralization. A gelatin gel diffusion system showed that DPP promotes the formation of HA at low concentrations, but

inhibits the growth of HA at higher concentrations [123]. The authors suggest that DPP may inhibit secondary nucleation [123].

The affinity of an NCP for calcium ions, collagen fibrils and HA have also been used to predict their role in mineralization [13]. For instance, the potent nucleator BSP has a high affinity for calcium ions, HA, and type I collagen [69]. ON is hypothesized to act as a mineral nucleator *in vivo* because it binds to collagen fibrils *in vitro* and also has a high affinity for calcium ions and HA [70]. DPP binds strongly to calcium ions, it was found to induce the formation of new nuclei, but inhibits the growth of already formed crystals [123].

1.3.5.3 Mineralization solutions

As mentioned in section 1.3.5.1, a number of *in vitro* mineralization systems involved incubating a collagen substrate in a mineralization solution containing calcium and phosphate ions supersaturated with respect to HA. The simpler solutions contained only calcium and phosphate ions at a similar (or higher) ion concentration as the blood plasma, buffered at pH 7.4 [32, 112, 113, 114]. However, these solutions do not take into account the rest of the ions present in blood serum (e.g. magnesium, carbonate) which are also very important to the process of mineralization.

In the late 1980s, Kokubo and his colleagues came up with a solution that was especially formulated to mimic the ion concentrations of the blood plasma, which later came to be known as simulated body fluid (SBF) [124]. It has been used widely in the biomaterials field for depositing a thin layer of HA onto bioactive implant materials [125, 126, 127]. It also gained widespread use with re-mineralization studies due to its increased stability compared to simple formulations of mineralization solutions that contain only calcium and phosphate ions [116, 128, 129]. Slight modifications were made by each investigator to suit his/her experiment. For

instance, when depositing HA onto de-mineralized fishbone, the concentration of the ions was adjusted to match that of the fish serum fluid [116].

Several additional formulations of SBF have also been studied in hopes of finding a solution that more closely mimics the ion concentration of the blood serum; this is because the original formulation of SBF, conventional SBF (c-SBF), contained elevated levels of chloride ions and decreased levels of carbonate ions [130]. Modified SBF (m-SBF) was found to be the optimum solution because it was more stable compared to revised SBF (r-SBF) and ionized SBF (i-SBF), and had an ion concentration closer to the blood plasma compared to c-SBF (see Table 5 for the ion concentrations of each SBF solution). The thermodynamics and kinetics of calcium phosphate precipitation of these SBF solutions have been studied in detail [34]. Experiments utilizing a range of SBF solution concentrations (e.g. 0.75x, 1.25x, and 1.5x) have found that both the crystallinity and Ca/P molar ratio of the calcium phosphate minerals deposited onto PLGA scaffolds decreased with increasing SBF concentration [128].

	Ion concentration (mM)										
Solution	**Na^+**	**K^+**	**Mg^{2+}**	**Ca^{2+}**	**Cl^-**	**HCO_3^-**	**HPO_4^{2-}**	**SO_4^{2-}**	**Buffer**	**pH**	**Ref**
blood plasma	142.0	5.0	1.5	2.5	103.0	27.0	1.0	0.5	None	7.4	[34]
blood plasma (dissociated)	142.0	5.0	1.0	1.3	103.0	27.0	1.0	0.5	None	7.4	[34]
c-SBF	142.0	5.0	1.5	2.5	147.8	4.2	1.0	0.5	Tris	7.4	[130]
r-SBF	142.0	5.0	1.5	2.5	103.0	27.0	1.0	0.5	HEPES	7.4	[130]
i-SBF	142.0	5.0	1.0	1.6	103.0	27.0	1.0	0.5	HEPES	7.4	[130]
m-SBF	142.0	5.0	1.5	2.5	103.0	10.0	1.0	0.5	HEPES	7.4	[130]
1.5-SBF (fish)	213.0	7.5	2.3	3.8	187.5	40.5	1.5	0.8	Tris	7.4	[116]

Table 5 Ion concentration of various SBF solutions.

1.4 Experimental approach

As presented by the current literature, the role of the individual non-collagenous macromolecules in regulating mineralization is not well understood. A more suitable *in vitro* model system is needed to carry out further investigations, specifically one that closely mimics the physiological conditions in both the collagen substrate and extracellular fluid composition.

This study utilizes a unique *in vitro* experimental approach to investigate the independent roles of collagen and non-collagenous macromolecules in regulating the deposition of calcium phosphate minerals. Paraformaldehyde-fixed murine periodontium tissues containing the three molars intact with the surrounding alveolar bone are utilized as the collagen substrate. The minerals from these tissues are gently extracted from the collagen matrix with ethylene-diamine-tetra-acetic acid (EDTA); very little tissue damage is observed with this de-mineralization method [116]. The tissues were then processed and embedded in paraffin wax, sectioned, and mounted onto microscope slides. The 5 µm thick tissue sections mounted on microscope slides were utilized as the substrate for mineral deposition; they were de-waxed and incubated in a solution containing a supersaturation of calcium and phosphate ions with respect to HA.

Although the basic setup of this *in vitro* model system has been utilized in the literature (e.g. soaking a piece of de-mineralized tissue in a mineralization solution), the proposed model system is different from previous re-mineralization systems in several ways. The tissue sections used for mineralization solutions are much thinner than conventional samples (5 µm compared to ~ 1 mm) [55, 116]; the decreased dimension allows faster ion diffusion and better infiltration of ions and thus more uniform mineral deposition throughout the entire sample. Mounting tissue sections onto microscope slides allows histological staining to be performed directly post re-mineralization; this simplifies the procedures involved in studying the mineral deposits (e.g. it eliminates the need to section mineralized tissues, which is a very difficult task). The tissues utilized for these studies contains both soft and hard connective tissues, this provides an

interesting comparison between the mineral deposition behaviour of the two types of tissues. And lastly, the non-collageneous macromolecules can be easily removed from the collagen matrix with enzymatic digestion due to the simple geometry of the proposed *in vitro* model system.

1.5 Project objectives and hypotheses

1.5.1 Project objectives

The long term objective of this project is to gain a better understanding of the roles of the various macromolecules (e.g. collagenous and non-collagenous components) in regulating the deposition of minerals.

There are two specific objectives to this project:

1. To develop an *in vitro* model system with a defined set of experimental conditions (e.g. ion concentration of the solution, frequency of solution change) that will yield selective calcium phosphate mineral deposition onto de-mineralized tissues.

2. Investigate the role of collagen fibrils by removing the non-collagenous proteins from the collagen matrix with enzymatic digestion and compare the pattern of re-mineralization with that obtained from intact de-mineralized tissues.

1.5.2 Hypotheses

Objective 1:

The ECM of the periodontium tissues contains sufficient information to direct mineral deposition, and the naturally mineralized tissues, bone and cementum, will re-mineralize preferentially over the soft connective tissues (e.g. PDL). A mineralization solution containing a similar concentration of ions as the blood plasma would be optimal at inducing calcium phosphate formation onto the de-mineralized tissue sections. Physical experimental conditions such as stirring and frequent solution change will result in more selective mineral deposition and

an increased amount of mineral formation, respectively. This is due to the increase in ion diffusion and the constant replenishment of ions.

Objective 2:

The collagen fibrils do not regulate mineral deposition spatially, therefore the mineral deposition pattern will be non-selective since the non-collagenous components have been removed (e.g. the soft connective tissues will also re-mineralize).

Chapter 2
Materials and Methods

2 Materials and Methods

2.1 Sample preparation

CD1 strain mice (approximately 3-4 week old males) obtained from Charles River (Montreal, Quebec) were euthanized by cervical dislocation. Their mandibles were dissected fresh and immediately placed in 1x DPBS solution (Dulbecco's phosphate buffered saline, 1x, Sigma-Aldrich) at 4°C. Further dissection was performed under a dissection microscope (Model: SZ61, Olympus) to isolate the three molars intact with the alveolar process and remove adherent soft connective tissues. The "Molar blocks" were fixed immediately in 4% paraformaldehyde (PFA) following dissection for 24 hours at 4°C. The samples were then de-mineralized for 10 days in 12.5 % ethylene-diamine-tetra-acetic acid (EDTA) (Sigma-Aldrich) at 4°C in a fridge on a rotary shaker (Barnstead/Thermolyne, labQuake). The EDTA solution was changed daily and the sample to solution volume was approximately 5 ml/per sample.

Following de-mineralization, the samples were rinsed with PBS for 24 hours at 4°C under the same conditions as de-mineralization. The molar blocks were then immersed in formalin solution, (10 %, neural buffered, Sigma-Aldrich) for 30 minutes and processed for paraffin embedding at the "Special Histology" facility at Mt.Sinai Hospital (Toronto, Ontario, Canada). The samples were then embedded in paraffin wax using with a tissue embedding machine (Tissue Tek II, Tissue embedding center) and a 2x Illuminated stand magnifier (Bausch & Lomb, Opticsplanets.com). The detailed protocols for preparing PFA and EDTA solutions are found in Appendix II (see Protocols 1 & 2, respectively).

The molar blocks were sectioned along the mesial-distal direction into 5 µm thick sections with a microtome (Reichert-Jung 1150 Auto-cut). The sections were floated in a hot water bath (TissuePrep Floatation Bath, Model: 134, Fisher) and mounted onto three types of microscope slides, glass (Fisherbrand Superfrost/Plus, Fisher scientific), polyvinyl chloride (PVC) (Fisherbrand Microscope slides, 2R disposable, Fisher Scientific) and low density polyethylene (LDPE) (McMaster Carr, USA). Note: the LDPE slides were cut into the size of rectangular slides (1"x3") from a polymeric sheet (1'x1'). Three tissue sections were mounted onto each microscope slide in close proximity to each other, opposite the frosted end.

Tissue sections adherent on microscope slides were de-mineralized a second time for 24 hours at room temperature to ensure the thorough removal of minerals. Briefly, de-paraffinized and de-hydrated samples were placed in glass Coplin staining jars (EMS, Hatfield, PA, USA) containing 40 ml of 12.5 % EDTA solution. Two slides were placed in each jar, on opposite sides of the jar, with the tissue sections facing inward. The jars were sealed with Parafilm® M Barrier Film and set on a stir plate (Model: PC-420D, Corning, Thomas Scientific); the solution was stirred with a magnetic stir bar (size ½") at 120 rpm (VWR).

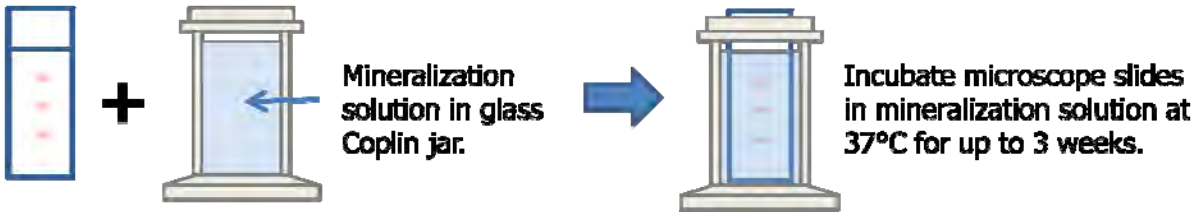

Figure 6 Experimental set-up for re-mineralization and 2nd de-mineralization.

2.2 Re-mineralization experiments

The slides were rinsed thoroughly with Mili-Q water (for 10 min.) and re-mineralized immediately in mineralization solutions. The experimental set up is similar to the second de-mineralization experiments, except that the glass Coplin jars containing the mineralization solutions were placed in an incubator (Model: 1525, General purpose incubator, VWR) in order to maintain a constant temperature of 37°C.

Two types of solutions were used for inducing mineral deposition onto the de-mineralized tissue sections, 1) CaP solution – a solution containing a supersaturation of calcium and phosphate ions with respect to hydroxyapaptite [32] and 2) simulated body fluid (SBF) – containing a similar ion concentration as the blood serum [130].

Four concentrations of each solution were tested. The composition (e.g. ion and buffer concentration) of each solution is shown in Table 6; the ion concentration of blood plasma is also included for comparison purposes. All solutions were prepared in-lab with reagent grade chemicals and ultrapure water (Milipore). Additional experimental conditions tested include constant stirring at 60 rpm with a magnetic stir bar, frequent solution change, and a combination of the two.

Solution	Concentration (mM)									pH
	Na^+	K^+	Mg^{2+}	Ca^{2+}	Cl^-	HCO_3^-	HPO_4^{2-}	SO_4^{2-}	Buffer	
Blood plasma	142.0	5.0	1.5	2.5	103.0	27.0	1.0	0.5	None	7.4
CaP soln. (1)	148.5	4.2	0.0	4.5	199.4	0.0	2.1	0.0	50.0 (Tris)	7.4
CaP soln. (2)	148.5	3.0	0.0	2.5	199.4	0.0	1.5	0.0	50.0 (Tris)	7.4
CaP soln. (3)	86.8	1.8	0.0	1.5	89.8	0.0	0.9	0.0	50.0 (Tris)	7.4
CaP soln. (4)	85.3	1.2	0.0	1.0	88.3	0.0	0.6	0.0	50.0 (Tris)	7.4
1x c-SBF	142.0	5.0	1.5	2.5	147.0	4.2	1.0	0.5	50.0 (Tris)	7.4
1.25x c-SBF	177.5	6.3	1.9	3.1	183.8	5.3	1.3	0.6	62.5 (Tris)	7.2
1.5x c-SBF	220.5	7.5	2.3	3.8	220.5	6.3	1.5	0.8	75.0 (Tris)	7.0
1x m-SBF	138.0	5.0	1.5	2.5	103.0	4.2	1.0	0.5	75.0 (HEPES)	7.4

Table 6 Ion and buffer concentration of the various mineralization solutions.

2.2.1 Preparation of CaP solutions

CaP solution (1) was prepared according to Olszta et al. [32]. Briefly, stock solutions containing 9 mM $CaCl_2$ and 4.2 mM K_2HPO_4 were prepared separately in 0.05 M Tris-saline buffer solution and stored in the fridge at 4°C. Equal amounts of each of the stock solution were mixed together immediately prior to use. The final solution contained 4.5 mM calcium ions and 2.1 mM phosphate ions. The CaP solution (2) was prepared in the same way; the stock solutions were obtained by diluting the original stock solutions with Tris-buffer.

CaP soln. (3) and CaP soln. (4) contained a significantly lower calcium and phosphate ion concentration; these were the highest calcium and phosphate ion concentrations in which the solutions were stable for a minimum of 5 days. The ionic strength of these solutions was adjusted with NaCl to match the ionic strength of the blood plasma.

2.2.2 Preparation of SBF solutions

The procedure for preparing the SBF solutions is adapted from Kokubo and his colleagues [124, 131]. All glassware were soaked in dilute hydrochloric acid for 2-3 hours and rinsed with ultrapure Mili-Q water prior to use. Respective amounts of reagent grade chemicals were added to ultrapure water in a polyethylene (PE) beaker in the order given in Table A4 (see Protocol 3 in Appendix II for details). All the c-SBF solutions were buffered with Tris and the m-SBF solution was buffered with HEPES; the use of different buffers in different SBF solutions allowed the cations and anions in each solution to balance out properly.

Each chemical was added after the previous one had dissolved completely; the Tris buffer was added in small quantities (approx. 0.1 g) at a time in order to prevent precipitate formation in solution. Final pH adjustment was carried out at 37°C. The solution was allowed to cool to room temperature prior to adjusting the volume with a 1000 mL volumetric flask (Chemglass Life Sciences, NJ, USA).

The solution was filtered with a sterile vented filter unit (Sterivex™-GP, VWR) that contains a 0.22 µm polyether sulfone membrane [130]. The solution was sealed immediately after filtering and stored at 4°C for up to 8 weeks. The as-prepared solution contained no visible precipitates; if visible precipitates were observed within 3-4 days of preparation, the solution was discarded and remade.

2.3 Enzymatic removal of non-collagenous macromolecules

The non-collagenous macromolecules bound to the collagen matrix were removed serially with proteolytic enzymes trypsin (Trypsin from porcine pancreas, BioReagent, lyophilized powder, 1047 BAEE units/mg solid, suitable for cell culture, Sigma-Aldrich, Oakville, Ontario, Canada) and papain (papain from papaya latex, buffered aqueous suspension, 2x crystallized, 16-40 units/mg protein, Sigma-Aldrich). Following second de-mineralization, the slides were rinsed with mili-Q water for two washes (5 minutes each).

The slides were then incubated with 40 ml of trypsin solution (1.25 mg/ml) at pH 7.6 in a glass Coplin jar at 37°C for 1 hour. The solution was stirred constantly with a magnetic stir bar at a speed of 60 rpm. Slides were rinsed with 2 washes of mili-Q water (5 minutes each) following trypsin digestion. Papain digestion was carried out for 30 minutes at room temperature in a 5 place-slide mailer (containing 15 ml of solution). The papain solution contained 2.5 mg/ml papain, 0.5 mM EDTA, 5 mM L-cysteine, 0.02 M sodium phosphate, 0.006 M sodium acetate, and 0.0012 % thymol; the pH of the solution was adjusted to 6.5. The slides were rinsed with mili-Q water following papain digestion. See Protocols 4 and 5 in Appendix II for detailed protocols of trypsin and papain digestions, respectively.

2.3.1 Visualization and quantitation of non-collagenous macromolecules

The amount of non-collagenous macromolecules contained in the collagen matrix before and after enzymatic removal was determined macroscopically with Fast Green staining (Fast Green FCF, Sigma-Aldrich). Since the Fast Green dye binds selectively to NCPs at a basic pH, therefore the intensity of staining was an indication of the amount of non-collagenous macromolecules present. The tissue sections mounted on glass microscope slides were stained

with 0.1% Fast Green dye for 6 minutes, dehydrated with graded ethanol and mounted (see Protocol 6 in Appendix II).

Quantitative analysis of the amount of non-collagenous macromolecules remaining in the collagen matrix after enzyme digestion was determined with amino acid analysis. Samples were freeze dried with a lyophilizer (ThermoSavant Modulyo D, Gibson-Air Mechanical Ltd, Toronto, Ontario) and taken to the Advanced Protein Technology Centre (SickKids Hospital, Toronto, Ontario, Canada) for amino acid analysis. The weight percentage of NCPs and collagen fibrils of each sample was calculated (see Appendix I for detailed procedure).

2.4 Mineral characterization

2.4.1 Light microscopy (LM)

Tissue sections adherent on glass slides were stained with Alizarin red and von Kossa methods to visualize the calcium phosphate deposits. Alizarin red detects calcium minerals and the von Kossa stain detects phosphate ions [132, 133]. Once the presence of calcium phosphate mineral was confirmed, Alizarin red was used for subsequent studies due to its high sensitivity and ease of operation. Immediately following the re-mineralization experiments, slides were rinsed in 2 washes of DI water (5 min. each) in order to remove the excess calcium and phosphate ions adsorbed onto the surface of tissue.

For Alizarin red staining, the slides were immersed in 1% Alizarin red S (Sigma-Aldrich) solution for 3.5 minutes. For the von Kossa method, slides were stained for 40 minutes in 5% silver nitrate solution (inside a glass Coplin staining jar) in the presence of direct light (Fiberlite illuminators for microscopy, Model: 180, Dolan-Jenner Industries, USA). See Appendix II, Protocols 7 and 8 for details.

The staining pattern was studied with the light microscope (Olympus BX51, Olympus America Inc.). Images were taken with a digital camera (Olympas, Infinity X, KCL) attached to the microscope using the Infinity Capture software.

2.4.2 Scanning electron microscopy (SEM) imaging

Tissue sections adherent on polyvinylchloride (PVC) and low density polyethylene (LDPE) slides were used for scanning electron microscopy (SEM) imaging. The slides were dried with hexamethyldisilazane (HMDS) (EMS, Hatfield, PA, USA) in order to preserve the tissue structure (see Protocol 9 in Appendix II).

The PVC slides were coated with a layer of carbon using a carbon evaporator (Model: Auto 306, BOC Edwards). A piece of carbon tape was placed around one side of the slide to prevent charge build up. The LDPE slides were left uncoated. High-resolution images were taken with an environmental scanning electron microscope (ESEM, Model: XL-30, Philips) with backscattered electrons (BSE). A beam intensity of 20 kV and spot size 6.0 were used. The variable pressure (VP) mode was used for uncoated samples, and when excessive charge buildup was observed on coated samples.

2.4.3 PMMA (poly (methyl-methacrylate)) embedded positive control sample

A naturally mineralized molar block was embedded in PMMA resin (Osteobed Bone embedding kit, Polysciences, Inc.); it was used as a positive control for both SEM imaging and EDX analysis (see Protocol 10 in Appendix II for detailed embedding procedure).

Half of the sample was cut into 5 µm thick sections with a sledge microtome (Model: PolycutS , Leica) and used for histological staining. The remaining sample block was used for EDX analysis. The surface of the sample was ground flat with a grinder (Model: Knuth-Rotor 2,

Struers) with sand paper grit sizes 80 µm & 120 µm and polished with a variable speed grinder-polisher (Model: Metaserv3000, Buehler) using 1 and 0.5 µm alumina particles at 150 rpm.

2.4.4 Energy-dispersive X-ray (EDX) analysis

Energy-dispersive X-ray (EDX) analysis was performed with an environmental scanning electron microscope (ESEM) (Model: XL-30, Philips) equipped with an X-ray detector. Samples adherent on PVC microscope slides were carbon coated and the analysis was performed in both variable pressure (VP) and High vacuum mode. The high vacuum mode was preferred because it yielded more precise results. A live time of 30 s and beam intensity of 20 kV were used. The dead time was kept in the range of 20-32%. The data was analyzed with the software "EDX control" and calculations were performed with Microsoft Excel. For each tissue, the EDX spectra taken from 3 different areas were averaged; 3-5 EDX spectra were obtained from each area.

When comparing the Ca/P and (Ca+Mg)/P molar ratios from multiple samples, statistical tests were done with Kruskal-Wallis One Way Analysis of Variance (ANOVA) on Ranks, using Dunn's method for pair-wise multiple comparisons at $p < 0.05$ (SigmaStat 10.0, Systat Software Inc., Germany). T-tests were utilized for pair-wise comparisons using Excel (Microsoft Excel); a two-tailed, two-sample unequal variance test was performed, and a confidence interval of 95 % was chosen.

The Ca/P and (Ca+Mg)/P molar ratios were corrected with the de-mineralized sample. The overall % of calcium, phosphorus and magnesium atoms of the de-mineralized sample was subtracted from each sample. The Ca/P molar ratio computed from the subtracted values was divided by the Ca/P molar ratio of the sample (based on the overall % Ca and P). This value was

then multiplied by the Ca/P molar ratio of the sample to give the corrected Ca/P ratio of each sample. This can be summarized with the following formula:

$$\frac{Ca}{P}_{corrected} = \frac{\frac{Ca}{P}overall(subtrated)}{\frac{Ca}{P}overall} \times \frac{Ca}{P}$$

The standard deviation of each value was calculated with error propagation formulas:

When subtracting two values: $u\{t_1 - t_2\} = \sqrt{(t_1)^2 + (t_2)^2}$

When dividing two values: $u\left\{\frac{A}{B}\right\} = \left(\frac{A}{B}\right) \times \sqrt{\left(\frac{u\{A\}}{A}\right)^2 + \left(\frac{u\{B\}}{B}\right)^2}$

Similar calculations were performed for (Ca+Mg)/P molar ratios.

2.4.5 Standard samples for EDX analysis

The software used for EDX analysis automatically corrects the samples with a ZAF standardless correction. In order to verify the validity of this standardless correction done by the software, compound standard corrections on samples that were similar in dimension and composition as the experimental samples were prepared.

For the PMMA embedded positive control sample, calcium pyrophosphate (CPP) ($Ca_2P_2O_7$) powder was embedded in Osteobed resin in the same way as the positive control sample (section 3.4.3). The sample was polished with a variable speed grinder-polisher (Model: Metaserv3000, Buehler) to yield a smooth surface.

For the PVC slides, calcium pyrophosphate ($Ca_2P_2O_7$) powder was suspended in 12% gelatin solution (Type A gelatin, Sigma-Aldrich) at a concentration of 0.2 g/ml. The liquid suspension was poured into a plastic mould and immersed in LN_2; the frozen sample was cut into 1 mm x 0.5 mm pieces and embedded in O.C.T. These samples were sectioned at -10°C with a cryo-microtome; 5 μm thick sections were mounted onto PVC microscope slides.

Chapter 3
Development of the *in vitro* model system

3 Development of the *in vitro* model system

An *in vitro* model system using de-mineralized tissues of the mouse periodontium was developed. Two types of mineralization solutions, CaP solution and simulated body fluid (SBF), were tested at several different concentrations. The effect of experimental conditions such as solution change and stirring on mineral deposition was also studied. The spatial deposition of minerals was studied at the LM level with Alizarin red and von Kossa staining. The arrangement of the mineral crystals was visualized with the SEM and the composition of the minerals was elucidated with EDX analysis.

3.1 Re-mineralization patterns at the LM level

The re-mineralization patterns obtained with each solution were studied at the LM level with histological stains, Alizarin red and von Kossa. Both types of staining methods were utilized in initial re-mineralization experiments to confirm the presence of calcium phosphate minerals; this is because each of these methods is specific for calcium and phosphate ions, respectively. The solution used in the von Kossa method contains silver ions that react with the phosphate groups in calcium phosphate salts and form sliver phosphate compounds that are black in colour [133]. However, the reaction is not specific to calcium phosphate, the silver compounds can also react with other phosphate salts such as sodium phosphate) [133]. The Alizarin red dye molecules bind selectively to calcium ions in the pH range of 4-10; however, it does not bind specifically to calcium phosphate salts and is used to demonstrate the presence of other calcium salts such as calcium carbonate [132, 133]. The binding of calcium ions is more specific at an acidic pH [133]; pH 4 is commonly used for cell culture studies [134]. pH 6.1 was chosen for this study

because it is closer to the physiological pH and would cause less damage to the organic tissue structure.

3.1.1 CaP solutions

CaP soln. (1) and CaP soln. (2) were the first solutions tested, since they were used by a previous study and yielded HA formation on collagen sponges [32]. The initial set of experiments did not include stirring or solution change.

Minerals were observed to deposit preferentially onto the de-mineralized hard tissues (e.g. dentin, cementum, and bone); the soft connective tissues (e.g. PDL) did not mineralize until at a much later time point. This means that the de-mineralized collagen matrix contains sufficient information to direct the spatial deposition of minerals. Figure 7 illustrates the progressive deposition of minerals on samples incubated in CaP soln. (1) after 4 and 14 days. After 4 days, mineral was only seen in dentin (see Figure 7b and Figure 7e). After 14 days, the intensity of staining in dentin had increased significantly when stained with the von Kossa method (compare Figure 7f and Figure 7e). At the same time point, Alizarin red staining shows mineral formation in alveolar bone as well as the cementum (see Figure 7c). No mineral staining was observed in the soft connective tissues in these samples up to 14 days of incubation.

Results from Figure 7 demonstrate that Alizarin red was a more sensitive staining method compared to von Kossa, compare the staining intensity of alveolar bone in Figure 7c and Figure 7f. The difference in sensitivity of the two staining methods could be a result of the sensitivity of the underlying chemical reactions. Another possible explanation for the higher sensitivity of alizarin red could be that there's a higher concentration of calcium ions present in mineralized tissues since the molar ratio of Ca/P is 1.67 in synthetic apatite. Regardless of the reason, Alizarin red was used for the remainder of this study due to its higher sensitivity and ease of use.

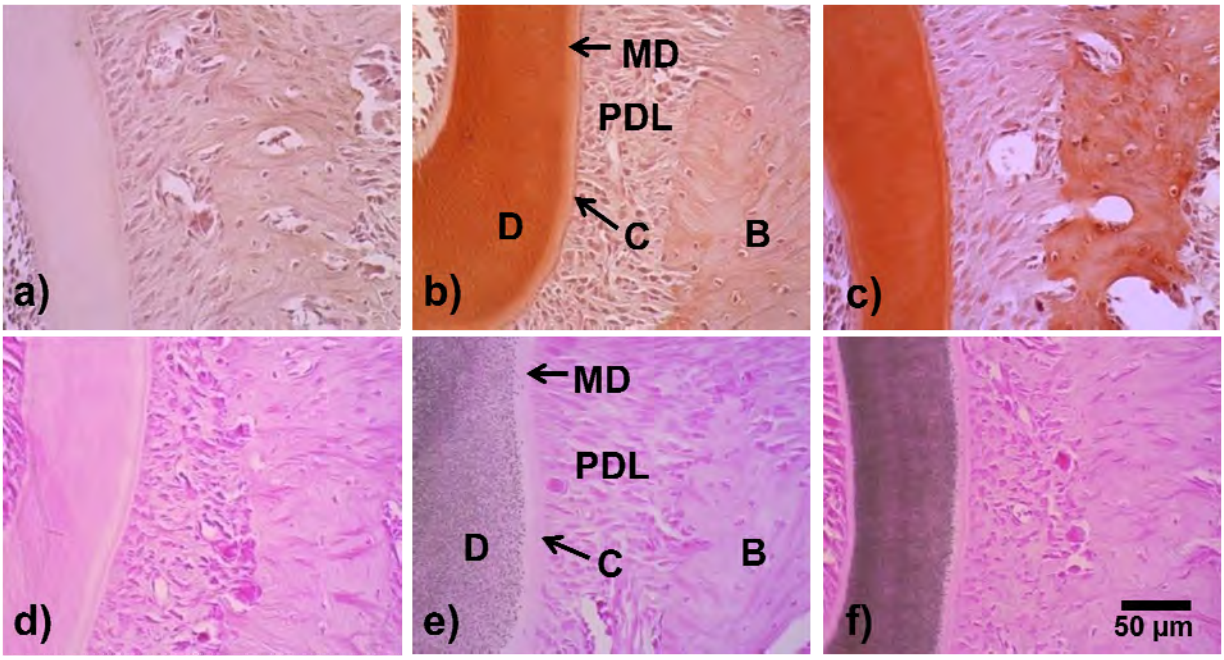

Figure 7 Samples incubated in CaP soln. (1) for 4 days (b, e) and 14 days (c, f); a de-mineralized control sample incubated in Tris buffer was also included for comparison (a, d). Images a)-c) were taken from samples stained with Alizarin red (with no counterstain), images d)-f) were taken from samples stained with von Kossa (counterstained with eosin). D: dentin, C: cementum, B: alveolar bone, PDL: periodontal ligament, MD: mantle dentin.

Different mineralized tissues induced mineral deposition at different rates. Dentin was always the first to re-mineralize, followed by bone, cementum, and mantle dentin. This order of mineral deposition was observed consistently with samples incubated in all mineralization solutions. The different rates of mineral formation in different tissues could be due to the type and amount of non-collagenous macromolecules present in each tissue, as is supported by the literature (see chapter 1 sections 1.3.1.2, and 1.3.2). Another possible cause is the arrangement of collagen fibrils. The collagen fibrils of dentin form well aligned tubular structures with a long range order; it is possible this directional structure makes mineral growth easier. The collagen fibrils of bone form wavy structures in the micron range, this could potentially make directional crystal growth more difficult.

Mineral deposition occurred at a much slower rate on samples incubated in CaP soln. (2) compared to CaP soln. (1). Dentin was stained with a light intensity even after 14 days of incubation (data not shown). This significant decrease in the amount of minerals formed on tissues incubated with this solution is due to its lowered calcium and phosphate ion concentration; it contained half the ion concentration as the CaP soln. (1).

It may be argued that the de-mineralized collagen of hard connective tissues were able to induce mineral deposition preferentially over the soft connective tissues because there were residual mineral nuclei left after the de-mineralization process. Preliminary experiments did show mineral staining in certain localized areas of dentin after the first de-mineralization process. In order to ensure complete removal of these residual mineral nuclei, a second de-mineralization was incorporated after sectioning of the tissues. Tissue sections mounted onto microscope slides were incubated in EDTA solution in a glass Coplin jar for 24 hours with constant stirring (at 120 rpm). This second de-mineralization step has been confirmed to remove all the mineral nuclei at the light microscopy level (see negative control samples in Figure 7a & Figure 7d).

One major drawback of these two solutions was homogenous precipitation. Precipitates always formed within a few hours of mixing the two stock solutions. And as the amount of precipitates formed in solution increased over time, the concentration of calcium and phosphate ions in solution decreased in proportion which resulted in less mineral formation on the tissue sections.

The homogenous precipitates also posed a problem when the solutions were stirred. The precipitates formed in solution could land on the tissue sections and act as crystal nuclei for subsequent mineral growth; this would obscure the effects of the organic matrix on mineral formation. Figure 8 shows the mineralization of samples incubated in CaP soln. (1) for 7 days with constant stirring. It is visible in the LM image that there are crystal nuclei deposited onto the PDL and the selectivity of mineral deposition is poor (Figure 8a); the SEM image shows loosely adherent particles in the dentin, alveolar bone, and PDL (Figure 8b).

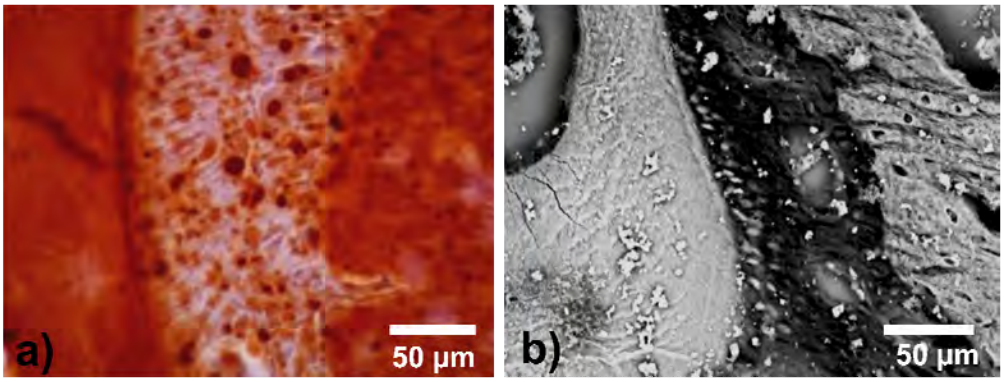

Figure 8 a) Samples incubated in the CaP soln. (1) for 7 days with constant stirring, stained with Alizarin red; b) SEM image taken with backscattered electrons.

In order to solve the problem of homogeneous precipitation, experiments were conducted to test the stability of solutions containing calcium and phosphate ions over a range of concentrations. The goal was to find a solution(s) with a relatively high calcium and phosphate ion concentration that would remain stable for a period of several days. The calcium ion concentrations tested were 3, 2.5, 2, 1.5, 1, and 0.5 mM; each solution contained a corresponding phosphate ion concentration in the molar ratio of Ca/P = 1.67. The three solutions with the highest ion concentration formed precipitates within the first day of the experiment. The remaining three solutions were stable for up to 7 days. The solutions containing calcium ion concentration of 1.5 and 1 mM were chosen for further re-mineralization studies, they were re-named as CaP soln. (3) and CaP soln. (4), respectively.

Staining results from sampled incubated in CaP soln. (3) and CaP soln. (4) for 7 and 14 days are shown in Figure 9. After 7 days of incubation in CaP soln. (3), dentin was intensely stained, bone was lightly stained, and mantle dentin was stained with a medium intensity; there was no staining in the PDL (Figure 9a). After incubation for 14 days in the same solution, all the hard tissues (alveolar bone, cementum, and dentin) were intensely stained; mineral staining was also seen on the cells in the PDL (Figure 9b).

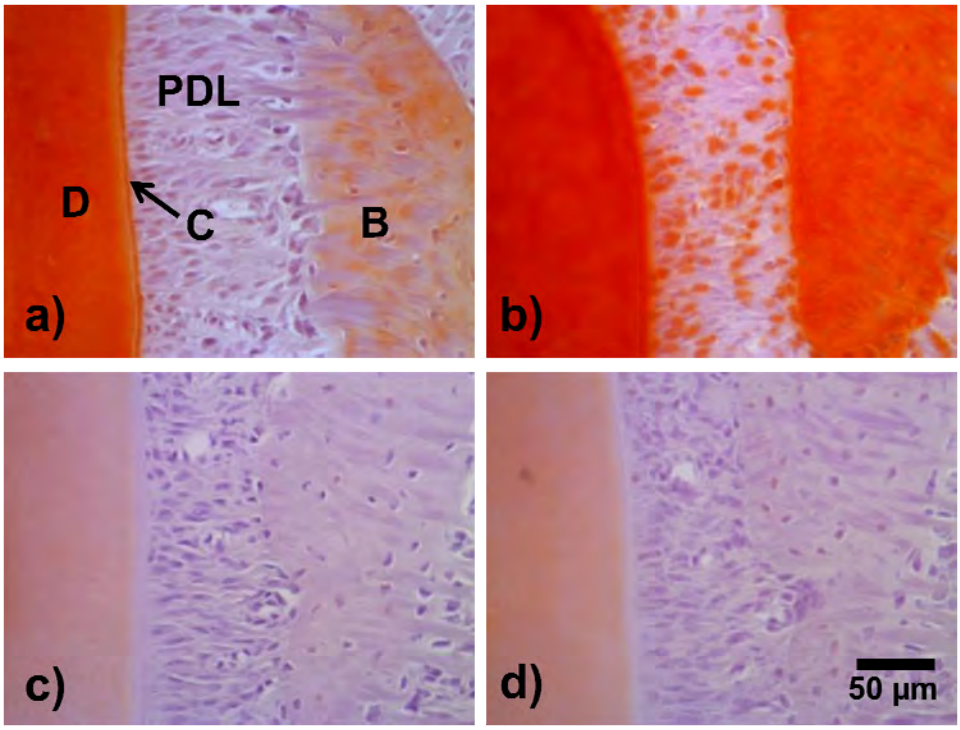

Figure 9 Samples incubated in the CaP soln. (3) (a & b) and CaP soln. (4) (c & d) for 7 (a & c) and 14 (b & d) days. All the solutions were changed every 7 days. D: dentin, C: cementum, B: alveolar bone, PDL: periodontal ligament.

CaP soln. (3) induced mineral deposition at a similar (or faster) rate compared to CaP soln. (1) even though it contained a much lower concentration of calcium and phosphate ions (compare Figure 7f and Figure 9b). This is due to the fact that CaP soln. (3) is much more stable compared to CaP soln. (1). Although CaP soln. (1) had a much higher concentration of calcium and phosphate ions initially, precipitates formed upon mixing of the two stock solutions and the concentration of calcium and phosphate ions in solution decreased overtime as the amount of precipitates increased over time, it may have reached a level lower than that found in CaP soln. (3) within a few days (or even hours) after the start of the experiment. On the other hand, all the calcium phosphate ions that precipitated from the CaP soln. (3) deposited onto the tissue sections and more minerals were formed on these samples as a result. These solutions were changed every 7 days in order to prevent homogenous precipitation.

Samples incubated in the CaP soln. (4) only showed staining in the dentin with a light intensity, even up to 14 days of incubation. Much less mineral was formed in these samples compared to those incubated in CaP soln. (3) (Figure 9b and 9d). This is a result of the lower supersaturation level of calcium and phosphate ions with respect to HA. Even though according to thermodynamics, the concentration of calcium and phosphate ions in this solution is 100 times above the superstaturation limit of HA (Ca: 3.7e-7 mM and PO_4: 2.3e-7 mM), the kinetics of mineral formation might take much longer compared to a solution containing a slightly higher calcium phosphate concentration (e.g. CaP soln. (3)). The difference in ion concentration of these two solutions might be sufficient to cause a drastic change in the kinetics in mineral deposition.

Staining was seen in the cells of the PDL after 14 days of incubation in CaP soln. (3). Soft tissue mineralization was also observed with other mineralization solutions such as 1x m-SBF (see Figure 12a in section 3.1.2.3) over an incubation time after which the hard connective tissues are stained intensely. The reason why the cells of soft connective tissues mineralize prior to the collagen fibrils could be due to the presence of phosphoproteins, which have been shown to induce the formation of calcium and phosphate minerals *in vitro*. More interestingly, calcium phosphate minerals deposited on the glass slides if incubated in the CaP soln. (1) for longer than 14 days under the stirred condition.

3.1.2 SBF solutions

3.1.2.1 Rate of mineral deposition in different SBF solutions

SBF solutions were tested because they contained a similar ion concentration as the blood plasma (see Table 6 in Materials and Methods section). SBF solutions were also expected to

form mineral crystals that are closer to HA in structure because these solutions have been reported in the literature to yield HA formation on the surface of bioactive materials [125, 126]. Two formulations of SBF solutions, c-SBF and m-SBF were tested (see Table 6 for the ion concentration of each solution). C-SBF was tested at three concentrations, 1x, 1.25x, and 1.5x.

Several experimental conditions such as constant stirring, solution change, and a combination of the two, were tested on the various SBF solutions. The incubation period used for each solution was based on preliminary experiments that determined the time frame in which a significant amount of mineral would be formed on the mineralized tissues, prior to the mineralization of soft tissues. The amount of minerals formed on samples was characterized with Alizarin red staining; a summary of the staining intensity of dentin, cementum, bone, and PDL tissues is shown in Appendix III (Table A6).

The rate of mineral deposition in different tissues was the same as the CaP solutions. Dentin was the first to mineralize, followed by bone and cementum. The PDL did not mineralize until intense staining was observed in the hard tissues.

Under similar experimental conditions, samples incubated in 1x m-SBF had the fastest rate of mineral formation, followed by 1.5x and 1.25x c-SBF (with similar rates of mineral formation), and 1x c-SBF was the slowest (see Table A6 in Appendix III). It was expected that solutions with a higher calcium and phosphate ion concentration would yield faster mineral formation due to a higher degree of ion supersaturation; this is observed with c-SBF solutions. The fact that 1.25x and 1.5x c-SBF solutions yielded similar rates of mineral formation is a result of the change in solution pH. The pH of 1.25x and 1.5x c-SBF solutions were decreased to 7.2 and 7.0, respectively, in order to keep the solutions stable and prevent precipitate formation during preparation [128]. And since the solubility of HA increases with decreasing pH, the actual supersaturation level of calcium and phosphate ions with respect to HA in the 1.25x and 1.5x c-SBF solutions could no longer be determined by ion concentration alone. It is conceivable that

the 1.25x c-SBF solution had a similar (or even higher) degree of supersaturation than the 1.5x c-SBF solution. Therefore, mineral formation on samples incubated in the two solutions occurred at similar rate.

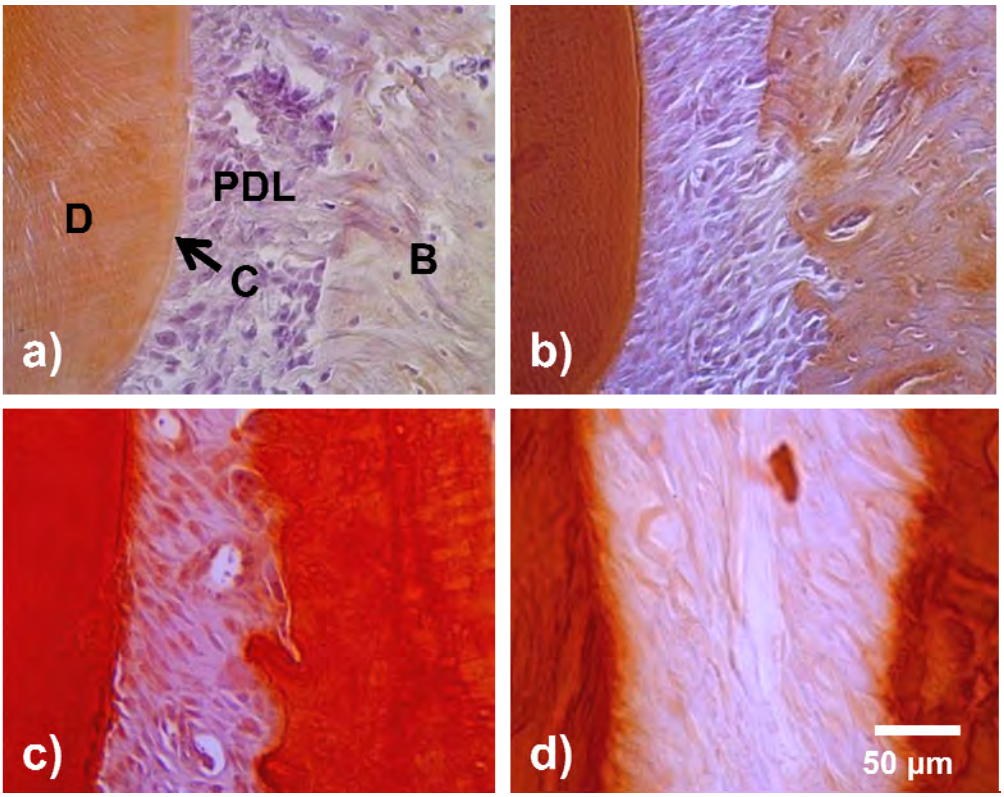

Figure 10 Samples incubated in 1x c-SBF (a) and 1.5x c-SBF (b) for 14 days, and in 1x m-SBF (c) for 3 days. All the samples were stirred constantly and the solutions were replaced every 3 days. The positive control sample (d) was embedded in Osteo-bed resin. D: dentin, C: cementum, B: alveolar bone, PDL: periodontal ligament.

Figure 10 shows a visual comparison of the staining intensity of samples incubated in the 1x and 1.5x c-SBF, and 1x m-SBF solutions. After 14 days of incubation, 1x c-SBF only showed light staining in dentin (Figure 10a), whereas the 1.5x c-SBF showed intense staining in dentin and light staining in bone (Figure 10b). Samples incubated in the 1x m-SBF solution for 3 days had a much greater amount of mineral deposition compared to all the c-SBF solutions; intense staining was observed in bone and dentin, and light staining was seen in the PDL (Figure 10c). The positive control samples (embedded in Osteo-Bed resin) had a similar staining intensity as the 1x m-SBF solution (Figure 10d). However, the tissue morphology of this sample is slightly

different from the ones embedded in paraffin and the cell nuclei of this sample are not as visible; these differences are a result of the different embedding methods.

The surprising result that 1x m-SBF induced mineral formation at a much faster rate compared to all the c-SBF solutions (especially 1.25x and 1.5x c-SBF which contained significantly higher concentrations of ions) could be explained by the different ionic activity products (IP) of these solutions [130]. 1x c-SBF has a lower IP compared to 1x m-SBF because it contained a much higher concentration of Cl^- ions; the increased concentration of Cl^- ions resulted in a lower activity coefficient of the solution which translates into a lower IP according to the formula presented by Oyane et al. [130]. The negative logarithm of IP of 1x c-SBF and 1x m-SBF calculated by Oyane et al. are shown in Table 7; these calculations involve a complex set of formulas that tried to account for various experimental conditions. For the purposes of this study, simple calculations were performed with "Visual MINTEQ" (a free equilibrium speciation model developed by the Department of Land and Water Resources Engineering at Kungliga Tekniska högskolan (KTH)) in order to draw a comparison between the IP of different SBF solutions; the calculated values are shown in Table 7. These calculations agree with the experimental observations of this study and confirm that 1x m-SBF is actually at a higher degree of supersaturation with respect to HA compared to 1x c-SBF, 1.25x c-SBF and 1.5x c-SBF.

Solution	**1x c-SBF [130]**	**1x m-SBF [130]**	**1x c-SBF**	**1.25x c-SBF**	**1.5x c-SBF**	**1x m-SBF**
-log (IP)	94.3	94.1	34.6	35.0	35.5	34.4

Table 7 Negative logarithms of Ionic Activity Products (IP) of the various c-SBF and m-SBF solutions with respect to HA, obtained from Oyane et al. [130] and from this study. All the solutions are supersaturated with respect to HA.

The c-SBF solutions were stable for a period of up to 2 weeks while the m-SBF solutions were only stable for up to a week. As a result, the c-SBF solutions did not need to be replaced for up to 2 weeks, but it was necessary to replace m-SBF solutions at least every week. Solution change at 3 day intervals was implemented in order to standardize the experiments and make straightforward comparisons between the different solutions.

3.1.2.2 Mineral morphology

SEM was utilized as a means to study the morphology of the minerals formed within the tissue sections due to its higher resolution compared to LM. Samples incubated in 1.5x c-SBF solution for 2 and 10 days are shown in Figure 11. The difference in intensity between the mineralized and non-mineralized tissues increased significantly from 2 days to 10 days. The PDL collagen fibrils that insert into the bone can be seen clearly at 2 days but are replaced by a defined layer of mineral deposits after 10 days of incubation. The cells of the PDL are also more visible after 10 days of incubation, demonstrating a small amount of minerals formed in them.

Figure 11c shows a close-up of the mineral morphology of the samples incubated in 1.5x c-SBF for 2 days. The mineral deposits have a sheet-like morphology arranged along the direction of the dentinal tubules. These crystals are much larger than those found in naturally mineralized dentin tissues (compare with Figure 11d). This means that the minerals formed with the proposed *in vitro* model system did not have the same morphology as the ones found in natural tissues; one possible explanation could be the difference between *in vitro* and *in vivo* extra-cellular environments.

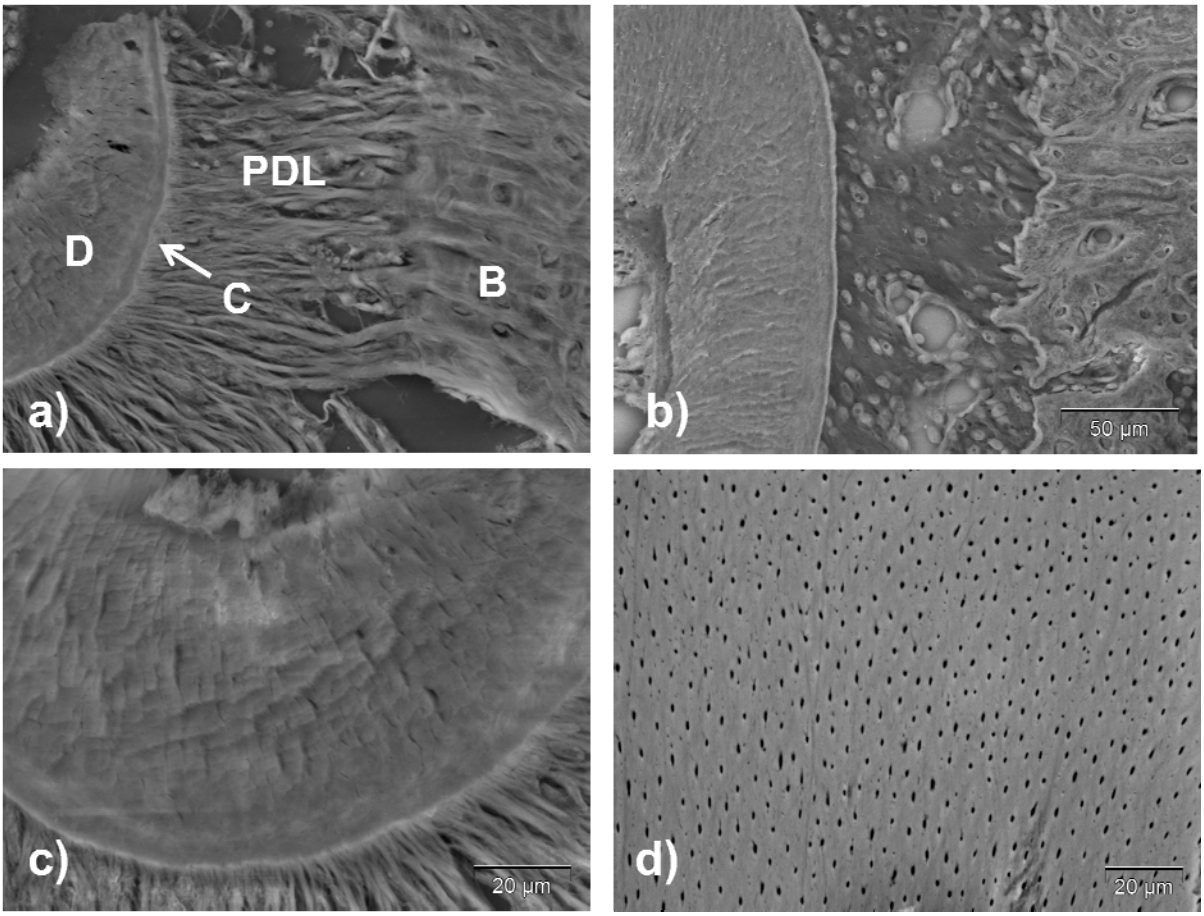

Figure 11 SEM images of samples incubated in 1.5x c-SBF solution for 2 (a) and 10 (b) days, with constant stirring; scale bar = 50 µm. Magnified view of the dentin from samples incubated in 1.5x c-SBF solution for 2 days (c). Dentin of the positive controls sample (d). All images were taken with BSE. D: dentin, C: cementum, B: alveolar bone, PDL: periodontal ligament.

3.1.2.3 Effect of stirring and solution change

Constant stirring of the solution and solution change were tested because they have been shown to increase the total amount of minerals formed on samples [135]. In this study, gentle stirring was carried out at a speed of 60 rpm and frequent solution change was implemented every three days.

Constant stirring increased the overall amount of minerals formed in samples incubated in all SBF solutions (see Table A6 in Appendix III). Figure 12 shows the effect of stirring on 1x m-SBF solution after 7 days of incubation. The amount of mineral formed on the stirred sample was substantially greater than the non-stirred sample (compared Figure 12a and Figure 12b); note the mineral staining in the PDL under the stirred condition. This significant increase in the amount of minerals formed under stirred conditions could be due to an increase in the local diffusion of ions. It is possible that crystal growth on already formed nuclei occur at a much faster rate.

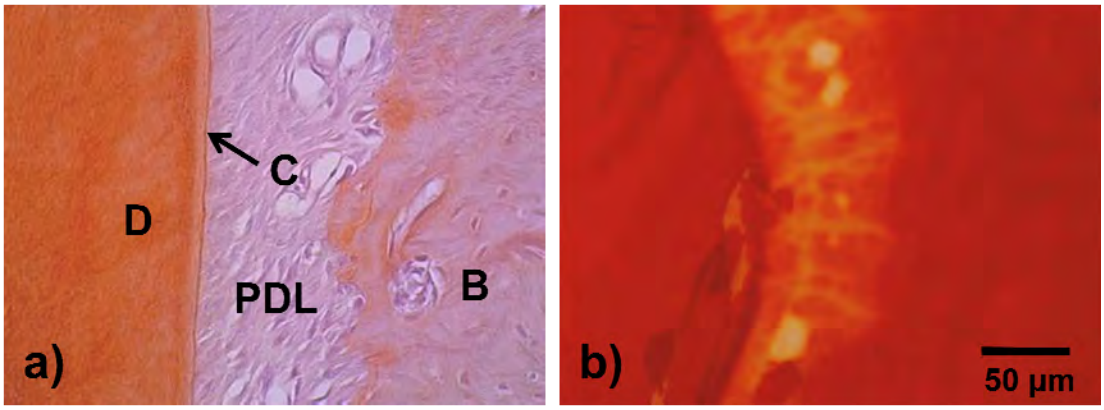

Figure 12 Samples incubated in the 1x m-SBF solution for 7 days, a) no stirring b) constant stirring at 60 rpm. Solution was replaced every 3 days for both samples. D: dentin, C: cementum, PDL: periodontal ligament, and B: bone.

Solution change at every 3 days had no significant effect on the overall amount of minerals formed (see Table A6 in Appendix III). This result is counter intuitive because the replenishment of ions should increase the amount of minerals formed [135]. One possible explanation could be that the nucleation of calcium phosphate crystals requires a certain amount of time, a period in which the calcium and phosphate ions diffuse to the site of mineral deposition, and solution change that takes place at short intervals could disrupt this process by changing the ion concentration of the bulk solution.

3.1.3 Summary: mineralization solutions

Two types of solutions were utilized for re-mineralization studies, CaP solutions and SBF. Preferential mineral deposition was observed with all mineralization solutions. The collagen of de-mineralized hard tissues mineralized preferentially over the soft connective tissues; this is an indication that the de-mineralized collagen matrix contains sufficient information to determine the spatial deposition of minerals.

The CaP solutions were not suitable for the *in vitro* models system because CaP soln. (1) and CaP soln. (2) produced homogenous precipitation which could act as potential sites of mineral nucleation on the tissue sections, and CaP soln. (3) and (4) did not result in sufficient mineral formation in order to yield precise EDX analysis. The SBF solutions were preferred over the CaP solution because they induced mineral formation at a much faster rate and did not result in homogenous precipitation. The minerals formed with these solutions were investigated with EDX analysis.

3.2 Mineral characterization with Energy Dispersive X-Ray (EDX) analysis

Energy dispersive X-ray analysis is often utilized for quantifying the amount and type of atoms present in solid samples. Since the different phases of calcium phosphate minerals (e.g. HA, OCP, HDCP) contain different calcium to phosphate (Ca/P) molar ratios, EDX can be utilized to determine the mineral phase present in each tissue. The Ca/P molar ratio of some of the common biological calcium phosphate minerals are shown in Table 1 (section 1.2.3); a list of the Ca/P molar ratio of all the calcium phosphate minerals can be found in Table A1 (see Appendix I). In some cases, the (Ca+Mg)/P molar ratio was computed because HA is known to contain a small amount of magnesium substitutions [3, 28].

3.2.1 Standard samples for EDX analysis

Standard samples are often utilized for EDX analysis to correct for factors such as X-ray absorption, fluorescence, and the atomic number effect [136]. The software utilized for this study, "EDX control", is capable of correcting for these factors automatically using internal standards. It also gives users the option of performing manual compound standard ZAF corrections. In order to check the accuracy of the internal "standardless" corrections, several compound standard ZAF corrections were performed.

Two types of standard samples were utilized for this study, one for the positive control sample embedded in Osteo-Bed rein and one for the tissue sections mounted on PVC microscope slides; each standard sample matched the experimental samples closely in dimension and composition [136]. Calcium pyrophosphate (CPP – $C_2O_2P_7$) powder was utilized as the standard compound

because the compound standard must not contain any atoms that are below the detection limit of EDX; HA contains hydrogen atoms that cannot be detected by the EDX detector.

The Ca/P molar ratios obtained from both of the standard samples were very close to the theoretical value of 1 (see Table 8), this means that the standardless correction performed automatically by the software was reasonably accurate and manual ZAF compound correction is not necessary.

Standard sample	**Ca/P molar ratio**	**N**
Embedded in Osteo-Bed (for positive control sample)	0.995 ± 0.020	15
Embedded in 12 % gelatin (for PVC slides)	1.043 ± 0.043	8

Table 8 Ca/P molar ratio obtained with standard samples.

3.2.2 The positive control sample

A non de-mineralized sample embedded in Osteo-Bed was utilized as the positive control. The Ca/P and (Ca+Mg)/P molar ratios were obtained for each mineralized tissues separately because there was some variation between the different tissues. The overall amount of calcium and phosphorus atoms (referred to as “overall % Ca” and “overall % P”) of each sample was also obtained; this value is the total amount of Ca or P atoms present in the entire sample, including the tissue itself, the carbon coating, and the substrate. This percentage was used as a standard of comparison for the total amount of mineral deposition in each tissue. A more accurate Ca/P and (Ca+Mg)/P molar ratio was obtained that contained only these atoms; these values are presented as the Ca/P and (Ca+Mg)/P molar ratios. Table 9 shows the Ca/P and Ca+Mg/P molar ratios of the positive control sample.

Tissue	Ca/P molar ratio	(Ca+Mg)/P molar ratio	N	Overall % Ca	Overall % P
Dentin	1.32 ± 0.01	1.36 ± 0.01	9	8.1 ± 0.1	6.4 ± 0.2
Bone	1.32 ± 0.02	1.38 ± 0.02	9	6.7 ± 0.5	5.4 ± 0.5
cementum	1.24 ± 0.06	1.29 ± 0.06	5	3.1 ± 0.9	2.6 ± 0.6

Table 9 The Ca/P and (Ca+Mg)/P molar ratios of dentin, bone and cementum obtained from the positive control sample (embedded in Osteo-Bed polymeric resin).

The average Ca/P molar ratios of dentin and bone obtained with the positive control sample were significantly lower compared to synthetic HA (1.67), but were close to that of OCP (1.33). The difference in molar ratio between biological HA and synthetic HA could be explained by the large amount of ionic substitutions present in biological HA [3]; both carbonate and magnesium substitutions may be present [3].

The Ca/P molar ratios obtained from this study match that of the chick bone and growing rat tibial diaphyses, which is between 1.35-1.39 [41, 42]. However, these values were much lower compared to human dentin (1.54) and cementum (1.64) tissues [137, 138]. These data suggest that there is a compositional difference between the HA crystals of different animal species (e.g. human vs. mice). Another explanation of the low Ca/P molar ratios obtained in this study could be due to the large amount of phosphorus present in the DNA of cells and the phosphorylated proteins bound to the collagen matrix.

The (Ca+Mg)/P molar ratios did not differ significantly from the Ca/P molar ratios. This could mean that a small amount of Mg substitution is present in naturally mineralized tissues.

3.2.3 Characterization of the mineral phase with EDX analysis

EDX analysis was performed on samples incubated in both types of solutions, CaP solutions and SBF solutions. The results for CaP solutions are not presented here because these solutions were unsuitable for the *in vitro* model system. CaP soln. (1) and (2) resulted in homogenous precipitation and CaP soln. (3) and (4) yielded a small amount of minerals on the tissue sections that could not be accurately analyzed with EDX. A minimum of 0.1 % overall calcium atomic concentration is needed to provide precise analysis, the CaP soln. (3) yielded values equal to or less than that value. SBF solutions yielded a considerably greater amount of minerals compared to CaP solutions, they were therefore investigated further.

Glass microscope slides were unsuitable for EDX analysis because the P peak appeared as a shoulder of the Si peak in EDX plots and made quantitation inaccurate. PVC microscope slides were utilized for EDX analysis because none of the peaks from this material interfered with the calcium or phosphorus peaks. The samples were coated with a thin layer of carbon and EDX spectra were collected in high vacuum mode (HV); the HV setting gave more accurate results compared to the variable pressure (VP) mode.

The experimental conditions for each SBF solution were chosen based on the criteria for producing the maximum amount of minerals while maintaining selectivity. All the conditions that were prescreened can be found in Appendix III (Table A6). The Ca/P and (Ca + Mg)/P molar ratios, as well as the total amount of mineral deposited on each sample incubated in the various SBF solutions are presented in Table 11.

The amount of minerals formed in each tissue correlates well with Alizarin red staining; compare the overall % Ca and P of each tissue with the staining intensity of each sample presented in Table A6 (Appendix III). The more intensely stained tissues such as dentin and cementum

contain a greater amount of overall % Ca and P, whereas the lightly stained tissue bone contained a significantly lower amount of overall % Ca and P. Tissues that yielded less than 0.1 % of the total amount of calcium (overall % calcium) did not yield precise data for EDX analysis and were not included in the analysis (e.g. the bone tissue of samples incubated in 1x SBF – stirring + solution change).

Tissue	Ca/P ratio	(Ca+Mg)/P ratio	Overall % Ca	Overall % P
1x m-SBF - soln change (7 d)				
Dentin	1.1 ± 0.2	1.3 ± 0.1	0.5 ± 0.2	0.5 ± 0.1
Bone	0.91 ± 0.06	1.26 ± 0.05	0.17 ± 0.04	0.175 ± 0.007
Cementum	0.96 ± 0.08	1.3 ± 0.1	0.34 ± 0.06	0.36 ± 0.05
1x m-SBF - stirring + soln change (7 d)				
Dentin	0.94 ± 0.03	1.21 ± 0.03	1.04 ± 0.04	1.125 ± 0.007
Bone	1.01 ± 0.03	1.34 ± 0.05	0.5 ± 0.1	0.50± 0.08
Cementum	0.91 ± 0.04	1.18 ± 0.04	1.4 ± 0.2	1.7 ± 0.3
1x c-SBF - stirring (21 d)				
Dentin	0.90 ± 0.06	1.1 ± 0.1	0.25 ± 0.05	0.30 ± 0.04
Bone	0.85 ± 0.08	1.2 ± 0.1	0.10 ± 0.02	0.12 ± 0.02
Cementum	1.01 ± 0.09	1.23 ± 0.09	0.4 ± 0.2	0.4 ± 0.2
1x c-SBF- stirring + soln change (21 d)				
dentin	0.83 ± 0.03	1.10 ± 0.04	0.19 ± 0.01	0.22 ± 0.01
bone	N/A	N/A	0.037 ± 0.006	0.05 ± 0.01
cementum	0.90 ± 0.07	1.3 ± 0.1	0.16 ± 0.01	0.17 ± 0.01
1.25x c-SBF - stirring (10 d)				
Dentin	0.90 ± 0.04	1.18 ± 0.05	0.44 ± 0.04	0.48 ± 0.07
Bone	0.89 ± 0.05	1.44 ± 0.06	0.098 ± 0.006	0.095 ± 0.006

cementum	0.87 ± 0.04	1.23 ± 0.04	0.5 ± 0.1	0.6 ± 0.1
1.25x c-SBF - stirring + soln change (21 d)				
dentin	0.86 ± 0.05	1.19 ± 0.09	0.20 ± 0.09	0.22 ± 0.10
bone	N/A	N/A	0.035 ± 0.007	0.035 ± 0.007
cementum	0.89 ± 0.07	1.3 ± 0.2	0.19 ± 0.02	0.18 ± 0.01
1.5x c-SBF - stirring (14 d)				
dentin	0.84 ± 0.10	1.10 ± 0.07	0.22 ± 0.05	0.24 ± 0.06
bone	1.0 ± 0.3	1.6 ± 0.4	0.30 ± 0.43	0.08 ± 0.03
cementum	1.0 ± 0.2	1.2 ± 0.2	0.23 ± 0.02	0.25 ± 0.02
1.5x c-SBF - stirring + soln change (14 d)				
Dentin	0.88 ± 0.06	1.12 ± 0.08	0.27 ± 0.03	0.29 ± 0.03
Bone	N/A	N/A	0.050	0.050
Cementum	0.81 ± 0.03	1.245	0.120	0.150

Table 10 The Ca/P and (Ca+Mg)/P molar ratio of the minerals formed with various SBF solutions. The overall atomic % of each type of atoms found in each sample is also included in the table. Solution change was carried out every 3 days. The solutions were stirred at a speed of 60 rpm.

The statistical significance of the Ca/P and (Ca+Mg)/P molar ratios of samples incubated in different solutions were computed with ANOVA, using Dunn's method for pair-wise multiple comparisons with $p < 0.05$ (see Figures 13-15).

Both of the Ca/P and (Ca+Mg)/P molar ratios were more statistically different in the dentin tissues compared to cementum and bone. This is due to the greater amount of precipitates formed in this tissue; dentin generally yielded a smaller standard deviation compared to the other two mineralized tissues (see Table 10). It can be inferred from these data that solutions which

yield a greater amount of mineral deposition are more suitable for the *in vitro* model system because they yield more precise data.

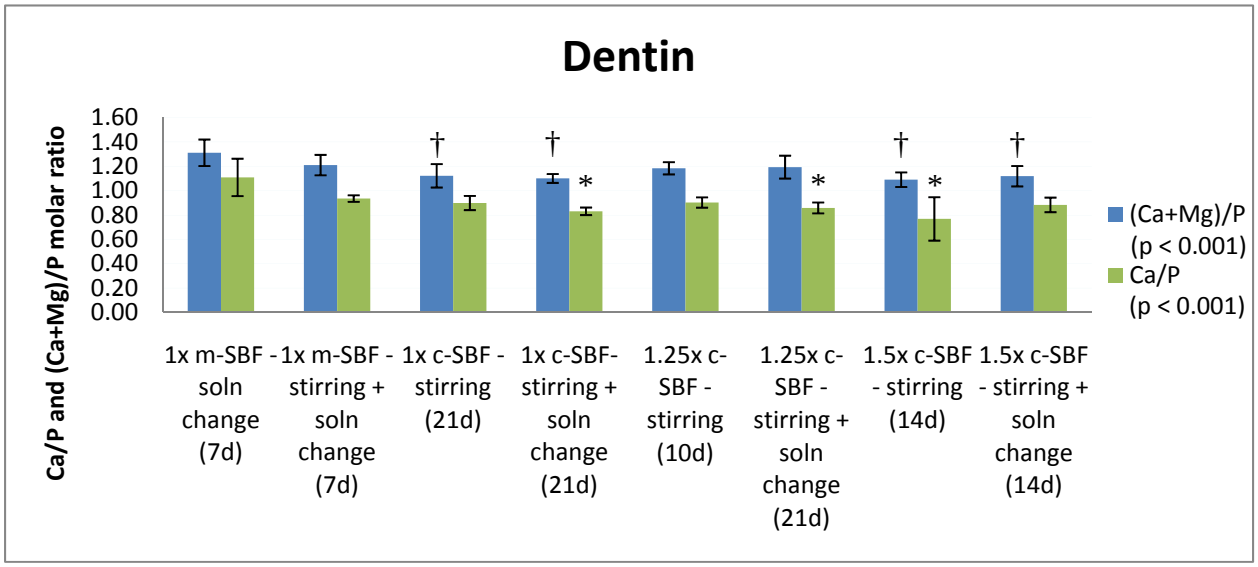

Figure 13 The Ca/P and (Ca+Mg)/P molar ratios of the dentin tissue of samples incubated in various SBF solutions. * p < 0.05 as compared with Ca/P molar ratio of 1x m-SBF – soln. change (7d); † p < 0.05 as compared with (Ca+Mg)/P molar ratio of 1x m-SBF – soln. change (7d).

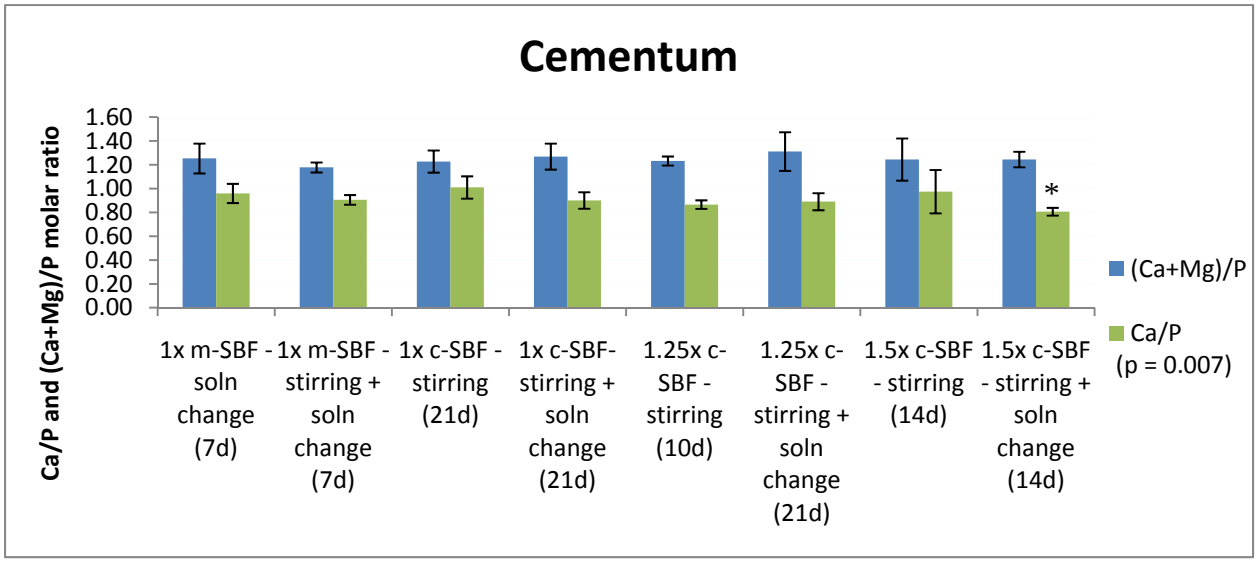

Figure 14 The Ca/P and (Ca+Mg)/P molar ratios of the cementum tissue of samples incubated in various SBF solutions. * p < 0.05 as compared with Ca/P molar ratio of 1x c-SBF – stirring (21 d).

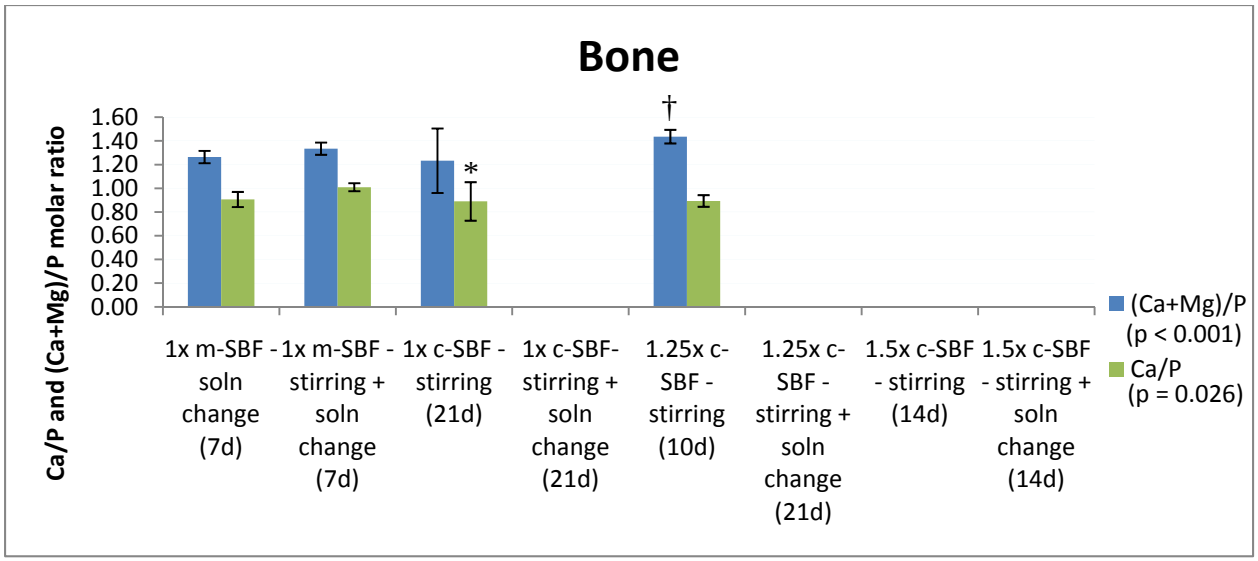

Figure 15 The Ca/P and Ca+Mg/P molar ratios of the bone tissue of samples incubated in various SBF solutions. * p < 0.05 as compared with Ca/P molar ratio of 1x m-SBF – stirring + soln. change (7d); † p <0.05 as compared with (Ca+Mg)/P molar ratio of 1x c-SBF – stirring (21d).

For the dentin tissue, the (Ca+Mg)/P molar ratio of samples incubated in 1x m-SBF (with solution change) was statistically different from 1x and 1.5x c-SBF solution (with both conditions). The Ca/P molar ratio of samples incubated in the same 1x m-SBF solution was statistically different from 1x c-SBF (with stirring and solution change), 1.25x c-SBF (with stirring and solution change), and 1.5x c-SBF (with stirring). The p values of these statistical tests were less than 0.001. The rest of the comparisons within the dentin tissue were not statistically significant. This means that the 1x-m SBF solution (with solution change) yielded higher Ca/P and (Ca+Mg)/P molar ratios compared to the rest of the SBF solutions and conditions.

Samples incubated in 1x m-SBF solution induced a significantly greater amount of mineral deposition compared to samples incubated in other solutions (see Table 10). However, the amount of minerals formed is not related to the Ca/P and (Ca+Mg)/P molar ratios of the mineral.

All the c-SBF solutions yielded minerals with similar Ca/P and (Ca+Mg)/P molar ratios (these values were not statistically different).

The (Ca+Mg)/P molar ratios were obtained from the samples incubated in SBF solutions in order to take into account magnesium substitution that may have taken place. The Ca/P molar ratio of samples incubated in 1x m-SBF solution was in the range of 1-1.1, but the (Ca+Mg)/P molar ratio was in the range of 1.2-1.3. For c-SBF solutions, the Ca/P and (Ca+Mg)/P molar ratio were in the range of 0.8-0.9 and 1.1-1.3, respectively. The significantly higher (Ca+Mg)/P molar ratios compared to Ca/P molar ratios in all the samples could mean that there is a significant amount of magnesium formed in the calcium phosphate minerals.

The Ca/P molar ratios of these samples were closer to DCPD rather than OCP and HA, but the (Ca+Mg)/P molar ratios of these samples were the closest to OCP (Table 10). The mineral phase present in these samples is inconclusive based on these EDX data; additional analysis techniques such as Raman spectroscopy or X-Ray diffraction are required to draw further conclusions. It is conceivable that inter-layers of different mineral phases are formed, e.g. layers of DCPD and OCP [28]. It is also possible that a magnesium containing phase of calcium phosphate such as whitlockite is present in addition to calcium phosphate [29]. The standard deviations of these samples are relatively low (less than 10 % of the molar ratios) which means the results are fairly precise.

Since the difference between the Ca/P and (Ca+Mg)/P molar ratios is greater than that observed in the positive control sample, it is reasonable to conclude based on the EDX analysis data that the minerals formed with this *in vitro* model system is different from the ones found in native tissue. These minerals have a different Ca/P molar ratio compared to the ones found in the position control sample. This may be related to the morphology of the minerals observed with SEM (see Figure 14 in Section 3.1.2.2). Again, additional characterization techniques are required to further characterize the minerals.

3.2.4 Ca/P and (Ca+Mg)/P molar ratio corrections

The amount of phosphorus atoms present in de-mineralized samples is much higher compared to the amount of calcium atoms (approximately 0.05 % and 0.01 %, respectively). The phosphorus atoms are likely from phosphoproteins, phospholipids, and the DNA of cells. The difference of the amount of calcium and phosphorus atoms could potentially change the Ca/P ratio of the minerals formed in tissues, especially for samples with a fairly low overall percentage of calcium and phosphate atoms. Therefore, a correction was performed to see how much a difference this "background" calcium and phosphorus atoms would make on the Ca/P ratios of different tissues. Table 11 shows the corrected Ca/P and (Ca+Mg)/P molar ratios for the dentin tissues of samples incubated in each solution.

Solutions	**Original molar ratios**		**Corrected molar ratios**	
	Ca/P	**(Ca+Mg)/P**	**Ca/P**	**(Ca+Mg)/P**
1x m-SBF - soln change (7 d)	1.1 ± 0.2	1.3 ± 0.1	1.4 ± 0.6	1.2 ± 0.6
1x m-SBF - stirring + soln change (7 d)	0.93 ± 0.03	1.21 ± 0.03	0.97 ± 0.07	1.20 ± 0.09
1x c-SBF - stirring (21 d)	0.90 ± 0.06	1.13 ± 0.11	1.3 ± 0.3	0.8 ± 0.4
1x c-SBF- stirring + soln change (21 d)	0.83 ± 0.03	1.10 ± 0.04	1.0 ± 0.2	1.0 ± 0.2
1.25x c-SBF - stirring (10 d)	0.90 ± 0.04	1.18 ± 0.05	1.0 ± 0.2	1.2 ± 0.2
1.25x c-SBF - stirring + soln change (21 d)	0.86 ± 0.05	1.19 ± 0.09	1.1 ± 0.8	1.1 ± 0.9
1.5x c-SBF - stirring (14 d)	0.84 ± 0.10	1.10 ± 0.07	1.0 ± 0.4	1.0 ± 0.5
1.5x c-SBF - stirring + soln change (14 d)	0.88 ± 0.06	1.12 ± 0.08	1.3 ± 0.2	1.1 ± 0.2

Table 11 Ca/P and (Ca+Mg)/P molar ratio corrections of dentin, from samples incubated in various SBF solutions.

Generally, the corrected Ca/P molar ratios increased and the corrected (Ca+Mg)/P molar ratios decreased. The Ca/P and (Ca+Mg)/P ratios were comparable after corrections for samples

incubated in four of the solutions (e.g. 1.5x c-SBF), but it became lower for the other four solutions. However, when the standard deviation is taken into consideration, the change in the Ca/P and (Ca+Mg)/P molar ratios after corrections become insignificant. In fact, due to the high standard deviation of the corrected molar ratios (up to 50% in some cases), these data cannot be used with the same certainty as the raw molar ratios. It can be concluded from these corrections that it is worthwhile to correct for the amount of calcium and phosphorus ions that are unbound to the tissues, however, a more accurate correction method is required for further analysis of these data.

3.2.5 Summary: EDX analysis

EDX analysis was conducted on all the samples incubated in SBF solutions. 1x m-SBF yielded the greatest amount of mineral deposition onto the de-mineralized tissue sections, possibly due to its high IP compared to c-SBF solutions. Stirring of the solution increased the total amount of minerals formed on the tissue sections and solution change had very little effect. The minerals formed with the SBF solutions had Ca/P molar ratios in the range of 0.8-1 and (Ca+Mg)/P molar ratios in the range of 1.1 – 1.4. The phase of the mineral is likely DCPD or OCP; however, further characterization with a secondary technique is required to make definitive conclusions.

Chapter 4
The role of collagen fibrils in mineralization

4 The role of collagen fibrils in mineralization

Collagen fibrils have been hypothesized to act as a template for mineral deposition rather than actively inducing mineral deposition [1, 13]. In this chapter, the proposed *in vitro* model system was utilized to investigate the role of collagen fibrils in regulating mineral deposition. The effect of collagen fibrils in inducing mineral formation was studied with de-mineralized samples that have their non-collagenous components removed with proteolytic enzymes. These samples were then mineralized with 1x m-SBF solution for 7 and 10 days. The staining patterns obtained from these enzyme-treated samples were compared with the control samples (non enzyme-treated).

4.1 Enzymatic removal of non-collagenous components

The non-collagenous components (NCPs and PGs) of the de-mineralized tissue sections were removed with proteolytic enzymes, trypsin and papain. Both types of enzymes were used because they have different specificity. Trypsin cleaves the peptides on the C-terminal side of lysine and arginine amino acid residues [139]; it is commonly used for dissociating cells from culture plates. Papain, on the other hand, exhibits a broad range of specificity and is generally more effective compared to the pancreatic proteases (e.g. trypsin) [140]. It cleaves peptide bonds of lysine, arginine, histidine, leucine, and glycine; it also hydrolyzes esters and amides [140]. Papain has been shown to hydrolyze the protein core of PGs without disrupting the structure of collagen fibrils when used for a short duration [141, 142]. Digestion of the collagen matrix will occur with both types of enzymes over an extended period of time [139, 140].

The Fast Green dye was used to detect the non-collagenous proteins. It is an acidic dye that binds to the basic groups of amino acid residues [143]. A solution pH of 8 was utilized because the basic functional groups of amino acids are in their ionized form at this pH; these functional groups have a pK value range of 9-13. The McIlvaine's buffer was used because it contains very few acidic ions that compete with the binding of Fast Green molecules. Some of the functional groups that are detected by the Fast Green dye include the phenolic group of tyrosine, the sulphydryl group of cysteine, the ε-amino group of lysine, and the guanidine group of arginine [143]. These basic amino acid residues are contained in large proportions in NCPs are therefore characteristic of their presence; collagen contains a fixed proportion of lysine residues and therefore stained with a light intensity.

A series of preliminary experiments were conducted with both types of enzymes separately to determine the optimum digestion time which allowed the maximum amount of NCPs and PGs to be removed while introducing the least amount of damage to collagen fibrils. Trypsin was more effective at digesting the NCPs and PGs of soft connective tissues (PDL and pulp) but not very effective at removing the non-collagenous components of hard tissues (e.g. bone and dentin), compare Figure 16a and Figure 16b; substantial degradation of the PDL collagen fibrils occurred before the intensity of staining of bone and dentin started to decrease (Figure 16a). Papain was effective at removing the non-collagenous components of both PDL and bone; it was less effective at removing the NCPs and PGs of dentin and began to disintegrate the tubule structure before the staining intensity of dentin started to increase (Figure 16a). Incubation with either enzyme for an extended period of time resulted in an excessive amount of tissue degradation (see Figure 16a).

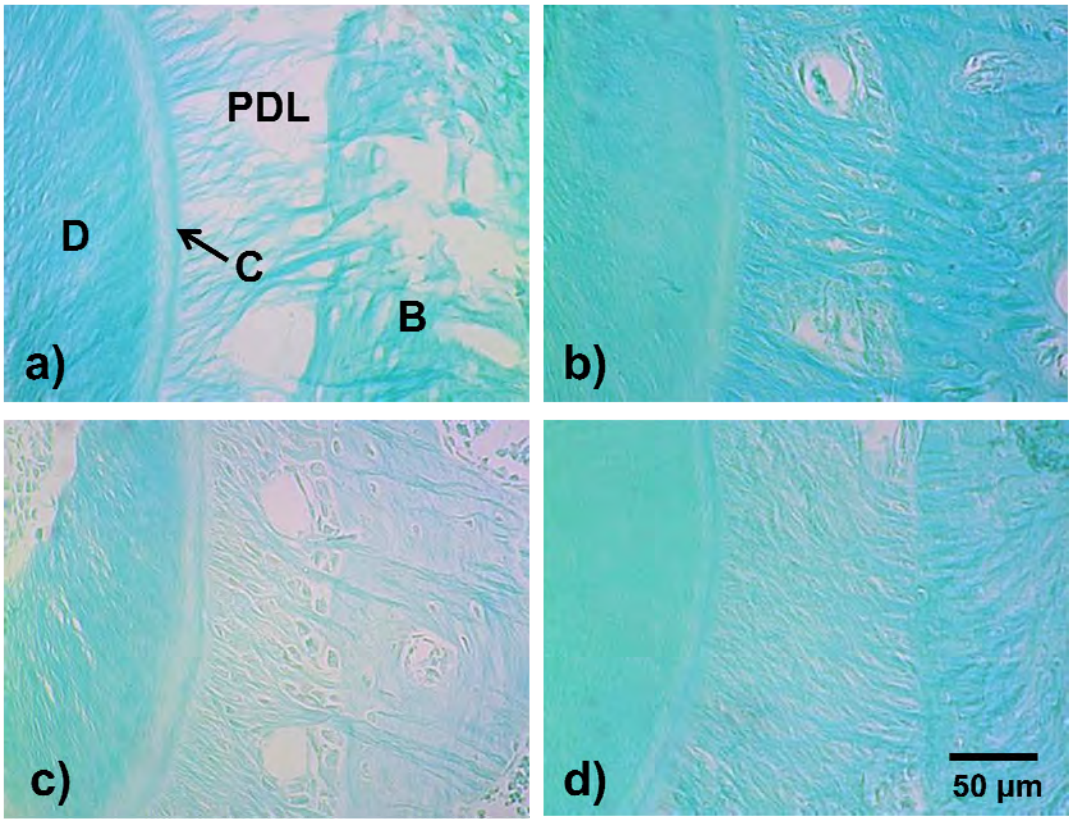

Figure 16 a) Sample digested with crude trypsin with a concentration of 2.5mg/ml for 25 hours; note the degradation of collagen fibrils in the PDL and bone. c) Sample digested with papain for 1 hour at 37°C; note the apparently lighter staining intensity of the PDL and bone. Images b) and d) are untreated control samples for a) and c), respectively. D: dentin, C: cementum, PDL: periodontal ligament, and B: bone.

The optimum digestion time determined initially for each enzyme separately was 1 hour at a concentration of 2.5 mg/ml at 37°C for papain, and 2 hours at a concentration of 2.5 mg/ml at 37°C with constant stirring for trypsin. However, when the two procedures were combined serially, a substantial amount of collagen degradation was seen. Therefore, an additional set of experiments was then conducted to explore more experimental conditions such as shorter incubation periods, lower concentrations and incubation at a lower temperature. The optimum digestion protocol was 1) trypsin at a concentration of 1.25 mg/ml for 1 hour at 37°C with stirring, followed by 2) papain at a concentration of 2.5 mg/ml for 30 minutes at room temperature.

4.1.1 Fast green staining

Samples treated with the serial proteolytic digestion of trypsin and papain was studied closely at the LM level with Fast Green staining. The collagen fibrils of all the tissues were still intact after proteolytic digestion, but the cells of the connective tissues have been removed. It is also conceivable that a small proportion of collagen fibrils have been removed from the PDL, characterized by the increased amount of empty space in the PDL where its collagen fibrils attach to bone (Figure 17).

The staining intensity of samples treated serially with trypsin and papain was compared with the untreated (control) sample (Figure 17). The PDL of the treated sample stained significantly lighter compared to the control, this is an indication that a large number of bound NCPs and PGs were removed from this tissue. The staining in bone was slightly lighter, indicating the removal of a portion of bound non-collagenous components. The intensity of dentin, however, remained roughly the same; this means only a relatively small portion of NCPs and PGs were removed from this tissue.

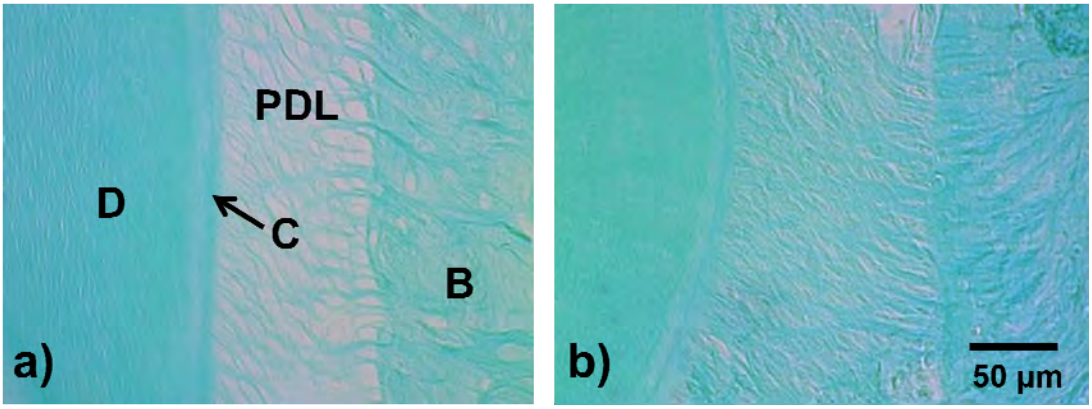

Figure 17 a) Sample treated with trypsin (for 1 hr at 37°C) and papain (for 30 minutes at room temperature), b) Untreated sample. D: dentin, C: cementum, PDL: periodontal ligament, and B: bone.

Although it has been reported that de-mineralization removes a large amount of NCPs from hard connective tissues [13], Fast Green staining still demonstrated the presence of a fair amount of NCPs and PGs after de-mineralization. It is possible that tissue fixation with formaldehyde prior to de-mineralization decreased the loss of NCPs and PGs during the de-mineralization process; since it has been reported that tissues fixed with glutaldehyde retained a larger portion of phosphoprotein (osteopontin) during the de-mineralization process compared to unfixed samples [144]. Further analysis is required to determine the exact amount of NCPs post de-mineralization. The proteolytic enzymes utilized in this study were effective at removing NCPs and PGs from the PDL, but less effective on bone and almost ineffective on dentin. This is due to the close association of the NCPs and PGs of dentin with the collagen matrix; this fraction of proteins (including phosphoproteins and Gla-proteins) has been hypothesized to play an important role in mineral formation [13, 145, 146].

4.1.2 Amino acid analysis

Amino acid analysis was performed on samples treated serially with trypsin and papain. It was used as a means to quantify the amount of non-collagenous proteins that are removed from the collagen matrix during the proteolytic digestion. The hydroxyproline (OH-Pro) and tyrosine (Tyr) content of the enzyme-treated sample were compared with the non enzyme-treated sample. OH-Pro is characteristic of collagen fibrils and was used for computing the content of collagen fibrils, and Tyr was used to compute non-collagenous proteins since it is present in very small amounts in collagen fibrils.

The mass percentage of the total amount of NCPs and collagen fibrils contained in the enzyme-treated and control samples were computed based on the amount of OH-Pro and Try present in each tissue. The control samples contained approximately 39 % of NCPs by weight and the sample treated with serial trypsin and papain digestion contained approximately 46 % of NCPs by weight. This means the total amount of collagen in the tissues decreased after enzyme

treatment. At first glance, this data does not seem to agree with the Fast Green staining results since the amount of NCPs was shown to decrease, and very little damage to collagen fibrils was seen. However, it is possible that a significant amount of collagen fibrils were degraded along with NCPs; the NCP and collagen fibril content was difficult to quantify with Fast Green staining. Additional analysis will be required to quantify the amount of NCPs and collagen fibrils present in each tissue prior to and after enzyme treatment(s).

A preliminary experiment performed with trypsin alone for 48 hours at 37°C showed that the NCP content decreased from approximately 37 % in the control sample to 16 % in the enzyme-treated sample. The trypsin used for this experiment was TPCK-treated and it was much less effective at removing the NCPs in the mineralized tissues compared to the crude trypsin utilized in the serial digestion experiments (see Figure 18). The corresponding Fast Green staining from these samples showed very light staining in the pulp (data not shown) and slightly lighter staining in the PDL, but all other tissues were stained with a similar intensity after enzyme-treatment. This means that for these samples, the NCP removal likely occurred in the pulp rather than the mineralized tissues.

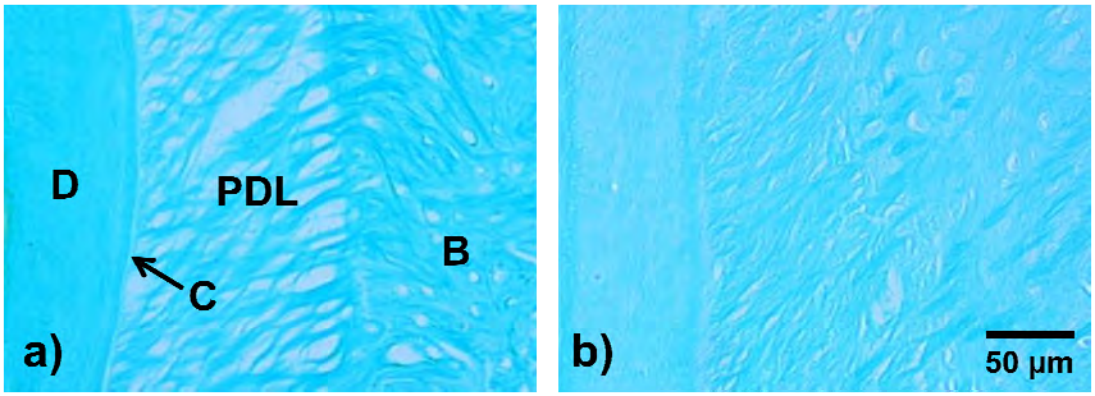

Figure 18 a) Sample treated with trypsin (TPCK-treated, 2.5 mg/ml) for 48 hours at 37°C; b) Untreated sample. D: dentin, C: cementum, PDL: periodontal ligament, and B: bone.

The amino acid analysis data obtained from this study only provide a crude comparison of the weight percent of NCPs and collagen fibrils because all the tissues of the periodontium are included in the analysis, including tissues that do not contain collagen (e.g. pulp). Therefore, it is difficult to infer the NCP content of each tissue from these analyses. In future studies, it is imperative to analyze each of the tissue of interest separately, especially the mineralized tissues such as dentin and bone.

4.1.3 Summary: enzymatic digestion of NCPs and PGs

Trypsin and papain were used serially to remove the non-collagenous contents from the de-mineralized tissue sections. A number of preliminary experiments were conducted to determine the optimum conditions which resulted in the maximum amount of NCP and PG removal and the least amount of damage to collagen fibrils. Fast Green staining showed that the enzymes were very effective for removing the non-collagenous components of the PDL, and less effective on bone and dentin. Amino acid analysis showed that a certain amount of collagen fibrils as well as NCPs were removed from the de-mineralized matrix.

4.2 Re-mineralization of the enzyme-treated samples

The de-mineralized samples digested with proteolytic enzymes trypsin and papain were re-mineralized in the same manner as the non enzyme-treated (control) samples with 1x m-SBF solution. The 1x m-SBF solution was chosen for this study because it yielded the greatest amount of mineral deposition onto the tissue sections. The solutions were changed every 3 days and no stirring was introduced; this condition was chosen because it produced the highest Ca/P and (Ca+Mg)/P molar ratios in the control samples. The mineral morphology and the Ca/P and (Ca+Mg)/P molar ratios of the enzyme treated samples were compared with the control.

4.2.1 Re-mineralization pattern at the LM level

The staining pattern obtained from enzyme-treated and control samples mineralized in 1x m-SBF solution for 7 and 10 days are shown in Figure 19. The enzyme-treated samples only showed light staining in the dentin at both time points; all other tissues did not show mineral staining (Figure 19a and Figure 19c). The control sample exhibited intense staining in the dentin and light staining in the bone at the 7 day time point (Figure 19b). After 10 days of incubation, the staining intensity in both dentin and bone increased proportionally; the PDL also started to mineralize (Figure 19d).

The mineralization behavior of the enzyme-treated samples is significantly different from the untreated samples. This means that the NCPs and PGs that were removed with enzyme treatment plays an important role in initiating mineral deposition, and that the collagen fibrils alone are not sufficient to induce mineral formation on de-mineralized tissues *in vitro*. Some may argue that the change in mineralization behavior of the enzyme-treated samples is due to an alteration in the collagen fibril structure. Although it is true that some collagen fibrils of the PDL have been removed, as is demonstrated by amino acid analysis, this argument cannot hold true because dentin still retained some of its ability to induce mineral formation. If the enzyme

digestions had altered the structure of collagen fibrils enough for them to lose their ability to initiate mineral formation, it should be true for all the tissues, and this was not the case for dentin. And since Fast Green showed lighter staining intensity in bone, it is likely that the small amount of mineral formed in dentin is due to the NCPs that remained bound to the collagen matrix after enzyme treatment.

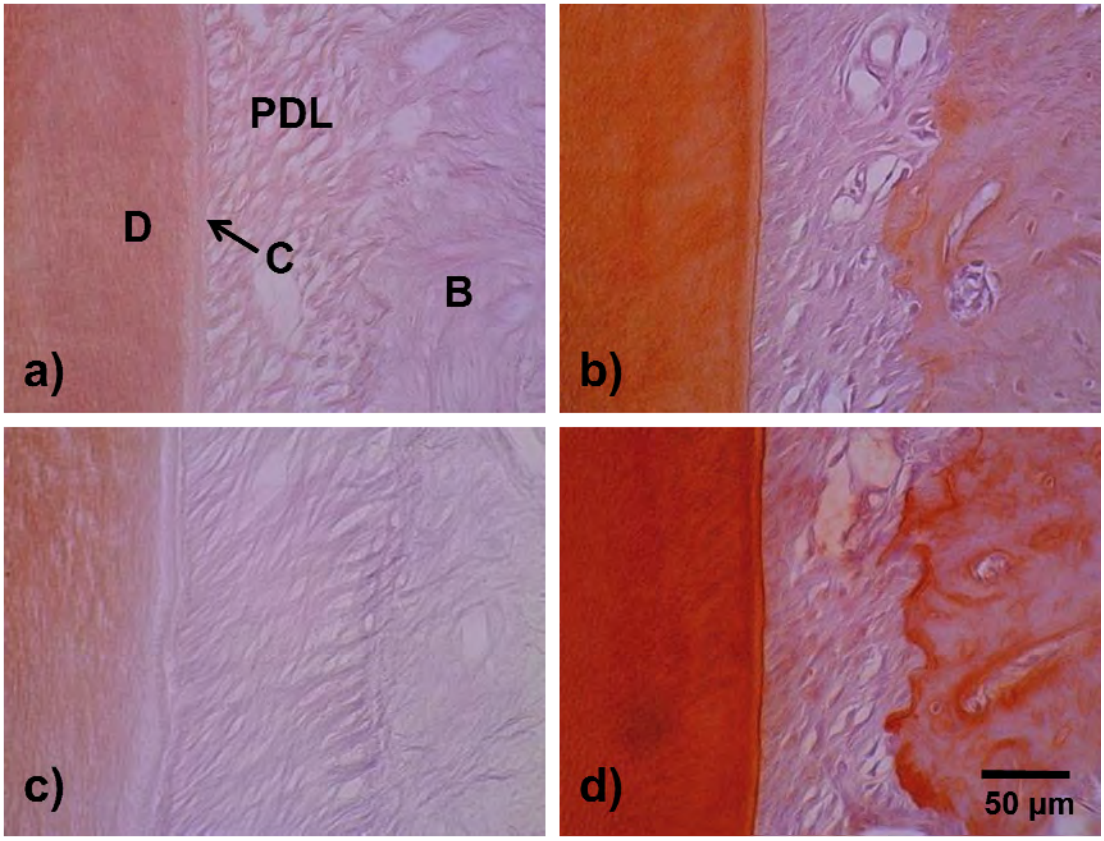

Figure 19 Samples mineralized with 1x m-SBF solution for 7 (a & b) and 10 days (c & d). a) and c) were treated with trypsin and papain, and b) and d) were not treated with enzymes. All the solutions were replaced every three days. D: dentin, C: cementum, B: alveolar bone, PDL: periodontal ligament.

It can be inferred from these re-mineralized enzyme-treated samples that the NCPs play a more critical role in mineral nucleation than mineral inhibition. This is supported by a previous study in which the PDL collagen fibrils were able to mineralize after the selective removal of GAGs

from the tissue [58]; it could be interpreted that it was the remaining NCPs in the tissue, not collagen fibrils which induced mineral deposition onto those tissues.

It is likely that the observed difference in the mineralization behavior between the enzyme-treated and non enzyme-treated samples is not simply delayed but altered. There was no change in the staining pattern observed between the 7 and 10 day time points for the enzyme-treated samples while an increase in mineral staining was observed with the control sample. Samples incubated for a longer duration is necessary to test this hypothesis. If the hypothesis is true, it means that both dentin and bone have a decreased affinity for calcium phosphate formation due to the loss of NCPs. Dentin was able to induce a small amount of mineral formation because it still contained more NCPs bound to its collagen fibrils compared to bone as demonstrated by Fast Green staining (Figure 17a).

4.2.2 Mineral morphology

The enzyme-treated samples were different from the non-treated sample in several ways when viewed with the SEM. The enzyme-treated samples did not contain any cells, as demonstrated with Alizarin red staining at the LM level. The collagen fibrils of the dentinal tubules of these samples appeared less compact compared to the positive control sample (compare Figure 20b and Figure 11d). In these samples, the mineral deposits did not form sheet-like structures as is observed with c-SBF solutions. There are two possible explanations for this: 1) the amount of minerals formed in these tissues is so low that they cannot be detected at the current magnification; 2) the mineral crystals are very fine and deposited within collagen fibrils that a much higher magnification is required in order to detect them.

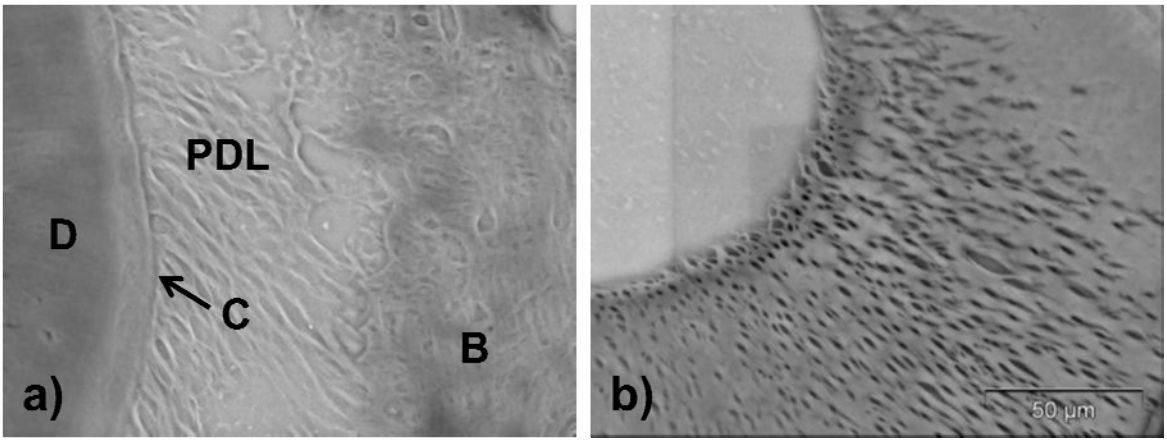

Figure 20 SEM image of an enzyme treated sample incubated in 1x m-SBF for 7 days (a). Image (b) shows the structure of dentinal tubules of the enzyme treated samples. Both samples were coated with a thin layer of carbon and imaged with backscattered electrons (BSE). D: dentin, C: cementum, B: alveolar bone, PDL: periodontal ligament.

4.2.3 Mineral characterization with EDX analysis

The overall amount of minerals formed on the enzyme treated samples decreased significantly compared to the non enzyme-treated samples, the overall % Ca decreases from 0.5 to 0.1 % in the dentin tissue (see Table 13). For the enzyme-treated samples, only dentin yielded a sufficient amount of mineral (> 0.1 %) for accurate EDX analysis. A negligible amount of calcium phosphate minerals was formed in bone tissues even up to 10 days of incubation in the 1x m-SBF. This result agrees with the staining pattern obtained with Alizarin red, no mineral staining was seen in bone (see Figure 19a and Figure 19c).

The Ca/P and (Ca+Mg)/P molar ratios of the enzyme-treated samples were much lower compared to the control samples (compare Table 12 with Table 10). This could mean that the

phase of the calcium phosphate minerals formed on these samples is different from samples not treated with enzymes as a result of the decreased content of NCPs and PGs in these tissues.

	Ca/P molar ratio	(Ca+Mg/P) molar ratio	overall % Ca	overall % P	overall % Mg
1x m-SBF – soln. change (7 days)					
Dentin	0.58 ± 0.02	0.99 ± 0.07	0.11 ± 0.03	0.17 ± 0.04	0.08 ± 0.02
1x m-SBF – soln. change (10 days)					
Dentin	0.8 ± 0.1	1.2 ± 0.2	0.12 ± 0.04	0.15 ± 0.07	0.10 ± 0.03

Table 12 The Ca/P and (Ca+Mg)/P molar ratios of the dentin tissue of the enzyme-treated samples incubated in 1x m-SBF solution (Please see Table 10 for the control sample incubated in 1x m-SBF for 7 days).

An interesting observation is that both of these ratios increased with time, compared the ratios obtained after 7 and 10 days of incubation (Table 12). This could be evidence for the initial formation of a less ordered phase of calcium phosphate which then transforms into a more ordered and mature mineral over time. One possibility is that DCPD is formed initially which then transforms into OCP over time [32, 33] (also see Section 1.2.3). However, upon a closer examination, the difference between the Ca/P and (Ca+Mg)/P molar ratios of the two samples were not statistically different according to t-test analysis (data not shown); therefore, this data cannot be used as evidence for the existence of a precursor phase to HA. Nonetheless, the values of Ca/P and (Ca+Mg)/P molar ratios of each sample were statistically different (data not shown). This supports the hypothesis of magnesium substitutions in the minerals formed on these tissues.

An important observation with the enzyme-treated samples is that they were highly susceptible to beam damage; the tissue started to degrade after approximately 10 s of exposure to the electron beam. Therefore, only one EDX spectra was obtained from each area because repeated spectrum collection yielded data with very low precision. Therefore, a total of 3-5 EDX spectra were obtained for each tissue from each sample. One possible explanation for the decreased

stability of these tissues is the loss of bound PGs and NCPs. These macromolecules may help stabilize the collagen fibrils [13].

Corrections for the Ca/P and (Ca+Mg)/P ratios for the enzyme treated samples followed a similar trend as the non enzyme-treated samples (compare Table 13 and Table 8). The Ca/P molar ratio of corrected samples increased while the (Ca+Mg)/P molar ratio decreased; however, they do not converge to the same degree as the non enzyme-treated samples. The standard deviation in these samples are very large, therefore it is difficult to draw definitive conclusions from these results.

Enzyme treated samples	**Original molar ratios**		**corrected molar ratios**	
Solutions	**Ca/P**	**(Ca+Mg)/P**	**Ca/P**	**(Ca+Mg)/P**
1x m-SBF - soln change (7 d)	0.58 ± 0.02	0.99 ± 0.07	0.7 ± 0.5	0.9 ± 0.5
1x m-SBF - soln change (10 d)	0.8 ± 0.1	1.2 ± 0.2	0.8 ± 0.7	1.0 ± 0.6

Table 13 The corrected values of Ca/P and (Ca+Mg)/P molar ratios of the enzyme digested samples incubated in 1x m-SBF solution.

4.2.4 Summary: re-mineralization of enzyme-treated samples

The enzyme treated samples were re-mineralized with 1x m-SBF for 7 and 10 days. The staining pattern of these samples was different from the control samples; a small amount of mineral was formed in bone and not in other tissues. This substantial decrease of mineral formation in the enzyme-treated samples supports the hypothesis that collagen fibrils alone cannot nucleate minerals, but it is the NCPs that promote mineral deposition. The Ca/P and (Ca+Mg)/P molar ratios of the enzyme treated samples were significantly lower compared to the control samples.

Chapter 5
Conclusions and suggested future work

5 Conclusions and suggested future work

5.1 Conclusions

This study presented the development of an *in vitro* model system that is useful for investigating the role of collagenous and non-collagenous proteins in regulating collagen mineralization. Native de-mineralized murine tissue was utilized as the collagen substrate and several solutions containing calcium and phosphate ions supersaturated with respect to HA were tested. Preferential mineral formation onto the de-mineralized hard tissues was observed with samples incubated in all the mineralization solutions.

Non-collagenous proteins were removed from the de-mineralized collagen matrix with serial digestion of proteolytic enzymes, trypsin and papain. The staining observed on the enzyme-treated samples was substantially less compared to the control samples. These results show that NCPs play the role of mineral nucleation in collagen mineralization

5.1.1 Objective 1 – Development of the *in vitro* model system

An *in vitro* model system utilizing mouse periodontium tissues was developed. Two types of mineralization solutions, CaP solution and SBF, were tested for their ability to induce mineral formation on the de-mineralized tissue sections. LM studies with histological staining showed that most mineralization solutions were able to induce preferential mineral deposition onto the

de-mineralized tissues. This means that the de-mineralized collagen matrix (containing non-collagenous macromolecules) contained sufficient information to determine the spatial deposition of minerals, this validates the first hypothesis.

SBF solutions were more suitable for the *in vitro* model system because they induced a greater amount of mineral formation onto the tissue sections and did not induce homogenous precipitation in solution. 1x m-SBF induced the greatest amount of mineral formation and had the highest Ca/P and (Ca+Mg)/P molar ratios. Both the Ca/P and (Ca+Mg)/P molar ratios obtained from this study were significantly lower compared to those found in the literature, further characterization such as Raman spectroscopy and X-Ray diffraction will be utilized to confirm the phase of the calcium phosphate minerals.

5.1.2 Objective 2 – The role of collagen fibrils in mineralization

Serial digestion with proteolytic enzymes trypsin and papain was performed to remove the non-collagenous components from the collagen matrix. Fast Green staining demonstrated that these enzymes were effective at removing the NCPs and PGs of PDL, but less effective at removing the NCPs and PGs of bone and dentin. This is due to the close association of the NCPs and PGs with collagen fibrils in mineralized tissues. Amino acid analysis demonstrated the loss of collagen fibrils in the enzyme-treated samples.

The enzyme digested samples were re-mineralized with 1x m-SBF for 7 and 10 days. Similar staining patterns were obtained for both time points, only dentin was stained with a light intensity, no staining was seen in other tissues. The loss of the ability of bone collagen to induce mineral formation is an indication that collagen fibrils do not promote mineral deposition; it is the NCPs and PGs that were removed which have the role of promoting mineral nucleation.

The Ca/P and (Ca+Mg)/P molar ratios of dentin were much lower compared to the untreated samples. Both of these ratios increased significantly with time, this could be evidence for the initial formation of a less ordered precursor mineral phase that transforms into a more stable phase over time. Again, further mineral characterization with additional characterization techniques is required to draw definitive conclusion regarding the phase and composition of the minerals formed.

5.2 Suggested future work

Here are a few suggested areas in which this project could be conducted further.

Further characterization of the mineral phase is required in order to better understand the proposed *in vitro* model system. Definitive conclusions cannot be made regarding each mineralization solution unless the phase of the calcium phosphate minerals can be identified. Sample preparation methods for Raman spectroscopy and X-Ray diffraction (XRD) with TEM are currently being developed in the laboratory; these techniques will provide more insight into the phase and morphology of the minerals formed on the tissue sections.

The removal of non-collagenous macromolecules was only characterized on a rough scale with Fast Green staining. The exact amounts of NCPs and PGs removed from each tissue, and the amount of collagen fibrils remaining in each tissue were not known. The amino acid analysis technique should be further developed to carry out analysis on each of the hard and soft connective tissues separately; this will provide useful information on the amount of NCPs and collagen fibrils remaining in each tissue after enzyme treatment.

Once these characterization techniques have been further developed, the next step for this project will be implementing the proposed *in vitro* model system for investigating the effect of specific groups of NCPs and PGs on mineral deposition. Enzymes will be utilized to remove specific groups of NCPs from the collagen matrix; the resulting mineralization pattern of these samples will then be characterized and compared with the non enzyme-treated (control) samples.

Two specific suggestions for further investigation are the role of PGs and the state of phosphorylation of phosphoproteins. PGs have been hypothesized to inhibit mineral formation

in the sheep PDL, and it would be interesting to see what happens to the proposed *in vitro* models system when the PGs are removed. De-phosphorylated proteins have been reported to lose their function to inhibit or promote mineral formation *in vitro*, thus, it would also be interesting to test the function of de-phosphorylated proteins with this *in vitro* model system.

References

1. A.R. Ten Cate, *Oral histology: Development, structure, and function*, 5th ed., Mosby, 1998.

2. C. Burger, H.W. Zhou, H. Wang, I. Sics, B.S. Hsiao, B. Chu, L. Graham, and M.J. Glimcher, "Lateral packing of mineral crystals in bone collagen fibrils," *Biophys. J.*, vol. 95, pp. 1985-1992, 2008.

3. M. D. Grynpas, L.C. Bonar, and M.J. Glimcher, "X-ray diffraction radial distribution function studies on bone mineral and synthetic calcium phosphates," *J. Mater. Sci., vol. 19*, pp. 723-736, 1984.

4. A. Posner, and P.J. Tannenbaum, "The mineral phase of dentin," in *Dentin and Dentinogensis*, vol. 1, A. Linde, Ed., Boca Raton, FL: CRC Press 1984, pp. 17.

5. A.S. Posner, "Bone mineral and the mineralization process," in *Bone and Mineral Research, vol. 5*, W.A. Peck, Ed., New York: Elsevier, 1987, pp. 65.

6. E.D. Eanes, "Physico-chemical principles of biomineralization", in *Bone Regulatory Factors, vol. 1*, A. Pecile, and B. de Bernard, Eds., NATO ASI Series, New York: Plenum Press, 1990.

7. H.P. Wiesmann, U. Meyer, U. Plate, and H.J. Höhling, "Aspects of collagen mineralization in hard tissue formation," *Int. Rev. Cytol.*, vol. 242, pp. 121-156, 2005.

8. M. Raspanti, C. Cesari, V. De Pasquale, V. Ottani, R. Strocchi, G. Zucchelli, and A. Ruggeri, "A histological and electron-microscopic study of the architecture and ultrastructure of human periodontal tissues," *Arch. Oral Biol.*, vol. 45, pp. 185-192, 2000.

9. "Periodontitis," MedlinePlus, *A service of the U.S. National Library of Medicine, National Institutes of Health (NIH),* 2010 [Online]. Available: http://www.nlm.nih.gov/medlineplus/ency/article/001059.htm [Accessed: August 1, 2010]

10. A. Viidik, and J. Vuust, Eds., *Biology of collagen*, Academic Press, 1980.

11. H.F. Lodish, A. Berk, P. Matsudaira, C.A. Kaiser, M. Krieger, M.P. Scott, L. Zipursky, and J. Darnell, *Molecular cell biology*, 5th ed., W.H. Freeman, 2003.

12. J. Habermehl, "Chapter 1: Introduction," *Collection Mémoires et thèses électroniques, Université Laval*, 2005. [Online]. Available: http://archimede.bibl.ulaval.ca/archimede/files/e8ebe68d-1ee7-4e8e-b018-852786824b4d/ch01.html [Accessed July 5, 2010].

13. E. Bonucci, Ed., *Calcification in biological systems*, CRC press, 1992.

14. K.E. Kadler, D.F. Holmes, J.A. Trotter, and J.A. Chapman, "Collagen fibril formation," *Biochem. J.*, vol. 316, pp. 1-11, 1996.

15. M.J. Glimcher, and S.M. Krane, "The organization and structure of bone, and the mechanisms of calcification," in *Treatise on Collagen, vol.2, part B, Biology of Collagen*, G.S. Ramachandran, Gen. ed., B.S. Gould, Ed., London: Academic Press, 1968, pp. 67.

16. H.C. Anderson, "Matrix vesicles and calcification," *Curr. Rheumatol. Rep.*, Vol. 5, pp. 222-226, 2003.

17. M. J. Glimcher, L.C. Bonar, M.D. Grynpas, W.J. Landis, and A.H. Roufosse, "Recent studies of bone mineral: is the amorphous calcium phosphate theory valid," *J. Cryst. Growth*, vol. 53, pp. 100-119, 1981.

18. R.A. Robinson, and M.L. Watson, "Collagen crystal relationships in bone as seen in the electron microscope," *Anat. Rec.*, vol. 114, pp. 383-410, 1952a.

19. R.A. Robinson, "An electron-microscope study of the crystalline inorganic component of bone and its relationship to the organic matrix," *J. Bone Joint Surg.*, vol. 34, pp. 389-434, 1952b.

20. P. Osdoby, and A.I. Caplan, "First bone formation in the developing chick limb," *Dev. Biol.*, vol. 86, pp. 147-56, 1981.

21. W.J. Landis, M.C. Paine, and M.J. Glimcher, “Electron microscopic observations of bone tissue prepared anhydrously in organic solvents,” *J. Ultrastruct. Res.*, vol. 59, pp. 1-30, 1977.

22. B. F. McEwen, M.J. Song, and W.J. Landis, “Quantitative determination of the mineral distribution in different collagen zones of calcifying tendon using high voltage electron microscopic tomography,” *J. Comput. Assist. Microsc.*, vol. 3, pp. 201-210, 1992.

23. W. J. Landis, M.J. Song, A. Leith, L. McEwen, and B.F. McEwen, “Mineral and organic matrix interaction in normally calcifying tendon visualized in three dimensions by high-voltage electron microscopic tomography and graphic image reconstruction,” *J. Struct. Biol.*, vol. 110, pp. 39-54, 1993.

24. L. Addadi, S. Weiner, and M. Geva, “On how proteins interact with crystals and their effect on crystal formation,” *Z. Kardiol.*, vol. 90, suppl. 3, pp. 92-98, 2001.

25. H. C. Anderson, “Molecular biology of matrix vesicles,” *Clin. Orthop. Relat. Res.*, vol. 314, pp. 266-280, 1995.

26. W. Traub, T. Arad, and S. Weiner, “Three-dimensional ordered distribution of crystals in turkey tendon collagen fibers,” *Proc. Natl. Acad. Sci. USA*, vol. 86, pp. 9822-9826, 1989.

27. R.Z. LeGeros, *Calcium Phosphates in Oral Biology*, Basel: Karger, 1991.

28. Zahid Amjad, Ed., *Calcium phosphates in biological and industrial systems*, Kluwer Academic Publishers, 1998.

29. C.A. Orme, and J.L. Giocondi, “Chapter 9: Model systems for formation and dissolution of calcium phosphate materials,” in *Handbook of Biomineralization*, Lawrence Livermore National Laboratory, August 2, 2006.

30. J.C. Voegel, and R.M. Frank, “Ultrastructural study of apatite crystal dissolution in human dentine and bone,” *J. Biol. Buccale*, vol. 5, pp. 181-194, 1977.

31. A.L. Arsenault, and M.D. Grynpas, “Crystals in calcified epiphyseal cartilage and cortical bone of the rat,” *Calcif. Tissue Int.*, vol. 43, pp. 219-225, 1988.

32. M. J. Olszta, X.G. Cheng, S.S. Jee, R. Kumar, Y.-Y. Kim, M.J. Kaufman, E.P. Douglas, and L.B. Gower, “Bone structure and formation: A new perspective,” *Mater. Sci. Eng. R*, vol. 58, pp. 77-116, 2007.

33. L.C. Chow, E.D. Eanes, Eds., *Octacalcium phosphate*, Karger, 2001.

34. X. Lu, and Y. Leng, “Theoretical analysis of calcium phosphate precipitation in simulated body fluid,” *Biomaterials*, vol. 26, pp. 1097-1108, 2005.

35. L. Addadi, and S. Weiner, “Control and design principles in biological mineralization,” *Angew. Chem. Int. Ed. Engl.*, vol. 31, pp. 153-169, 1992.

36. J. Mahamid, A. Sharir, L. Addadi, and S. Weiner, “Amorphous calcium phosphate is a major component of the forming fin bones of zebrafish: Indications for an amorphous precursor phase,” *Proc. Natl. Acad. Sci. USA*, vol. 105, pp. 12748-12753, 2009.

37. J.D. Termine, and A.S. Posner, “Infrared analysis of rat bone: age dependency of amorphous and crystalline mineral fractions,” *Science*, vol. 153, pp. 1523-1525, 1966.

38. J.D. Termine, E.D. Eanes, D.J. Greenfield, M.U. Nylen, and R.A. Harper, “Hydrazine-deproteinated bone mineral,” *Calcif. Tissue Res.*, vol. 12, pp. 73-90, 1974.

39. R.E. Wuthier, G.S. Rice, J.E.B. Wallace Jr., R.L. Weaver, R.Z. LeGeros, and E.D. Eanes, “*In vitro* precipitation of calcium phosphate under intracellular conditions: formation of brushite from an amorphous precursor in the absence of ATP,” *Calcif. Tissue Int.*, vol. 37, pp. 401-410, 1985.

40. N.J. Crane, V. Popescu, M.D. Morris, P. Steenhuis, and M.A. Ignelzi Jr., “Raman spectroscopic evidence for octacalcium phosphate and other transient mineral species deposited during intramembranous mineralization,” *Bone*, vol. 39, pp. 434-442, 2006.

41. E.D. Pellegrino, and R.M. Biltz, “Mineralization in the chick embryo. I. monohydrogen phosphate and carbonate relationships during maturation of the bone crystal complex,” *Calcif. Tissue Res.*, vol. 10, pp. 128-135, 1972.

42. J.E. Wergedal, and D.J. Baylink, “Electron microprobe measurements of bone mineralization rate in vivo,” *Am. J. Physiol.*, vol. 226, pp.345-352, 1974.

43. E.D. Eanes, and J.L. Meyer, “The maturation of crystalline calcium phosphates in aqueous suspensions at physiologic pH,” *Calcif. Tissue Res.*, vol. 23, pp. 259-269, 1977.

44. J.L. Meyer, and E.D. Eanes, “A thermodynamic analysis of the amorphous to crystalline calcium phosphate transformation,” *Calcif. Tissue Res.*, vol. 25, pp. 59-68, 1978a.

45. J.L. Meyer, and E.D. Eanes, “A thermodynamic analysis of the secondary transition in the spontaneous precipitation of calcium phosphate,” *Calcif. Tissue Res.*, vol. 25, pp. 209-216, 1978b.

46. E.D. Eanes, “Crystals growth of mineral phases in skeletal tissues,” *Prog. Crystal Growth Character. Mater.*, vol. 3, pp. 3-15, 1980.

47. W.E. Brown, “Crystal growth of bone mineral,” *Clin. Orthop.*, vol. 44, pp. 205-220, 1966.

48. M.A. Walters, Y.C. Leung, N.C. Blumenthal, R.Z. LeGeros, and K.A. Konsker, “A Raman and Infrared spectroscopic investigation of biological hydroxyapatite,” *J. Inorg. Chem.*, vol. 39, pp. 193-200, 1990.

49. I. Rehman, R. Smith, L.L. Hench, and W. Bonfield, “Structural evaluation of human and sheep bone and comparison with synthetic hydroxyapatite by FT-Raman spectroscopy,” *J. Biomed. Mater. Res.*, vol. 29, pp. 1287-1294, 1995.

50. R. Smith, and I. Rehman, “Fourier transform Raman spectroscopic studies of human bone,” J. Mater. Sci. Mater. Med., vol. 5, pp. 775-778, 1995.

51. A. Carden, and M.D. Morris, “Application of vibrational spectroscopy to the study of mineralized tissues (review),” *J. Biomed. Opt.*, vol. 5, pp. 259-268, 2000.

52. A. Boskey, “FT-IR imaging of native and tissue-engineered bone and cartilage,” *Biomaterials*, vol. 28, pp. 2465-2478, 2007.

53. N. J. Crane, v. Popescu, M.D. Morris, P. Steenhuis, and M.A. Ignelzi, “Raman spectroscopic evidence for octacalcium phosphate and other transient mineral species deposited during intramembranous mineralization,” *Bone*, vol. 39, pp. 434-442, 2006.

54. A. Wopenka, A. Kent, J.D. Pasteris, Y. Yoon, and S. Thomopoulos, “The tendon-to-bone transition of the rotator cuff: a preliminary Raman spectroscopic study documenting the gradual mineralization across the insertion in rat tissue samples,” *Appl. Spectrosc.*, vol. 62, pp. 1285-1294, 2008.

55. B.N. Bachra, “Mineral deposition in collagen *in vitro*,” *Calc. Tissue Res.*, vol. 2, pp. 343-352, 1968.

56. B.N. Bachra, “Calcification *in vitro* of demineralized bone matrix: electron microscopic and chemical aspects,” *Calc. Tisssue Res.*, vol. 8, pp. 287-303, 1972.

57. D.B. Boyer, and F.R. Eirich, “Remineralization of dentin *in vitro*,” *Calcif. Tissue Res.*, vol. 21, pp. 17-28, 1976.

58. J. Kirkham, S.J. Brookes, R.C. Shore, W.A. Bonass, and C. Robinson, “The effect of glycosylaminoglycans on the mineralization of sheep periodontal ligament *in vitro*,” *Connet. Tissue Res.*, vol. 33, pp. 23-29 [345-351], 1995.

59. K. Hoshi, S. Kemmotsu, Y. Takeuchi, N. Amizuka, and H. Ozawa, “The primary calcification in bones follows removal of decorin and fusion of collagen fibrils,” *J. Bone Miner. Res.*, vol. 14, pp. 273-280, 1999.

60. G. He and A. George, “Dentin matrix protein I immobilized on type I collagen fibrils facilitates apatite deposition in vitro,” *J. Biol. Chem.*, vol. 279, pp. 11649-11656, 2004.

61. E. Embery, “An update on the biochemistry of the periodontal ligament,” *Eur. J. Orthod.*, vol. 22, pp. 77-80, 1990.

62. E.P. Katz, and S.T. Li, “The intermolecular space of reconstituted collagen fibrils,” *J. Mol. Biol.*, vol. 73, pp. 351-369, 1973a.

63. E.P. Katz, and S.T. Li, "Structure and function of bone collagen fibrils," *J. Mol. Biol.*, vol. 80, pp. 1-15, 1973b.

64. L.C. Bonar, and M.J. Glimcher, "Supramolecular structure and packing differences between tendon and bone collagens," in *The chemistry and biology of mineralized connective tissues*, Veis, A., Ed., North Holland, New York: Elsevier, 1981, pp. 119-121.

65. M.J. Glimcher, and E.P. Katz, "The organization of collagen in bone: the role of the non-covalent bonds in the relative insolubility of bone collagen," *J. Ultrastruct. Res.*, vol. 12, pp. 705-729, 1965.

66. M. Gelinsky, S. Lenhard, P. Simon, R. Born, H. Domaschke, and W. Pompe, "Influence of osteocalcin on *in vitro* mineralization of collagen type I," *8th ICCBMT*, Banff, Alberta, Canada, October 17-22, 2004, pp. 230-233, 2004.

67. A.S. Dashpande, and E. Beniash, "Bioinspired synthesis of mineralized collagen fibrils," *Cryst. Growth Des.*, vol. 8, pp. 3084-3090, 2008.

68. M.J. Glimcher, "Mechanism of calcification: role of collagen fibrils and collagen-phosphoprotein complexes *in vitro* and *in vivo*," *Anat. Rec.*, vol. 224, pp. 139-153, 1989.

69. A. George, and A. Veis, "Phosphorylated proteins and control over apatite nucleation, crystal growth, and inhibition," *Chem. Rev.*, vol. 108, pp. 4670-4693, 2008.

70. P.G. Robey, "The biochemistry of bone," *Endocrinol. Metab. Clin. North Am.*, vol. 18, pp. 859-902, 1989.

71. C.A. Shuttleworth and J.W. Smalley, "Periodontal ligament," *Int. Rev. Connect. Tissue Res.*, vol. 10, pp. 211-247, 1983.

72. P. G. Robey, "Vertebrate mineralized matrix proteins. Structure and function," *Connect. Tissue Res.*, vol. 35, pp. 131-136, 1996.

73. G.K. Hunter, P.V. Hauschka, A.R. Poole, L.C. Rosenberg, H.A. Goldberg, "Nucleation and inhibition of hydroxyapatite formation by mineralized tissue proteins," *Biochem. J.*, vol. 317, pp. 59-64, 1996.

74. A. Alberts, *Molecular biology of the cell*, 4th ed., Garland Science: Taylor & Francis Group, 2002.

75. P. M. Bartold, "Proteoglycans of the periodontium: structure, role and function," *Periodont. Res.*, vol. 22, pp. 431-444, 1987.

76. L.C.U. Junqueira, and G.S. Montes, "Biology of collagen-proteoglycan interaction," *Arch. Histol. Jap.*, vol. 46, pp. 589-629, 1983.

77. L. Hakkinen, O. Oksala, T. Salo, F. Rahemtulla, and H. Larjava, "Immunohistochemical localization of proteoglycans in human periodontium," *J. Histochem. Cytochem.*, vol. 41, pp. 1689-1699, 1993.

78. H. Cheng, B. Caterson, P.J. Neame, G.E. Lester, and M. Yamauchi, "Differential distribution of lumican and fibromodulin in tooth cementum," *Connect. Tissue Res.*, vol. 34, pp. 87-96, 1996.

79. A. Hjerpe, C.A. Antonopoulos, B. Engfeldt, and B. Wikstrom, "Analysis of dentine glycosaminoglycans using high-performance liquid chromatography," *Calcif. Tissue Int.*, vol. 35, pp. 496-501, 1983.

80. L.W. Fisher, "The nature of the proteoglycans of bone," *Proceedings of the Second International Conference on the Chemistry and Biology of Mineralized Tissues*, W.T. Butler, Ed., Alabama, Session VII, pp. 188-196, 1984.

81. A. Linde, A. Lussi, and M.A. Crenshaw, "Mineral induction by immobilized polyanionic proteins," *Calcif. Tissue Int.*, vol. 44, pp. 286-295, 1989.

82. D.S. Howell, and J.C. Pita, "Calcification of growth plate cartilage with special reference to studies on micropuncture fluid," *Clin. Orthop.*, vol. 118, pp. 208-229, 1976.

83. N.C. Blumenthal, "Mechanism of proteoglycan inhibition of hydroxyapatite formation," in *The Chemistry and Biology of Mineralized Connective Tissues*, A. Veis, Ed., North Holland, New York: Elsevier, 1981, pp. 509-515.

84. C.-C. Chen, A.L. Boskey, and L.C. Rosenberg, “The inhibitory effect of cartilage proteoglycan on hydroxyapatite growth,” *Calcif. Tissue Int.*, vol. 36, pp. 285-290, 1984.

85. A.L. Boskey, “Hydroxyapatite formation in a dynamic collagen gel system: Effects of type I collagen, lipids, and proteoglycans,” *J. Phys. Chem.*, vol. 93, pp. 1628-1633, 1989.

86. K. Verdelis, Y. Ling, T. Sreenath, N. Haruyama, M. MacDougall, M.C. van der Meulen, L. Lukashova, L. Spevak, A.B. Kulkami, and A.L. Boskey, “DSPP effects on *in vivo* bone mineralization,” *Bone*, vol. 43, pp. 983-990, 2008.

87. A. Domenicucci, H.A. Goldberg, T. Hofmann, D. Isenman, S. Wasi, and J. Sodek, “Characterization of porcine osteonectin extracted from foetal calvariae,” *Biochem. J.*, vol. 253, pp. 139-151, 1988.

88. G. K. Hunter, and H.A. Goldberg, “Nucleation of hydroxyapatite by bone sialoprotein,” *Proc. Natl. Acad. Sci.*, vol. 90, pp. 8562-8565, 1993.

89. H. A. Goldberg, G.K. Hunter, “The inhibitory activity of osteopontin on hydroxyapatite formation in vitro,” *Ann. NY Acad. Sci.*, vol. 760, pp. 305-308, 1995.

90. A. Nanci, and D.D. Bosshardt, “Structure of periodontal tissues in health and structure,” *Periodontology 2000*, vol. 40, pp. 11-28, 2006.

91. M.P. Mark, C.W. Prince, T. Oosawa, S. Gay, A.L. Bronckers, and W.T. Butler, “Immunohistochemical demonstration of a 44-KD phosphoprotein in developing rat bones,” *J. Histochem. Cytochem.*, vol. 35, pp. 707-715, 1987a.

92. M.P. Mark., C.W. Prince, S. Gay, R.L. Austin, M. Bhown, R.D. Finkelman, and W.T. Butler, “A comparative immunocytochemical study on the subcellular distributions of 44 kDa bone phosphoprotein and bone gamma-carboxyglutamic acid (Gla)-containing protein in osteoblasts,” *J. Bone Min. Res.*, vol. 2, pp. 337-346, 1987b.

93. M.D. McKee, and A. Nanci, “Osteopontin at mineralized tissue interfaces in bone, teeth, and osseointegrated implants: ultrastructural distribution and implications for mineralized tissue formation, turnover, and repair,” *Microsc. Res. Tech.*, vol. 33, pp. 141-64, 1996.

94. M.P. Mark, W.T. Butler, C.W. Prince, R.D. Finkelman, and J.V. Ruch, “Developmental expression of 44-kDa bone phosphoprotein (osteopontin) and bone gamma-carboxyglutamic acid (Gla)-containing protein (osteocalcin) in calcifying tissues of rat,” *Differentiation*, vol. 37, pp. 123-136, 1988.

95. H. I. Roach, “Why does bone matrix contain non-collageneous proteins? The possible roles of osteocalcin, osteonectin, osteopontin and bone sialoprotein in bone mineralization and resorption,” *Cell Biol. Int.*, vol. 18, pp. 617-628, 1994.

96. K.M. Conn, J.D. Termine, “Matrix protein profiles in calf bone development,” *Bone*, vol. 6, pp. 33-36, 1985.

97. P.V. Hauschka, J.B. Lian, and P.M. Gallop, “Direct identification of the calcium-binding amino acid, gamma-carboxyglutamate, in mineralized tissue,” *Proc. Natl. Acad. Sci. USA*, vol. 72, pp. 3925-3929, 1975.

98. Y. Otawara, and P.A. Price, “Developmental appearance of matrix Gla protein during calcification in the rat,” *J. Biol. Chem.*, vol. 261, pp. 10828-10832, 1986.

99. A.L.J.J. Bronckers, S. Gay, M.T. DiMuzio, and W.T. Butler, “Immunolocalization of gamma-carboxyglutamic acid containing proteins in developing rat bones,” *Coll. Relat. Res.*, vol. 5, pp. 273-281, 1985.

100. A.L.J.J. Bronckers, S. Gay, R.D. Finkelman, and W.T. Butler, “Developmental appearance of Gla proteins (osteocalcin) and alkaline phosphatase in tooth germs and bone of the rat,” *Bone Miner.*, vol. 2, pp. 361-373, 1987.

101. A.J. Camarda, W.T. Butler, R.D. Finkelman, and A. Nanci, “Immunocytochemical localization of gamma-carboxyglutamic acid-containing proteins and osteocalcin in rat bone and dentin,” *Calcif. Tissue Int.*, vol. 40, pp. 349-355, 1987.

102. J.D. Fraser, and P.A. Price, “Lung, heart and kidney express high levels of mRNA for the vitamin K-dependent matrix Gla protein. Implications for the possible functions of matrix Gla protein and for the tissue distribution of the gamma-carboxylase,” *J. Biol. Chem.*, vol. 263, pp. 11033-11036, 1988.

103. G. Luo, P. Ducy, M.D. McKee, G.J. Pinero, E. Loyer, R.R. Behringer, & G. Karsenty, Spontaneous calcification of arteries and cartilage in mice lacking matrix GLA protein, *Nature*, vol. 386, pp. 78-81, 1997.

104. M. Ketteler, C. Wanner, T. Metzger, P. Bongartz, R. Westenfeld, U. Gladziwa, L.J. Schurgers, C. Vermeer, W. Jahnen-Dechent, and J. Floege, Deficiencies of calcium-regulatory proteins in dialysis patients: A novel concept of cardiovascular calcification in uremia, *Kidney Int.*, vol. 63, pp. S84-S87, 2003.

105. J.E. Aubin, A. Gupta, R. Zirngibl, and J. Rossant, "Bone sialoprotein knockout mice have bone abnormalities," *Bone*, vol. 17, pp. 558-558, 1995.

106. S. C. Cowin, *Bone mechanics handbook*, 2nd ed., Informa HealthCare, 2001.

107. S.R. Rittling, H.N. Matsumoto, M.D. McKee, A. Nanci, X.R. An, K.E. Novick, A.J. Kowalski, M. Noda, and D.T. Denhardt, "Mice lacking osteopontin show normal development and bone structure but display altered osteoclast formation *in vitro*," *J. Bone Miner. Res.*, vol. 13, pp. 1101-1111, 1998.

108. P. H. Tartaix, M. Doulaverakis, A. George, L.W. Fisher, W.T. Butler, C. Qin, E. Salih, M. Tan, Y. Fujimoto, L. Spevak, and A.L. Boskey, "*In vitro* effects of dentin matrix protein-1 on hydroxyapatite formation provide insight into *in vivo* functions," *J. Biol. Chem.*, vol. 279, pp. 18115-18120, 2004.

109. A.L. Boskey, L. Spevak, E. Paschalis, S.B. Doty, and M.D. McKee, "Osteopontin deficiency increases mineral content and mineral crystallinity in mouse bone," *Calcif. Tissue Int.*, vol. 2, pp. 145-154, 2002.

110. G.K. Hunter, C.L. Kyle, and H.A. Goldberg, "Modulation of crystal formation by bone phosphoproteins: structural specificity of the osteopontin-mediated inhibition of hydroxyapatite formation," *Biochem. J.*, vol. 300, pp. 723-728, 1994.

111. A.L. Boskey, M. Maresca, W. Ullrich, S.B. Doty, W.T. Butler, and C.W. Prince, "Osteopontin-hydroxyapatite interactions *in vitro*: inhibition of hydroxyapatite formation and growth in a gelatin-gel," *Bone Miner.*, vol. 2, pp. 147-159, 1993.

112. J-H Bradt, M. Mertig, A. Teresiak, and W. Pompe, “Biomimetic mineralization of collagen by combined fibril assembly and calcium phosphate formation,” *Chem. Mater.*, vol. 11, pp. 2694-2701, 1999.

113. M. Iijima Y. Moriwake, and Y. Kuboki, “*In vitro* growth of octacalcium phosphate on type I collagen fiber,” *J. Cryst. Growth*, vol. 137, pp. 553-560, 1994a.

114. M. Iijima, K. Iijima, Y. Moriwaki, and Y. Kuboki, “Oriented growth of octacalcium phosphate crystals on type I collagen fibrils under physiological conditions,” *J. Cryst. Growth*, vol. 140, pp. 91-99, 1994b.

115. I. Yamaguchi, T. Kogure, M. Sakane, S. Tanaka, A. Osaka, and J. Tanaka, “Microstructure analysis of calcium phosphate formed in tendon,” *J. Mater. Sci. Mater. Med.*, vol. 14, pp. 883-889, 2003.

116. J. Chen, C. Burger, C.V. Krishnan, B. Chu, B.S. Hsiao, and M.J. Glimcher, “*In vitro* mineralization of collagen in demineralized fish bone,” *Macromol. Chem. Phys.*, vol. 206, pp. 43-51, 2005.

117. S. Ito, T. Saito, and K. Amano, “*In vitro* apatite induction by osteopontin: interfacial energy for hydroxyapatite nucleation on osteopontin,” *J. Biomed. Mater. Res. A*, vol. 69, pp. 11-16, 2004.

118. D.A. Pampena, K.A. Robertson, O. Litvinova, G. Lajoie, H.A. Goldberg, and G.K. Hunter, “Inhibition of hydroxyapatite formation by osteopontin phosphopeptides,” *Biochem. J.*, vol. 378, pp. 1083-1087, 2004.

119. A.L. Boskey, “Osteopontin and related phosphorylated sialoproteins: effects on mineralization,” *Ann. N.Y. Acad. Sci.*, vol. 760, pp. 249-256, 1995.

120. G. He, T. Dahl, A. Veis, and A. George, “Nucleation of apatite crystals *in vitro* by self-assembled dentin matrix protein 1,” *Nature materials*, vol. 2, pp. 552-558, 2003a.

121. G. He, T. Dahl, A. Veis, and A. George, “Dentin matrix protein 1 initiates hydroxyapatite formation *in vitro*,” *Connect. Tissue Res.*, vol. 44 (suppl. 1), pp. 240-245, 2003b.

122. T. Saito, A.L. Arsenault, M. Yamauchi, Y. Kuboki, and M.A. Crenshaw, "Mineral induction by immobilized phosphoproteins," *Bone*, vol. 21, pp. 305-311, 1997.

123. A.L. Boskey, M. Maresca, S. Doty, B. Sabsay, and A. Veis, "Concentration-dependent effects of dentin phosphoryn in the regulation of *in vitro* hydroxyapatite formation and growth," *Bone Miner.*, vol. 11, pp. 55-65, 1990.

124. C. Ohtsuki, "How to prepare the simulated body fluid (SBF) and its related solutions, proposed by Kokubo and his colleagues," *Graduate school of materials science, Nara Institute of Science and Technology*, 2009 [Online]. Available: http://mswebs.naist.jp/LABs/tanihara/ohtsuki/SBF/index.html [Accessed: Aug. 22, 2008].

125. T. Kokubo, S. Ito, Z.T. Huang, T. Hayashi, S. Sakka, T. Kitsugi, and T. Yamauro, "Ca, P-rich layer formed on high-strength bioactive glass-ceramic A-W," *J. Biomed. Mater. Res.*, vol. 3, pp. 331-343, 1990a.

126. T. Kokubo, H. Kushitana, S. Sakka, T. Kitsugi, and T. Yamauro, "Solutions able to reproduce *in vivo* surface-structure changes in bioactive glass-ceramic A-W," *J. Biomed. Mater. Res.*, vol. 6, pp. 721-734, 1990b.

127. M. Bohner, and J. Lemaitre, "Can bioactivity be tested in vitro with SBF solution?" *Biomaterials*, vol. 30, pp. 2175-2179, 2009.

128. K. Shin, A.C. Jayasuriya, and D.H. Kohn, "Effect of ionic activity products on the structure and composition of mineral self assembled on three-dimensional poly(lactide-co-glycolide) scaffolds," *J. Biomed. Mater. Res. A*, vol. 83, pp. 1076-1086, 2007.

129. G. Falini, S. Fermani, B. Palazzo, and N. Roveri, "Helical domain collagen substrates mineralization in simulated body fluid," *J. Biomed. Mater. Res. A*, vol. 87, pp. 470-476, 2008.

130. A. Oyane, H.-M. Kim, T. Furuya, T. Kokubo, T. Miyazaki, and T. Nakamura, "Preparation and assessment of revised simulated body fluids," *J. Biomed. Mater. Res. A*, vol. 65, pp. 188-195, 2003.

131. H.-M. Kim, T. Miyazaki, T. Kokubo, and T. Nakamura, “Revised simulated body fluid,” *Key Eng. Mater.*, vol. 192-195, pp. 47-50, 2001.

132. H. Puchtler, S.N. Meloan, and M.S. Terry, “On the history and mechanism of Alizarin red and Alizarin red S stains for calcium,” *J. Histochem. Cytochem.*, vol. 17, pp.110-124, 1969.

133. J. Kiernan, *Histological and histochemical methods: Theory and practice*, 4th ed., Cold spring harbor laboratory press, 2008.

134. “Alizarin red S staining protocol for calcium,” *IHCWorld*, 2007. [Online]. Available: http://www.ihcworld.com/_protocols/special_stains/alizarin_red_s.htm [Accessed September 14, 2009].

135. M. M. Beppu, M.A. Torres, C.G. Aimoli, G.A.S. Goulart, and C.C. Santana, “*In vitro* mineralization on chitosan using solutions with excess of calcium and phosphate ions,” *J. Mater. Res.*, vol. 20, pp. 3303-3311, 2005.

136. A. R. Spurr, “Choice and preparation of standards for X-ray microanalysis of biological materials with special reference to macrocyclic polyether complexes,” *J. Microsc. Biol. Cell.*, vol. 22, pp. 287-303, 1975.

137. T.D. Daley, A. Jarvis, G.P. Wysocki, and S.L. Kogon, “X-Ray microanalysis of teeth from healthy patients and patients with familial hypophosphatemia,” *Calcif. Tissue Int.*, vol. 47, pp. 350-355, 1990.

138. T. Kodaka, and K. Debari, Scanning electron microscopy and energy-dispersive X-ray microanalysis studies of afibrillar cementum and cementicle-like structures in human teeth, *J. Electron Microsc.*, vol. 51, pp. 327-335, 2002.

139. “Trypsin,” *Sigma-Aldrich*, 2010, [Online]. Available: http://www.sigmaaldrich.com/life-science/metabolomics/enzyme-explorer/analytical-enzymes/trypsin.html [Accessed January 12, 2010].

140. "Papain," *Sigma-Aldrich*, 2010, [Online]. Available: http://www.sigmaaldrich.com/life-science/metabolomics/enzyme-explorer/analytical-enzymes/papain.html [Accessed March 25, 2010].

141. L. C. U. Junqueira, G. Bignolas, P.A. Mourao, and S.S. Bonetti, "Quantitation of collagen-proteoglycan interaction in tissue sections," *Connect. Tissue Res.*, vol. 7, pp. 91-96, 1980.

142. N. Shepard, and N. Mitchell, "The localization of articular cartilage proteoglycans by electron microscopy," *Ant. Rec.*, vol. 187, pp. 463-476, 1977.

143. J. Chayen, and L. Bitensky, *Practical histochemistry*, 2nd ed., John Wiley & Sons, 1991.

144. M.D. McKee, A. Nanci, W.J. Landis, Y. Gotoh, L.C. Gerstenfeld, and M.J. Glimcher, Effects of fixation and demineralization on the retention of bone phosphoprotein and other matrix components as evaluated by biochemical analyses and quantitative imuunocytochemistry, *J. Bone Miner. Res.*, vol. 6, pp. 937-945, 1991.

145. A. Linde, M. Bhown, and W.T. Butler, Noncollagenous proteins of dentin, *J. Biol. Chem.*, Vol. 225, pp. 5931, 1980.

146. A. Veis, W. Stetler-Stevenson, Y. Takagi, B. Sabsay, and R. Fullerton, The nature and localization of the phosphorylated proteins of mineralized dentin, in *The Chemistry and Biology of Mineralized Connective Tissues*, A. Veis, Editor, Elsevier/North-Holland, New York, 1981, pp. 377-387.

147. "Von Kossa for Calcium," *Stainsfile*, 2005. [Online]. Available: http://stainsfile.info/StainsFile/stain/bone/vonkossa.htm [Accessed August 3, 2008].

148. C.F.A. Culling, *Handbook of histopathological and histochemical techniques*, 3rd ed, Butterworth, 1974.

149. W.T. Butler, H. Birkedal-Hansen, W.F. Beegle, R.E. Taylor, and E. Chung, "Proteins of the periodontium. Identification of collagens with the [alpha1(I)]2alpha2 and

[alpha1(III)]3 structures in bovine periodontal ligament," *J. Biol. Chem.*, vol. 250, pp. 8907-8912, 1975.

150. J.E. Eastoe, "The amino acid composition of proteins from the oral tissues-II," *Arch. Oral Biol.*, vol. 8, pp. 663-652, 1963.

151. E.J. Miller, G.R. Martin, K.A. Piez, and M.J. Powers, "Characterization of chick bone collagen and compositional changes associated with maturation," *J. Biol. Chem.*, vol. 242, pp. 5481-5489, 1967.

Appendix I

Abbreviation: Name	**Formula**	**Ca/P ratio**	**Log K_{sp} at 25°C**
MCPM: monocalcium phosphate monohydrate	$Ca(H_2PO_4)_2 \cdot H_2O$	0.50	Highly soluble
MCPA: monocalcium phosphate anhydrous	$Ca(H_2PO_4)_2$	0.50	Highly soluble
DCPD: dicalcium phosphate dihydrate	$CaHPO_4 \cdot 2H_2O$	1.00	6.59
DCPA: dicalcium phosphate anhydrous	$CaHPO_4$	1.00	6.90
OCP: octacalcium phosphate	$Ca_8H_2(PO_4)_6 \cdot 5H_2O$	1.33	96.6
α-TCP: α-tricalcium phosphate	$\alpha\text{-}Ca_3(PO_4)_2$	1.50	25.5
β-TCP: β-tricalcium phosphate	$\beta\text{-}Ca_3(PO_4)_2$	1.50	28.9
Whitlockite (mineral)	$Ca_{18}(Mg,Fe)_2H_2(PO_4)_{14}$ $Ca_{18}(Mg,Fe)_2(Ca)(PO_4)_{14}$	1.29 1.36	
OHAp (HA): hydroxyapatite	$Ca_5(PO_4)_3OH$	1.67	58.4
FAp: fluorapatite	$Ca_5(PO_4)_3F$	1.67	60.5
ClAp: chlorapatite	$Ca_5(PO_4)_3Cl$	1.67	
CO_3Ap: carbonated apatite	A-CO_3Ap: $Ca_{10}(PO_4)_6CO_3$ B-CO_3Ap: $Ca_{10}(PO_4)_{6-x}(CO3)_{3x/2}(OH)_2$		
TTCP: tetracalcium phosphate	$Ca_4(PO_4)_2O$	2.00	38

Table A1 Abbreviation, formula, and solubility products of calcium phosphates [28].

Non-collagenous macromolecule	**Function**
Phosphophoryn(s)	Mineralization
DMP-1	Potential regulator of mineralization in dentin
DSP-1	Potential regulator of mineralization in dentin
Versican	Captures space that will become bone
Decorin	Binds to collagen and TGF-β
Biglycan	Binds to collagen and TGF-β, high in sites undergoing morphogenesis
Osteonectin	Ca++ and hydroxyapatite binding, regulate cell shape, growth factor binding
Fibronectin	Binds to cells, fibrin, heparin, gelatin, collagen
Osteopontin	Binds to cells, may regulate proliferation, inhibits NOS, regulates viral infection
Bone sialoprotein	Binds to cells, may initiate mineralization
Matrix Gla protein	May function in cartilage metabolism
Osteocalcin	May regulate osteoclastic activity

Table A2 Hypothesized function of mineralized matrix proteins [72].

Amino acid analysis calculations:

The weight % of NCPs and collagen fibrils were calculated using Excel. The amino acid content was first converted to residues per 1000 residues. The amount of amino acid that's contained in collagen tissue alone was subtracted from the total amount of amino acid present in each tissue. The number of amino acid residues contained in collagen and NCPs were then multiplied by the molecular weight of each amino acid, and the weight percentage determined from that.

The amount of each amino acid residue contained in collagen was an average taken of the three mineralized tissues of the periodontium, dentin, cementum, and bone. The values of amino acid contained in each tissue were obtained from the literature and are shown in the Table below [149-151].

Amino acid residue	**Bovine PDL collagen [149]**	**Human dentin collagen [150]**	**Chick bone collagen [151]**
Asp	52.4	55	46
Glu	82.1	73	74
OH-Pro	83.1	101	98.9
Ser	39.9	38	28
Gly	318	319	326
His	6.8	5.3	6.5
Arg	47.4	47	49
Thr	21	19	20
Ala	103	112	121
Pro	111	115	114
Tyr	8	2.3	4.9
Val	23.6	25	19
Met	7.6	5.2	7.2
Cys	2.3	0	0
Ile	13.4	10	12
Leu	30.1	26	25
Phe	14.1	14	15
Lys	28.1	23	28
hydroxylysine	7	8.4	5.9

Table A3 Amino acid residue values of PDL, dentin, and bone collagen obtained from the literature [149-151]. Values are shown as number of amino acid residues per 1000 residues.

Appendix II: Experimental protocols

Protocol 1: Paraformaldehyde (PFA) preparation

To make 100 ml of 4 % PFA solution:

Materials: 10x Dulbecco's PBS solution; paraformaldehyde (Prill)

1. In Erlenmeyer flask, add 4 g of PFA to 80 ml of water (do in fumehood)
2. Start heating with stirring
3. Add 10 ml of 10x PBS
4. Add 0.2 ml of 5 N NaOH
5. Continue heating until PFA is in solution
6. Remove from hot plate and cool on ice
7. Adjust pH to 7.2 with 5 M and 1 M HCl
8. Adjust the volume to 100 ml with a volumetric flask
9. Filter through 0.45 µm filter and store at 4°C

Protocol 2: Ethylene-diamine-tetra-acetic acid (EDTA) preparation

To make 1 L of a 12.5 % EDTA solution:

Materials: EDTA disodium salt powder (Bio); 1x Dulbecco's phosphate buffered saline

1. Dissolve 125 g of EDTA powder in 800 ml of 1x PBS solution
2. Warm up the solution to approximately 60°C to allow the powder dissolve completely
3. Cool down the solution to 25°C with ice or cold water
4. Adjust the pH to 7.4 with 5 M NaOH (~ 60 ml)
5. Adjust the final volume of the solution to 1 L with a volumetric flask
6. Filter the solution and store in PETE bottle at room temperature

Protocol 3: SBF solutions preparation

Chemicals	**Solutions**			
	1x m-SBF	**1x c-SBF**	**1.25x c-SBF**	**1.5x c-SBF**
NaCl	5.377 g	8.025 g	9.994 g	12.000 g
$NaHCO_3$	0.840 g	0.353 g	0.441 g	0.529 g
KCl	0.224 g	0.224 g	0.280 g	0.335 g
K_2HPO_4	0.174 g	0.174 g	0.218 g	0.261 g
$MgCl_2 \cdot 6H_2O$	0.305 g	0.305 g	0.381 g	0.457 g
HCl (1M)	None	40 mL	50 mL	60 mL
NaOH (0.2M)	100 mL	None	None	None
HEPES	17.8733g	None	None	None
$CaCl_2 \cdot 2H_2O$	0.368 g	0.368 g	0.459 g	0.551 g
Na_2SO_4	0.071 g	0.071 g	0.089 g	0.107 g
$(CH_2OH)_3CNH_2$	N/A	6.057 g	7.571 g	9.086 g
NaOH (1M)	~ 15 mL	None	None	None
HCl (1M)	None	~ 1 mL	~ 1 mL	~ 1 mL

Table A4 Chemicals used for the preparation of 1x m-SBF, 1x c-SBF, 1.25x c-SBF, and 1.5x c-SBF. Note: HEPEs buffer was dissolved in 100 mL of 0.2 M NaOH prior to adding it to the solution.

Chemicals	Chemical Purity and manufacturer
NaCl	>99.0 % reagent ACS, ACP, Montreal, Quebec
$NaHCO_3$	>99.5 % reagent ACS, ACP, Montreal, Quebec
KCl	>99.0 % reagent ACS, ACP, Montreal, Quebec
K_2HPO_4	>98.0 % reagent ACS, ACP, Montreal, Quebec
$MgCl_2 \cdot 6H_2O$	>99.6 % ACS reagent grade, Bioshop
$CaCl_2 \cdot 2H_2O$	>99.0 % A.C.S reagent, Sigma-Aldrich
Na_2SO_4	>99.0 % ACS reagent, EMD, Merck
$(CH_2OH)_3CNH_2$ (Tris buffer)	>99.8 % ACS reagent, Sigma-Aldrich
HEPES buffer	>99.5 % cell culture tested, Sigma-Aldrich

Table A5: List of chemicals and manufactures for making SBF solutions.

Protocol 4: Trypsin solution preparation (1.25 mg/ml)

Prepare 40 ml of 1.25 mg/ml of trypsin solution (approximate activity = 10,000 BAEE units)

1. Re-constitute 0.5 g of trypsin in 10 ml of 1 mM HCl (stir and warm up the solution to 37°C on a hotplate)
2. Add 25 ml of 1x DPBS solution to the trypsin solution
3. Adjust the pH of the solution to 7.6 at 37°C with 1 M (~4 drops) and 0.1 M (~13 drops) NaOH
4. Adjust the volume of the solution to 40 ml with 1x DPBS (~4.4 ml)

Protocol 5: Papain solution preparation (2.5 mg/ml)

Materials: Papain suspension in 0.05 M sodium acetate (product # P3125); activity: 31 units/mg of protein; volume of solution: 4.77 ml; Enzyme concentration: 21 mg/ml

1. Prepare 50 ml of 20 mM sodium phosphate buffer
    - Add 0.1567 g of sodium phosphate powder to 45 ml mili-Q water
    - Adjust the pH of the solution to 6.5 and the volume of the solution to 50 ml
2. Prepare a buffered solution containing 5 mM L-cysteine and 0.5 mM EDTA:
    - Add 0.0341 g of L-cysteine and 0.0105 g of EDTA powder to 50 ml of phosphate buffer solution
3. Prepare 15 ml of 2.5 mg/ml papain solution:
    - Add 1.789 ml of papain to 13.212 ml of sodium phosphate buffer (solution 2)

Protocol 6: Fast Green staining protocol

Materials: Fast Green FCF powder (Sigma-Aldrich)

Solutions

1. 0.1 % Fast Green in citrate-phosphate buffer – dissolve 0.25 g of Fast Green FCF powder (Sigma-Aldrich) in McIlvaine's buffer [135].
    a. McIlvaine's buffer: combine the respective amounts of solution i and ii
        i. 2.75 ml of 0.1 M citric acid (0.48 g in 25 ml distilled water)
        ii. 97.25 ml of 0.2 M disodium phosphate (7.1 g Na_2HPO_4 anhydrous in 250 ml of distilled water)
2. 1 % glacial acetic acid – Dilute from concentrated acetic acid with Mili-Q water.

Staining Procedure

1. Dewax and hydrate paraffin embedded sections
2. Stain in Fast Green for 6 min.
3. Wash in 1 % acetic acid for 20 s, followed by 70 %, 95 %, 100 % and 100% ethanol, 30 seconds each
4. Clear in xylene and mount with paramount

Protocol 7: Alizarin red staining method [133]

Solutions

A. 1 % Alizarin red S solution – Dissolve 1 g of Alizarin red S powder in 100 ml of Mili-Q water, adjust the pH to 6.1 with 0.5 M ammonium hydroxide (NH_4OH) (add drop by drop).
B. Differentiating fluid – add one drop of concentrated HCl to 95 % ethanol; mix the solution well before using and discard when the solution turn yellow

Staining Procedure

1. De-wax and hydrate paraffin sections
2. Stain in Alizarin red solution for 3.5 min.
3. Wash in tap water for 20 s
4. Differentiate in solution B for 15 s
5. Complete the dehydration in 2 changes of absolute ethanol, 2 min. each
6. Clear in xylene and mount with Cytoseal

Results

Mineralized tissue bright orange to red, other connective tissues pale pink-orange.

Protocol 8: Von Kossa staining method [133, 147, 148]

Solutions

A. 5 % aqueous silver nitrate ($AgNO_3$) dissolved in mili-Q water,
B. 5 % aqueous sodium thiosulfate ($Na_2S_2O_3 \cdot 5H_2O$)
C. A counterstain – eosin (dissolve 2.5 g in 495 mL of distilled water, add 0.5 ml of glacial acetic acid)

Procedure

1. Place slides in a clear glass Coplin jar filled with 5% silver nitrate solution
2. Place the jar in front of a bright light for 40 min.
3. Remove slides from the jar and wash the slides well in 2 changes of distilled water (5 min each) to remove all traces of silver
4. Rinse slides in the thiosulfate solution for 5 min. to remove the un-reacted silver
5. Wash well in 3 changes of tap water (5 min each)
6. Counter-stain with eosin for 30 s to 1 min.
7. Rinse in distilled water for 20 s to remove excess dye
8. Dehydrate the slides with 70 %, 95 %, 100 %, and 100 % ethanol solutions progressively for 1 min. each
9. Clear in xylene for 1 min. and mount with Cytoseal

Results

Mineralized tissue brown/black, connective tissue pink

Protocol 9: Drying samples with hexamethyldisilazane (HMDS)
Important: Work in a **fumehood**.

1. Dehydrate the hydrated samples with graded ethanol, 50 %, 70 %, 95%, 100% (1 min. ea.)
2. Dehydrate with pure ethanol (2 min.)
3. Dehydrate with HDMS (2 min.)
4. Let sample dry in the fumehood for 30-60min.

Note: If working with slides, pipette drops of solutions onto the samples at regular time intervals (e.g. every 5-20 s); do not let the samples dry during the dehydration process.
Dispose of waste in properly labeled container (this is important for HMDS).

Protocol 10: Procedure for embedding the positive control sample in Osteo-bed resin
The sample was dehydrated with 70%, 95%, and 100 % ethanol for 2 days each, followed by infiltration with the Osteobed resin for 4 days and the Osteobed resin containing catalyst for 3 days at room temperature. The sample was then embedded in fresh Osteobed resin containing the catalyst for a total of 8 days with the temperature gradually increased to 60°C.

Appendix III

	1x c-SBF	**1.25x c-SBF**	**1.5x c-SBF**	**1x m-SBF**
5 d	N/A	N/A	N/A	**Soln change:** D-medium; B-light to very light; C-medium to light; PDL-none **Soln change + stirring:** D-medium to intense; B-medium; C-medium to intense; PDL-none
7 d	N/A	**None:** D-intense; B-light; C-medium to light; PDL-none; **Stirring:** D-medium to intense; B-light; C-light to medium; PDL-none **Soln change:** D-light; B-none; C-none; PDL-none **Soln change + stirring:** D-light to medium; B-light to very light; C-light to medium; PDL-none	**None:** D-intense; B-none to very light; C-medium to light; **Stirring:** D-intense to medium; B-light; C-medium to light; PDL-none **Soln change:** D-intense; B-very light; C-medium to light; PDL-none	**Soln change:** D-medium to intense; B-light; C-medium to intense; PDL-none **Soln change + stirring:** D-intense; B-intense; C-intense; PDL-light, nuclei stained medium intensity;
10 d	N/A	N/A	N/A	**Soln change:** D-intense; B-medium to light; C- intense; PDL-none **Soln change + stirring:**

				D-very intense; B-very intense; C-very intense; PDL-light, cell nuclei stained intense
14 d	**Stirring:** D-medium; B-light to very light; C-light; PDL-none **Soln change:** D-light to medium; B-nothing; C-very light; PDL-none **Soln change + stirring:** D-medium to intense; B-light to very light; C-light to very light; PDL-none	**None:** D-medium to intense; B-none to light; C-medium to light; PDL-none; **Stirring:** D-intense; B-medium to intense; C-intense; PDL-light, cell nuclei stained intense **Soln change:** D-medium to intense; B-light; C-light; PDL-none **Soln change + stirring:** D-medium to intense; B & C-light to medium; PDL-none	**None:** D-intense to medium; B-light; C-light to medium; PDL-none **Stirring:** D-intense; B-medium to intense; C-intense; PDL-none **Soln change:** D-medium to intense; B-light to medium; C-light; PDL-none	

Table A6 Intensity of mineral staining observed on samples incubated in different SBF solutions for various durations. Solution change was carried out every 3 days.